

NASA MEMO 3-9-59L

NASA

MEMORANDUM

TRANSONIC WIND-TUNNEL INVESTIGATION OF AN INLET MODEL
OF A SUPERSONIC FIGHTER-BOMBER AIRPLANE

By Arvo A. Luoma and Joseph D. Brooks

Langley Research Center
Langley Field, Va.

UNCLASSIFIED

NASA 10.71350 5/20/71

FACILITY FORM 602

N71-73444

(ACCESSION NUMBER)

(THRU)

(PAGES)

(CODE)

(NASA CR OR TMX OR AD NUMBER)

(CATEGORY)

NATIONAL AERONAUTICS AND
SPACE ADMINISTRATION

WASHINGTON

April 1959

CONFIDENTIAL

[REDACTED]
NATIONAL AERONAUTICS AND SPACE ADMINISTRATION

MEMORANDUM 3-9-59L

TRANSONIC WIND-TUNNEL INVESTIGATION OF AN INLET MODEL
OF A SUPERSONIC FIGHTER-BOMBER AIRPLANE*

By Arvo A. Luoma and Joseph D. Brooks

SUMMARY

L
2
0
8

An investigation of the internal aerodynamic characteristics of a 1/13-scale model of the inlet of a supersonic fighter-bomber airplane was made in the Langley 8-foot transonic tunnel at Mach numbers from 0.60 to 1.10. The model included the forward part of the airplane fuselage with wing stubs incorporating sweptforward twin-duct wing-root inlets. Various angles of attack, angles of sideslip, and mass-flow ratios were investigated. Information on pressure recovery and distortion of the duct flow at the station corresponding to the engine face was obtained.

The average total-pressure ratio and the total-pressure distortion at the engine face were primarily affected by changes in mass-flow ratio and angle of attack. Changes in angle of sideslip had slight effect on these flow parameters.

INTRODUCTION

The present investigation of the internal aerodynamic characteristics of a 1/13-scale model of the inlet of a supersonic fighter-bomber airplane was made in the Langley 8-foot transonic tunnel at Mach numbers from 0.60 to 1.10. The model had sweptforward twin-duct wing-root inlets designed for operation at Mach numbers up to 2.0. Other investigations of sweptforward inlets at Mach numbers from 1.0 to 2.0 are reported in references 1 to 3.

The purpose of the present investigation was to provide information at transonic speeds on the pressure recovery and the flow distortion at the duct station corresponding to the engine face and on the static-pressure fluctuations in the diffuser. The results on the static-pressure

[REDACTED]

[REDACTED]

fluctuations are presented in reference 4. The results on pressure recovery and on the magnitude and pattern of the total-pressure distortion at the duct station corresponding to the engine face are presented herein. These results were obtained at mass-flow ratios from approximately 0.52 to 0.88, at angles of attack from -4° to 10° , and at angles of sideslip from -5° to 10° . Tests were also made with a "glove" attached to each side of the body for reducing the height of the boundary-layer diverter.

SYMBOLS

A	cross-sectional area of duct at station corresponding to engine face	L 2 0 8
A_p	projected area of inlet (5.00 sq in. on model)	
M	Mach number of undisturbed stream	
p	local static pressure of flow in duct at station corresponding to engine face	
p_{av}	average (arithmetical) static pressure of static tubes on engine-face survey rake	
p_t	local total pressure of flow in duct at station corresponding to engine face	
$p_{t,\infty}$	total pressure of undisturbed stream	
$(p_t)_{av}$	mass-flow-weighted average total pressure of flow in duct at station corresponding to engine face, $\frac{\int_A p_t \frac{\rho V}{\rho_\infty V_\infty} dA}{\int_A \frac{\rho V}{\rho_\infty V_\infty} dA}$	
$(p_t)_{max}$	maximum value of local total pressure measured by engine-face survey rake	
$(p_t)_{min}$	minimum value of local total pressure measured by engine-face survey rake	
$\Delta p_t / (p_t)_{av}$	total-pressure distortion of flow in duct at station corresponding to engine face, $\frac{(p_t)_{max} - (p_t)_{min}}{(p_t)_{av}}$	

r	radial location in duct at station corresponding to engine face (see fig. 1)
R	radius to outer wall of duct at station corresponding to engine face
V	local velocity of flow in duct at station corresponding to engine face
V_{∞}	velocity of undisturbed stream
w	duct mass-flow rate, $\int_A \rho V \, dA$
w/w_{∞}	duct mass-flow ratio, $\frac{w}{\rho_{\infty} V_{\infty} A_p}$
α	angle of attack of model, based on reference line of body
β	angle of sideslip of model
θ	angular displacement of radial rows of total-pressure tubes on engine-face survey rake (see fig. 1)
ρ	local mass density of flow in duct at station corresponding to engine face
ρ_{∞}	mass density of undisturbed stream

APPARATUS AND METHODS

Tunnel

This inlet investigation was made in the Langley 8-foot transonic tunnel, which has a slotted test section that permits continuous testing through the transonic speed range. The tunnel operates at a stagnation pressure approximately equal to atmospheric pressure. A detailed description of the tunnel and the calibration are presented in reference 5.

Model

The model used in this investigation was a sting-supported, 1/13-scale model of a supersonic fighter-bomber airplane. The model included the forward part of the airplane fuselage with wing stubs incorporating sweptforward twin-duct wing-root inlets. A drawing of the model is shown in figure 2, and photographs of the model are shown as figures 3 and 4. The two ducts from the wing-root inlets merged into a single duct which had an exit at the body base. The station at which the ducts merged was 0.93 inch downstream of the station corresponding to the engine face. The cross section of each duct was semielliptical at the inlet and semi-circular at the merging station (fig. 2(a)). The variation of the total duct cross-sectional area (normal to the model center line) with fuselage station is shown in figure 5.

Tests were also made with a glove attached to each side of the fuselage (figs. 2 and 4). The gloves widened the fuselage and reduced the height of the boundary-layer diverter. A motor-driven throttling plug at the base of the model was used during the test runs to vary the mass flow in the model duct (fig. 2(a)).

Instrumentation and Tests

Two survey rakes consisting of total-pressure and static-pressure tubes were used in the model - one rake at the duct station corresponding to the engine face for pressure-profile studies and a second rake near the exit of the duct for mass-flow measurements. Mass-flow values were also computed from the pressure data obtained with the engine-face survey rake. The mass-flow values presented herein are the average of the two rake values, which agreed well.

The layout of the total-pressure and static-pressure tubes in the engine-face survey rake is given in figure 1; several of the rake tubes leaked or were plugged during the tests and are not shown in the figure. The duct divider in the model extended downstream of the engine-face survey rake, and a rake-support tube formed an inner wall of the flow (fig. 1).

A strain-gage attitude transmitter was used for measuring angle of attack for tests in which the model was pitched in a vertical plane, or for measuring angle of sideslip for tests in which the model was yawed in a vertical plane. The instrument was mounted in the fuselage and yielded angle-of-attack or sideslip data that were independent of balance and sting deflection due to load.

Data were obtained at mass-flow ratios which generally varied from approximately 0.68 to the maximum obtainable (throttling plug at downstream limit). Some data were obtained at mass-flow ratios down to 0.52. The angles of attack, angles of sideslip, and Mach numbers at which data were obtained are shown in table I. A transition strip consisting of a 0.2-inch-wide strip of no. 60 carborundum grains shellacked on the fuselage 5.5 inches from the fuselage nose was used for one run. The average Reynolds numbers of the undisturbed stream based on a length of 1 foot were 3.4×10^6 at the test Mach number of 0.60 and 4.0×10^6 at the test Mach numbers of 0.90, 0.95, and 1.10.

Accuracy

The estimated accuracy of the data is as follows:

$P_t/P_{t,\infty}$	± 0.003
M	± 0.003
w/w_∞	± 0.01
α , deg	± 0.1
β , deg	± 0.1

RESULTS

Basic Results

The basic data are presented in figures 6 to 10 as the radial variation of the local total-pressure ratio $P_t/P_{t,\infty}$ at the engine face for various mass-flow ratios, angles of attack, angles of sideslip, and Mach numbers. The total-pressure plots were faired to the static-pressure values at the inner and outer walls of the duct. The inner and outer walls of the duct were not instrumented for static-pressure measurements, and it was assumed that the static pressure on the walls was the same as that measured by the nearest static-pressure tube on the survey rake. Information about the configurations and test conditions and an index of the basic figures are given in table I.

Summary Results

The variation of the average total-pressure ratio $(P_t)_{av}/P_{t,\infty}$ and the average static-pressure ratio $P_{av}/P_{t,\infty}$ with mass-flow ratio is shown in figures 11 to 14 for the various configurations and test conditions. Contour plots of the local total-pressure ratio $P_t/P_{t,\infty}$

at the engine face as seen looking downstream are presented in figures 15 and 16 for the basic configuration at various test conditions. The effect of mass-flow ratio on the total-pressure distortion $\Delta p_t / (p_t)_{av}$ at the engine face is presented in figure 17 for various angles of attack and sideslip.

DISCUSSION

Pressure Recovery

The average total-pressure ratio at a given Mach number generally was a maximum at the lowest mass-flow ratio tested and gradually decreased with an increase in mass-flow ratio until inlet choking was approached (as indicated by the abrupt decrease in average total-pressure ratio with an increase in mass-flow ratio). The increase in average total-pressure ratio that occurred with a decrease in mass-flow ratio appears to be characteristic of sweptforward inlets, as shown by the results of reference 1. However, the improvement in pressure recovery at low mass-flow ratios is generally accompanied by an increase in external drag because of the increased spillage from the inlet. The average total-pressure ratio for the basic configuration was 0.98 at an angle of attack of 0° , an angle of sideslip of 0° , a mass-flow ratio of 0.70, and a Mach number of 0.90 (fig. 11). An increase in Mach number decreased the average total-pressure ratio by a small amount, at most by approximately 2 percent at mass-flow ratios below inlet choking (figs. 11 to 14).

The average total-pressure ratio at an angle of sideslip of 0° was essentially unaffected by changes in angle of attack from -4° to 4° at mass-flow ratios of 0.70 and less (fig. 11). At these low values of mass-flow ratio, an increase in angle of attack above 4° decreased the average total-pressure ratio. For example, at a mass-flow ratio of 0.70, an increase in angle of attack from 4° to 10° resulted in a decrease in average total-pressure ratio of 3 percent at subsonic speeds and of 4 percent at a Mach number of 1.10. At mass-flow ratios higher than 0.70, a change in angle of attack from 0° in either a positive or a negative direction decreased the average total-pressure ratio. At a mass-flow ratio of 0.80, for example, an increase in angle of attack from 0° to 10° resulted in a decrease in average total-pressure ratio of 5 percent at subsonic speeds and of 6 percent at a Mach number of 1.10. The maximum obtainable test mass-flow ratio at an angle of sideslip of 0° decreased as the angle of attack was changed from 0° . This decrease amounted to approximately 5 percent as the angle of attack was changed from 0° to 10° . The addition of a transition strip to the fuselage nose ahead of the inlet had no effect on the average total-pressure ratio, as is indicated by the flagged symbols in figure 11.

The effect of angle of attack on the average total-pressure ratio was somewhat different for the model at an angle of sideslip of -5.2° (fig. 12) than at an angle of sideslip of 0° (fig. 11). At angles of attack of 4° and above, the average total-pressure ratio was generally higher (at most by 1 percent) at an angle of sideslip of -5.2° than at an angle of sideslip of 0° .

The effect of angle of sideslip on the average total-pressure ratio at an angle of attack of 0° was small for the basic configuration (fig. 13) and for the basic configuration with fuselage gloves (fig. 14). The small effect of angle of sideslip on pressure recovery is attributed to the action of the fuselage vortices in thinning the fuselage boundary layer on the downstream side of the fuselage (ref. 2).

The addition of the fuselage gloves had small effect on the average total-pressure ratio (figs. 13 and 14); the maximum effect amounted to a reduction of 2 percent and occurred at a Mach number of 1.10 at mass-flow ratios near 0.70. The gloves also affected somewhat the variation of average total-pressure ratio with angle of sideslip at these test conditions.

Total-Pressure Contours

At an angle of attack of 0° , the flow was fairly uniform at the lower mass-flow ratios (fig. 15). An increase in mass-flow ratio at an angle of attack of 0° resulted in an increase in flow nonuniformity, particularly in the upper half of the duct. At a given mass-flow ratio, an increase in angle of attack from 0° to 10° resulted primarily in an increase in flow nonuniformity in the lower half of the duct. The effect of Mach number on the contour plots of figure 15 was rather small. A change in angle of sideslip caused some unsymmetrical changes in the contour plots, but the overall effects were small (fig. 16).

Total-Pressure Distortion

An increase in mass-flow ratio considerably increased the total-pressure distortion $\Delta p_t / (p_t)_{av}$ particularly as inlet choking was approached (fig. 17). At a constant mass-flow ratio, the total-pressure distortion increased with an increase in angle of attack starting at 0° (figs. 17(a) and 17(b)), as previously indicated by the contour plots. The effect of angle of attack on distortion increased with an increase in mass-flow ratio. The transition strip on the fuselage had a negligible effect on total-pressure distortion (fig. 17(b)). Adding the gloves to the fuselage or varying the angle of sideslip of the model had an

insignificant effect on the total-pressure distortion (fig. 17(c)). An increase in Mach number increased the total-pressure distortion slightly.

CONCLUSIONS

An investigation of the internal aerodynamic characteristics of a 1/13-scale model of the inlet of a supersonic fighter-bomber airplane was made in the Langley 8-foot transonic tunnel at Mach numbers from 0.60 to 1.10. The model included the forward part of the airplane fuselage with wing stubs incorporating sweptforward twin-duct wing-root inlets. Mass-flow ratios from 0.52 to 0.88, angles of attack from -4° to 10° , and angles of sideslip from -5° to 10° were investigated. The following conclusions applicable to the duct flow at the engine face are indicated:

1. The average total-pressure ratio at a given Mach number generally was a maximum at the lowest mass-flow ratio tested and gradually decreased with an increase in mass-flow ratio until inlet choking was approached. An increase in Mach number decreased the average total-pressure ratio by a small amount.

2. An increase in angle of attack from 0° to 10° decreased the average total-pressure ratio at most by approximately 6 percent at mass-flow ratios below inlet choking.

3. The average total-pressure ratio at an angle of attack of 0° was essentially unaffected by a change in angle of sideslip or a decrease in the height of the boundary-layer diverter by the addition of gloves to the fuselage.

4. The total-pressure distortion increased with an increase in mass-flow ratio and an increase in angle of attack from 0° , but it was essentially unaffected by a change in angle of sideslip or the addition of gloves to the fuselage.

Langley Research Center,
National Aeronautics and Space Administration,
Langley Field, Va., December 19, 1958.

REFERENCES

1. Trescot, Charles D., Jr.: Investigation at Transonic Speeds of the Effects of Inlet-Lip Sweep on the Internal-Flow Characteristics of a Semielliptical Air Inlet With an Inlet-Lip Stagger of 30° . NACA RM L57E16, 1957.
2. Robins, A. Warner: Wind-Tunnel Investigation of a Wing-Root Inlet Configuration With Various Modifications at Mach Numbers of 1.41, 1.81, and 2.01. NACA RM L57A28, 1957.
3. Hayes, Clyde, and Mackley, Ernest A.: An Investigation of the Performance of a Semielliptical Scoop Inlet at Mach Numbers of 1.60, 1.76, and 2.02. NACA RM L57G15, 1958.
4. Brooks, Joseph D.: Transonic Wind-Tunnel Investigation of Static-Pressure Fluctuations in Duct of a Scale Inlet Model of a Supersonic Fighter-Bomber Airplane. NACA RM L57C17, 1957.
5. Wright, Ray H., Ritchie, Virgil S., and Pearson, Albin O.: Characteristics of the Langley 8-Foot Transonic Tunnel With Slotted Test Section. NACA Rep. 1389, 1958. (Supersedes NACA RM L51H10 by Wright and Ritchie and NACA RM L51K14 by Ritchie and Pearson.)

TABLE I

CONFIGURATIONS, TEST CONDITIONS, AND INDEX OF BASIC FIGURES

Configuration	Model condition	M	α , deg	β , deg	Figure
Basic	Smooth	0.90, 0.95, and 1.10	-4 to 10	0	6
	Transition strip on fuselage	0.90 and 1.10	-4 to 10	0	7
	Smooth	0.90, 0.95 and 1.10	-4 to 10	-5.2	8
	Smooth	0.60, 0.90, 0.95, and 1.10	0	-5 to 10	9
Basic with fuselage gloves	Smooth	0.90 and 1.10	0	-5 to 10	10

L
2
0
8

Description	Radial location, r	$\frac{r}{R}$
Inner wall	0.312	0.217
Ring 1	.444	.309
Ring 2	.638	.444
Ring 3	.905	.629
Ring 4	1.110	.772
Ring 5	1.285	.894
Outer wall	1.438	1.000

○ Total-pressure tube

△ Static-pressure tube

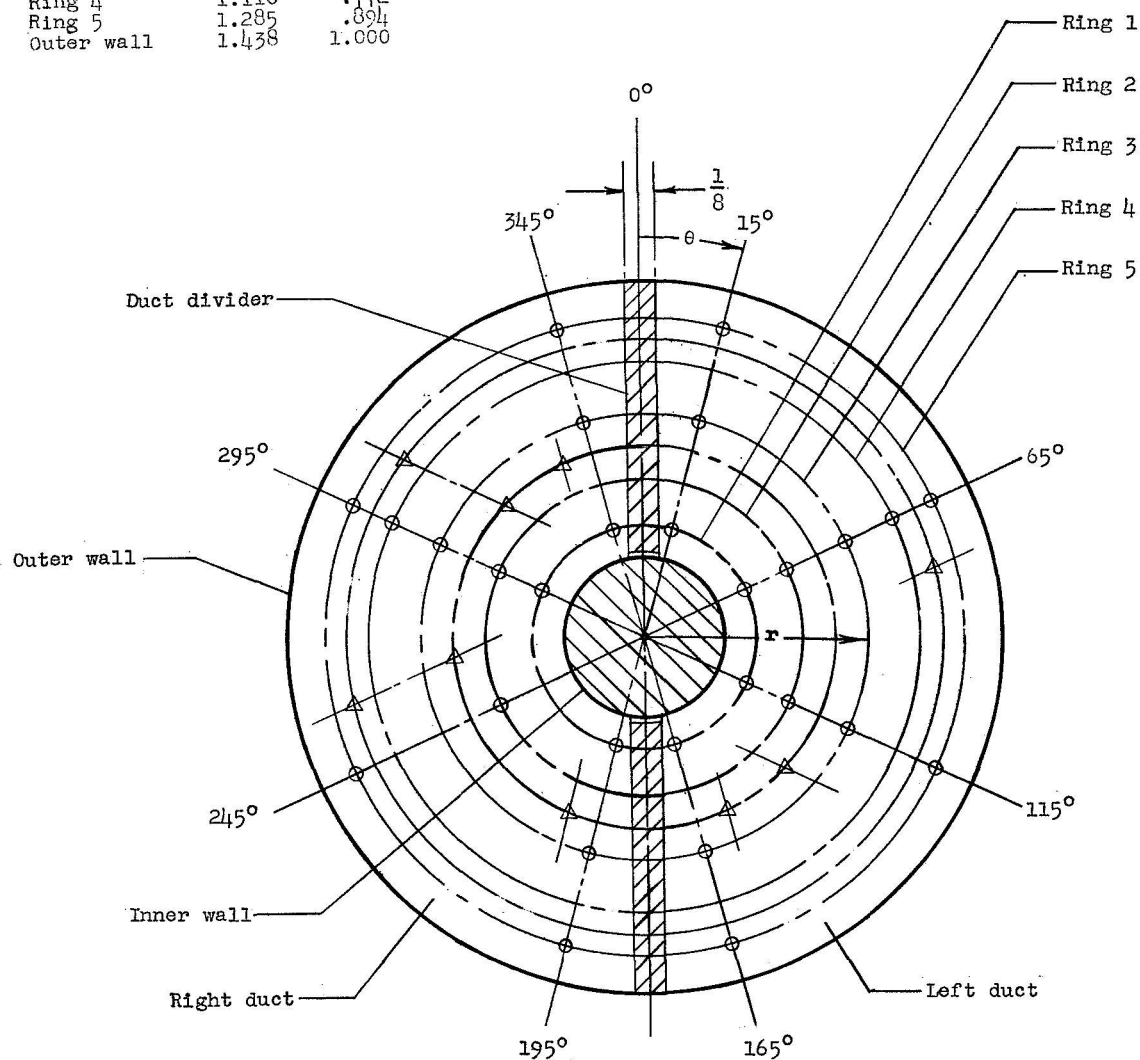
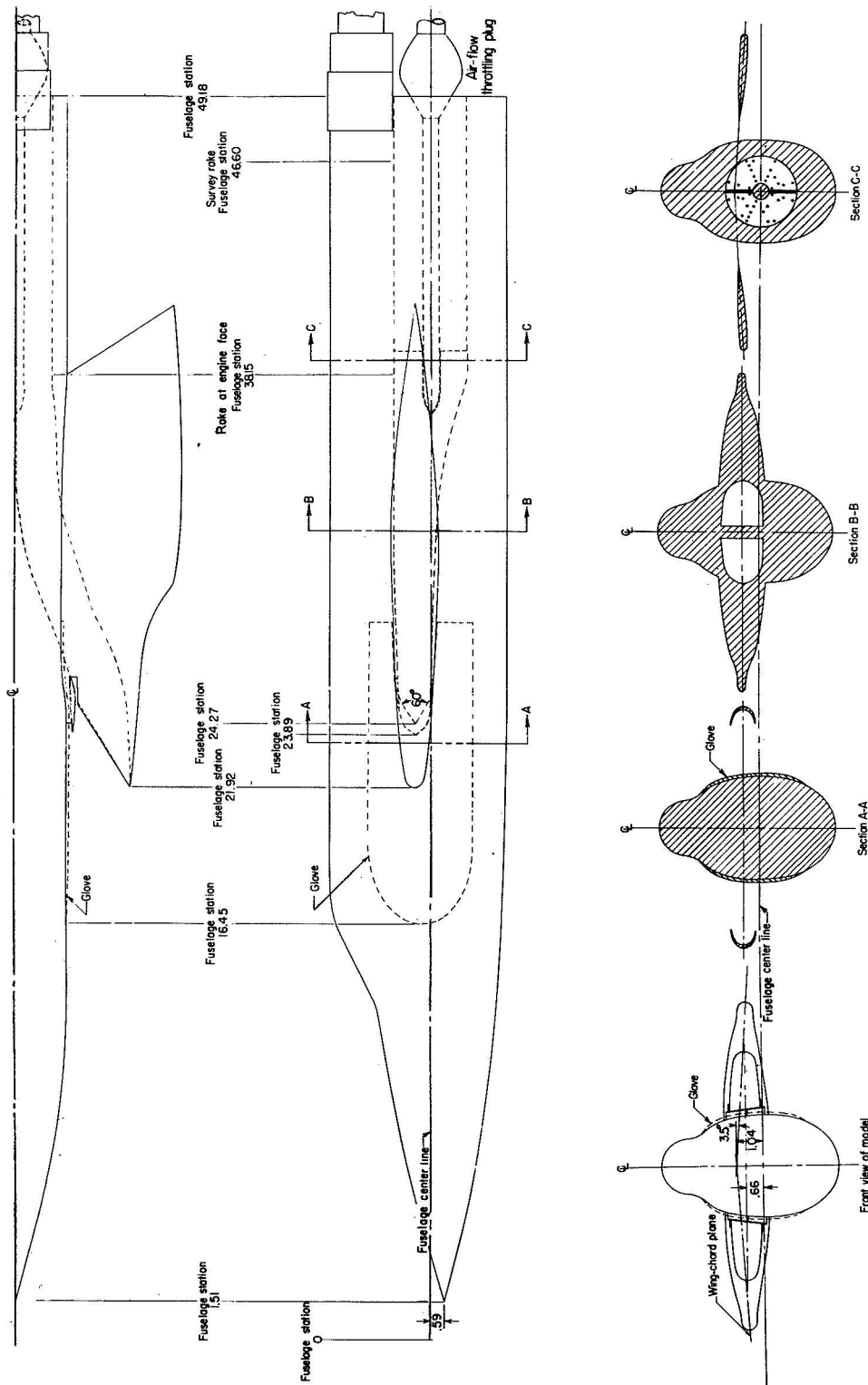
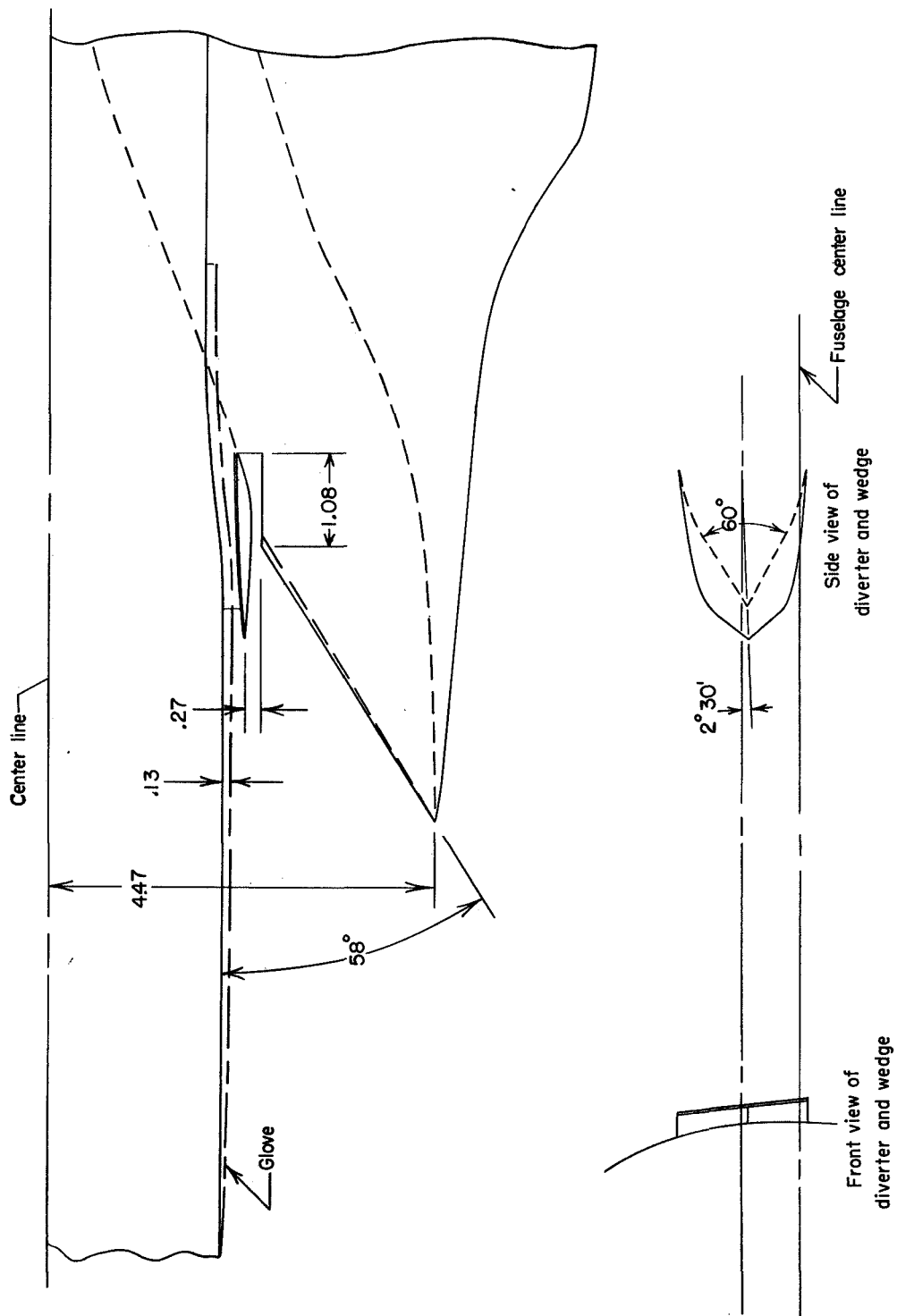


Figure 1.- Location of total-pressure and static-pressure tubes on survey rake in duct at station corresponding to engine face. View looking downstream. All dimensions are in inches unless otherwise indicated.



(a) General arrangement.

Figure 2.- Drawing of inlet model. All dimensions and fuselage stations are in inches.



(b) Details of inlet and diverter.

Figure 2.- Concluded.

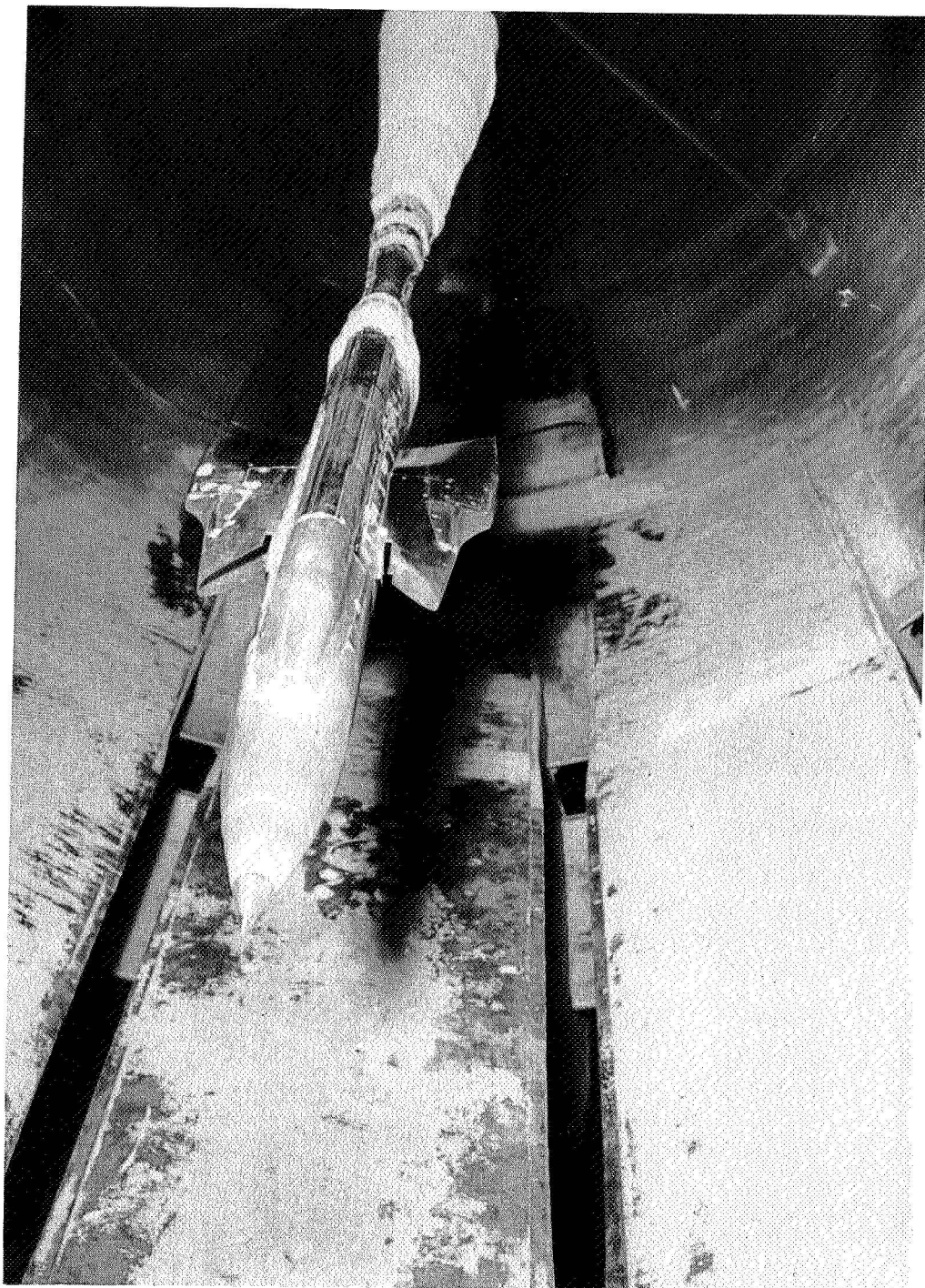
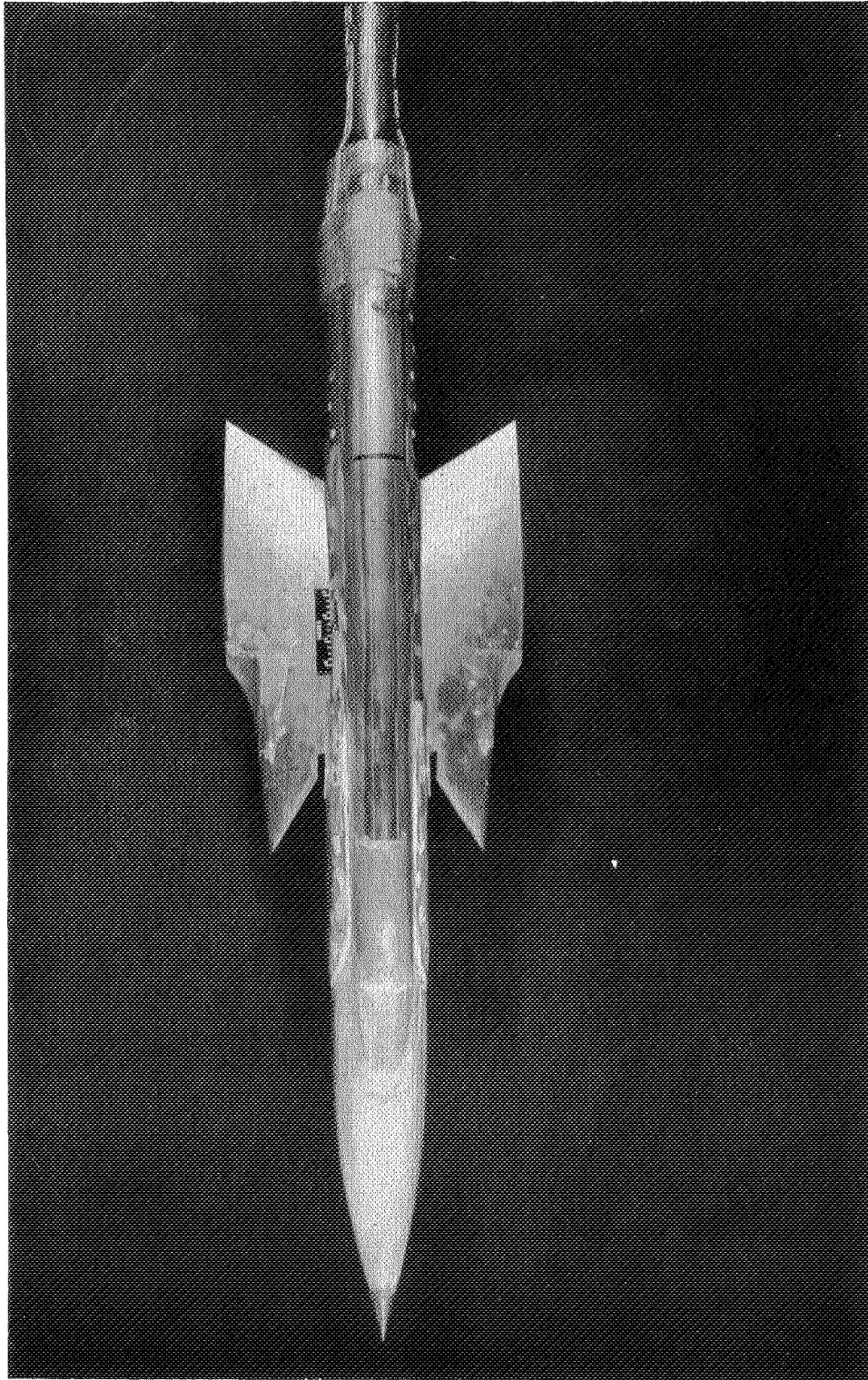


Figure 3.- Basic configuration installed in Langley 8-foot transonic tunnel. L-89261



(a) Plan view. L-89411

Figure 4.- Basic configuration with fuselage gloves.



(b) Side view. L-89410

Figure 4.- Concluded.

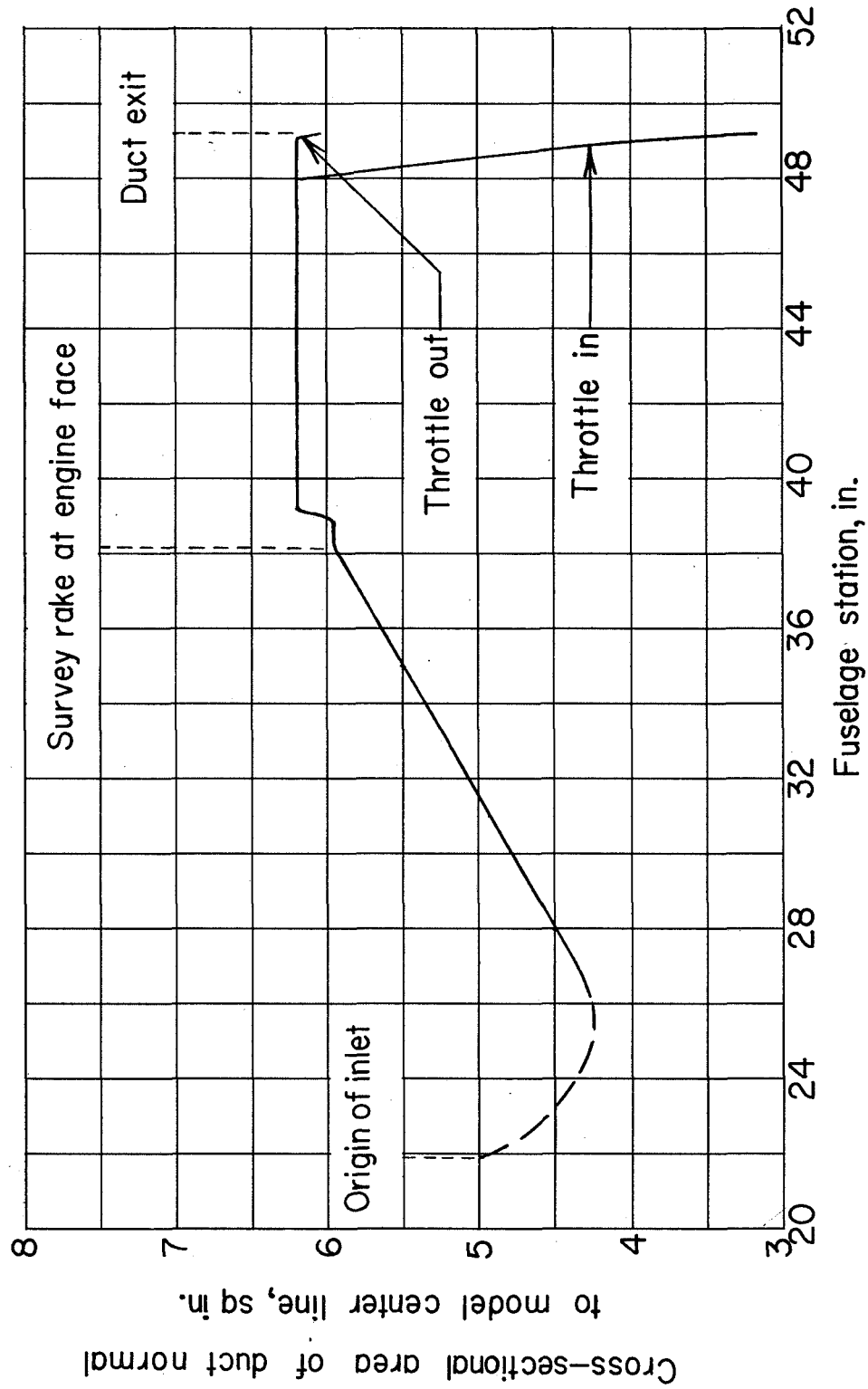
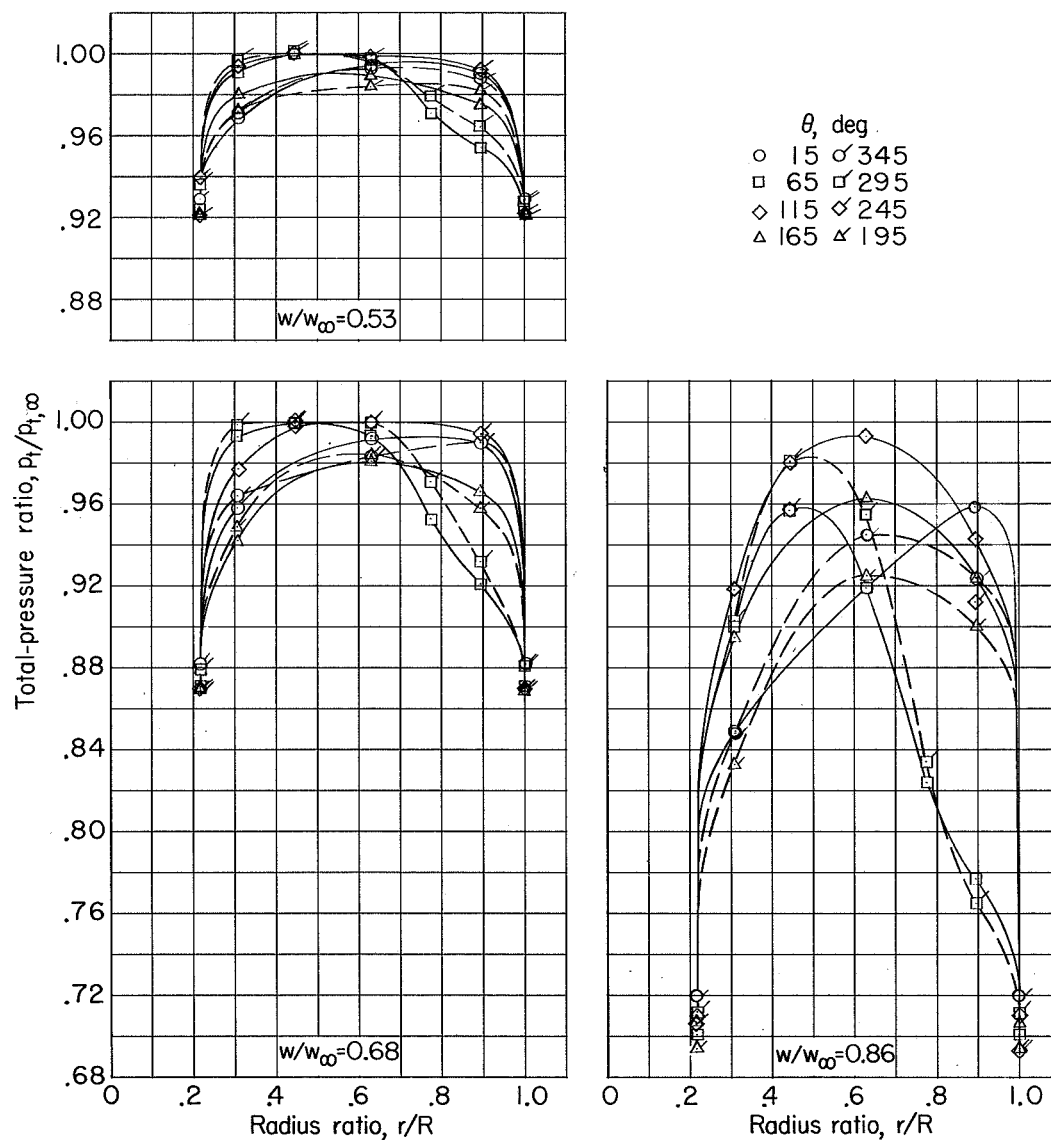
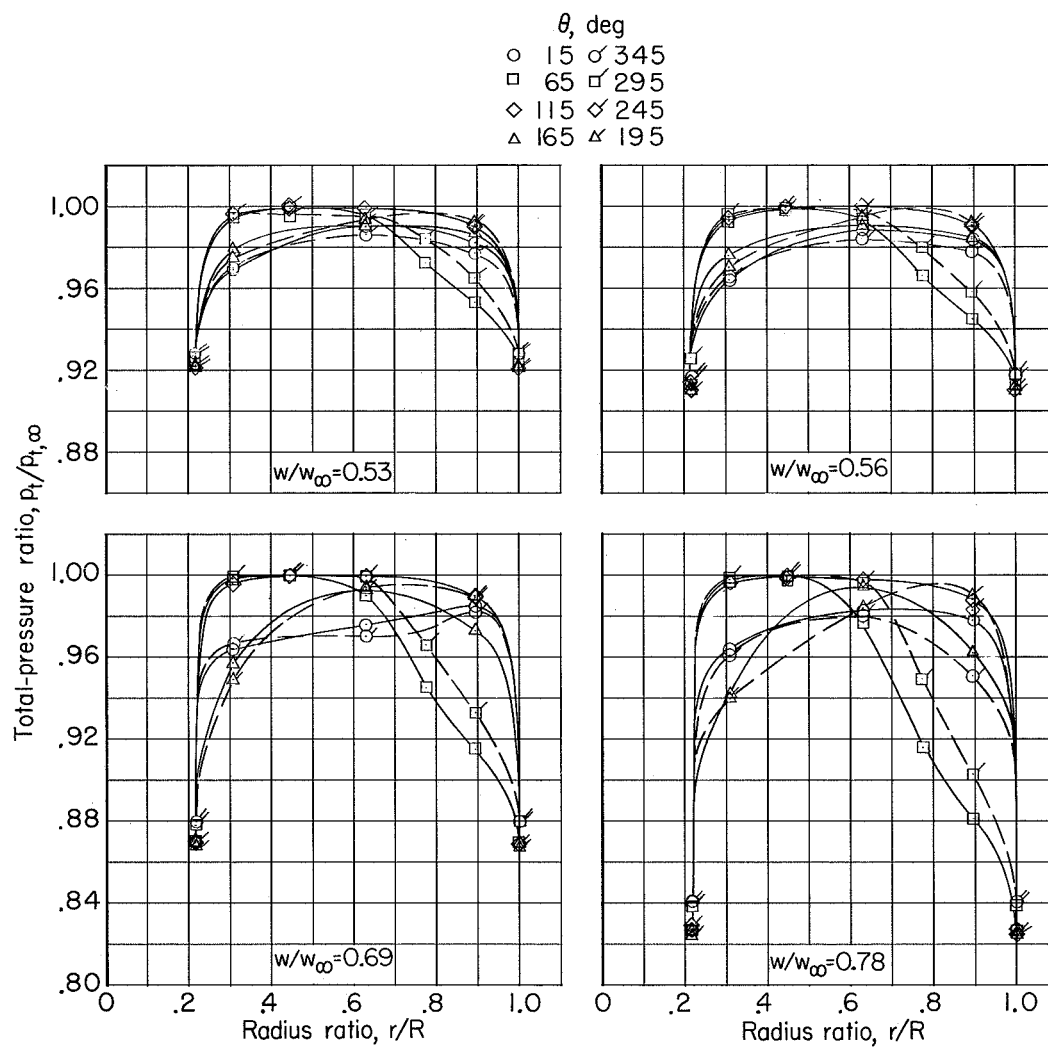


Figure 5.- Variation of total cross-sectional area of duct with fuselage station.



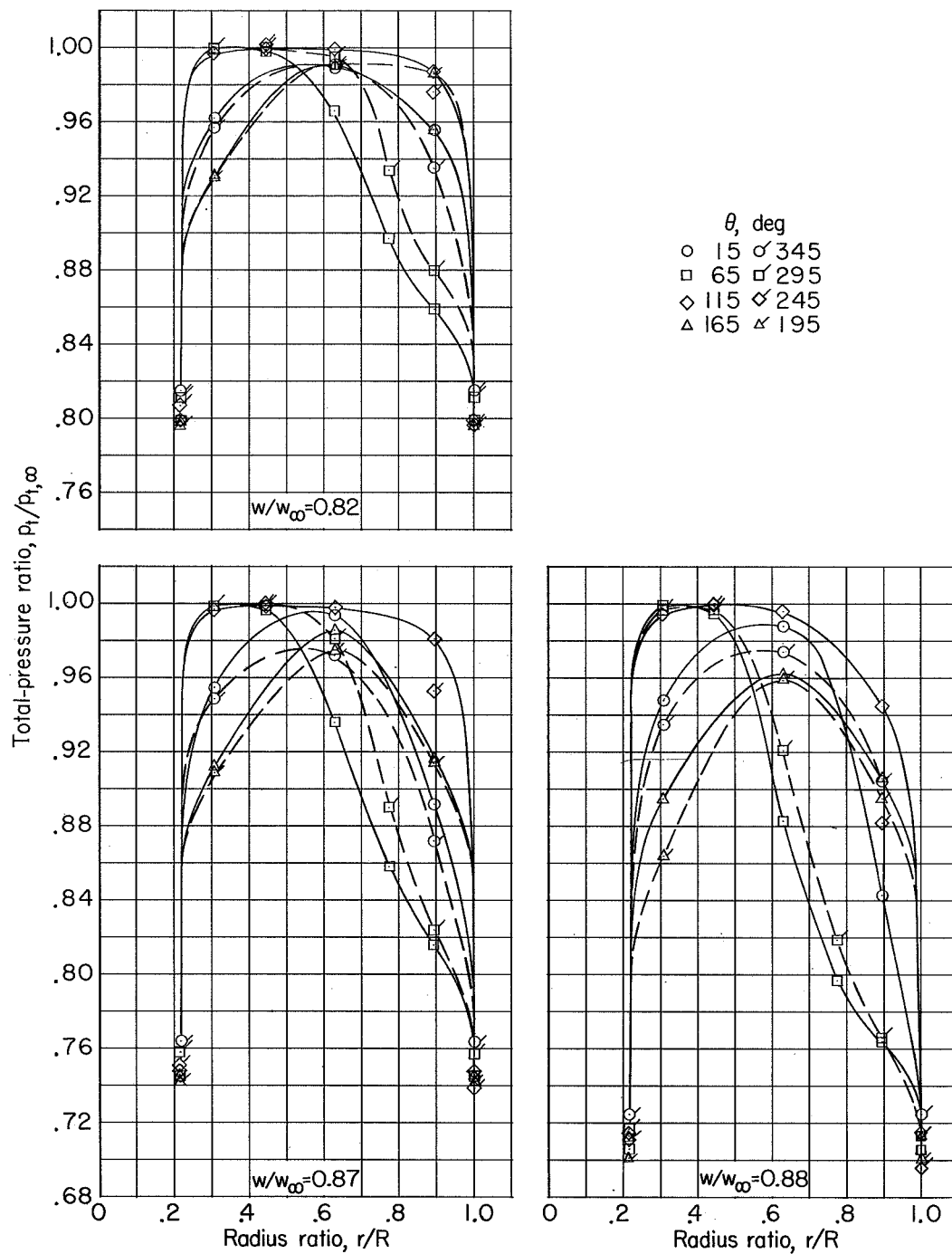
(a) $M = 0.90$; $\alpha = -4^\circ$.

Figure 6.- Radial variation of total-pressure ratio at various angles of attack, mass-flow ratios, and Mach numbers. Basic configuration. $\beta = 0^\circ$.



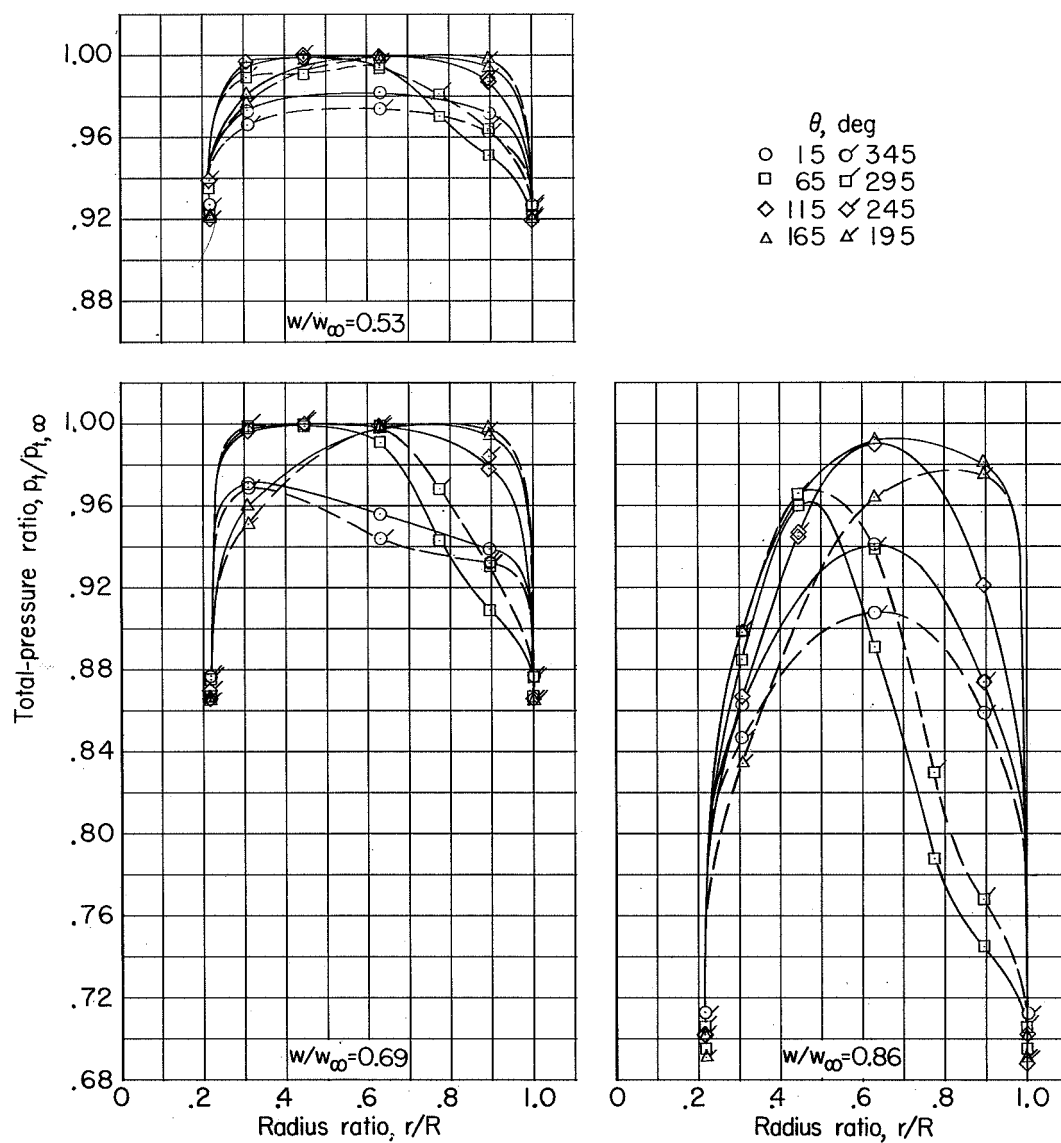
(b) $M = 0.90$; $\alpha = 0^\circ$.

Figure 6.- Continued.



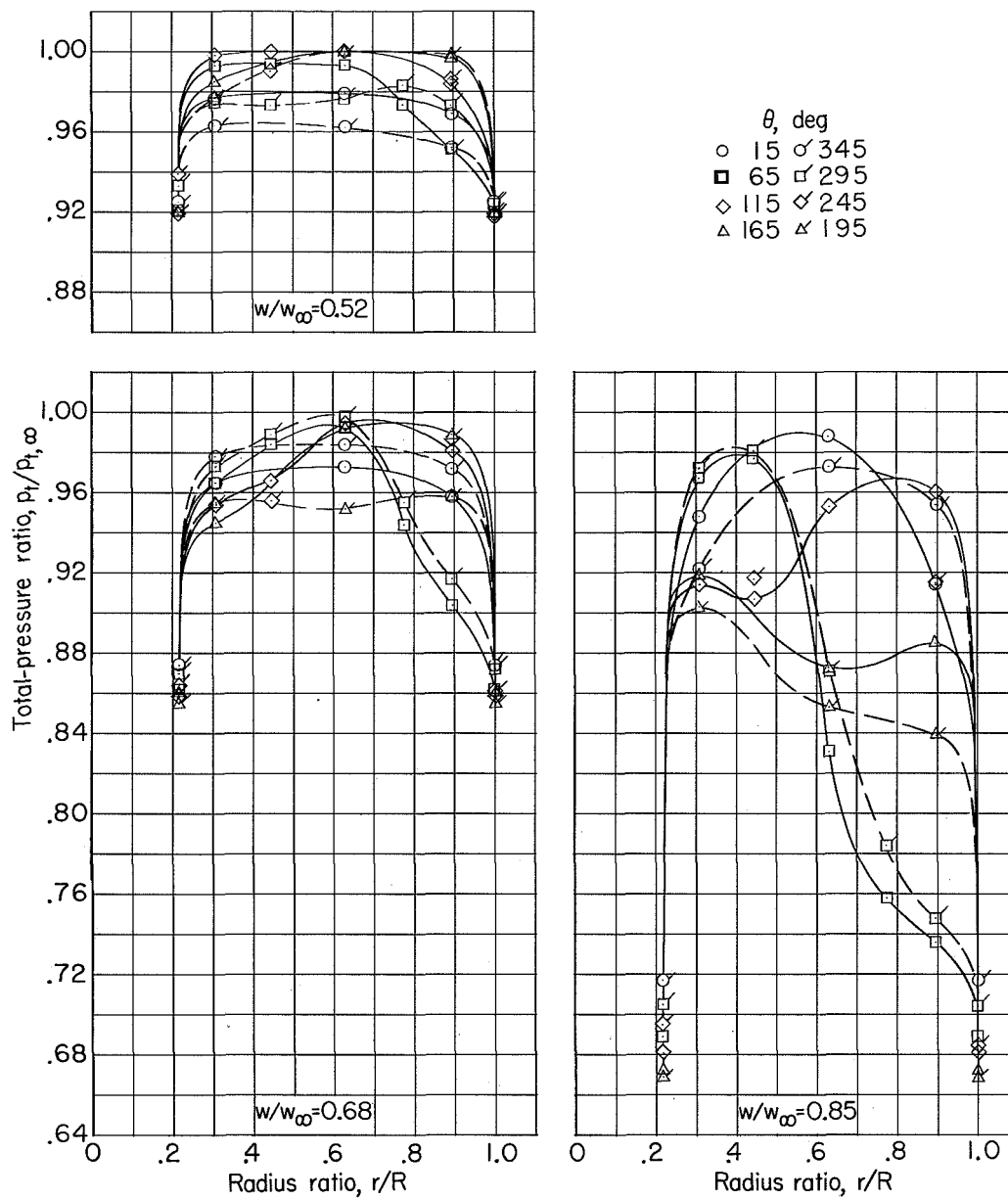
(b) Concluded.

Figure 6.- Continued.



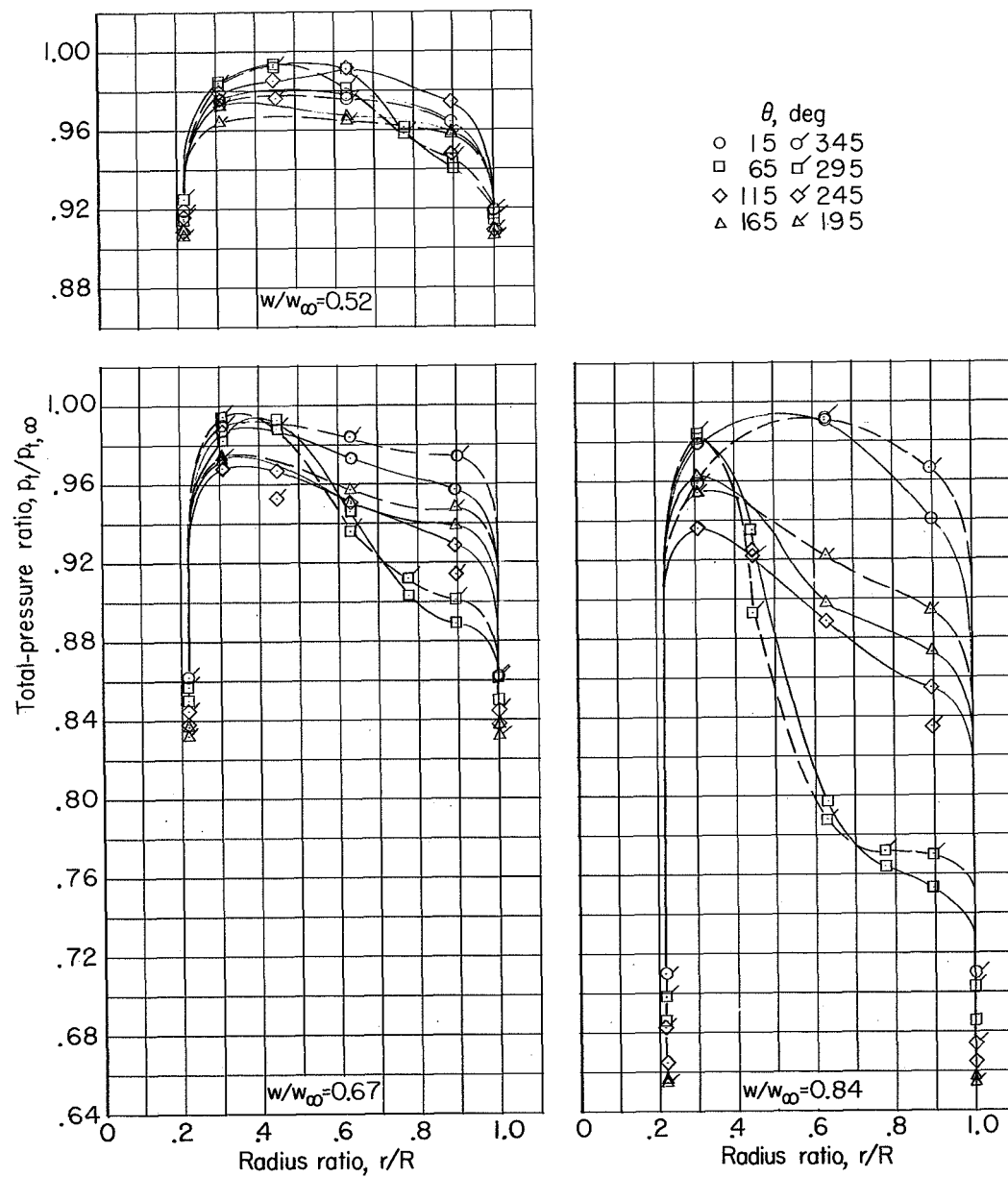
(c) $M = 0.90$; $\alpha = 4^\circ$.

Figure 6.- Continued.



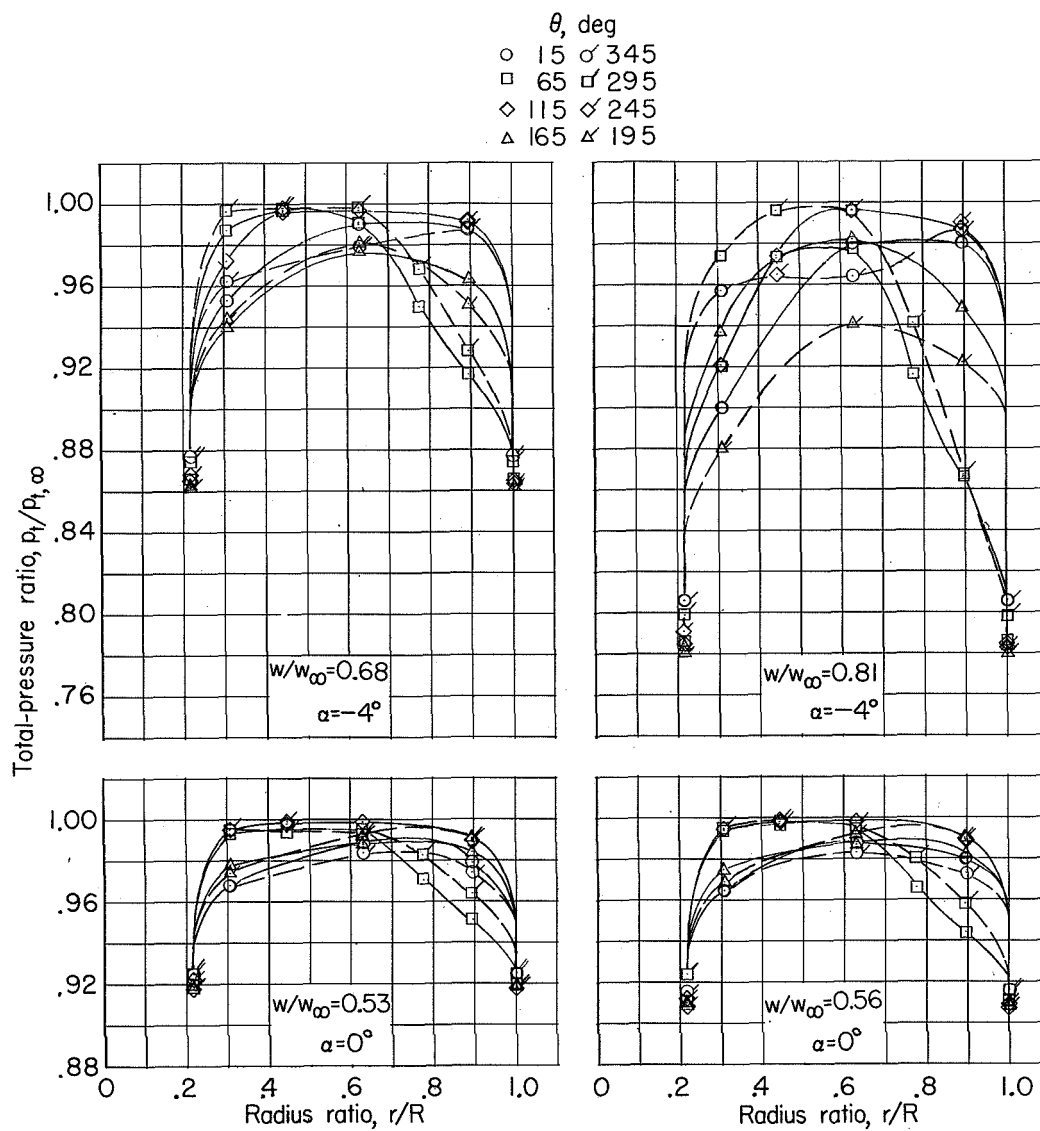
(d) $M = 0.90$; $\alpha = 7^\circ$.

Figure 6.- Continued.



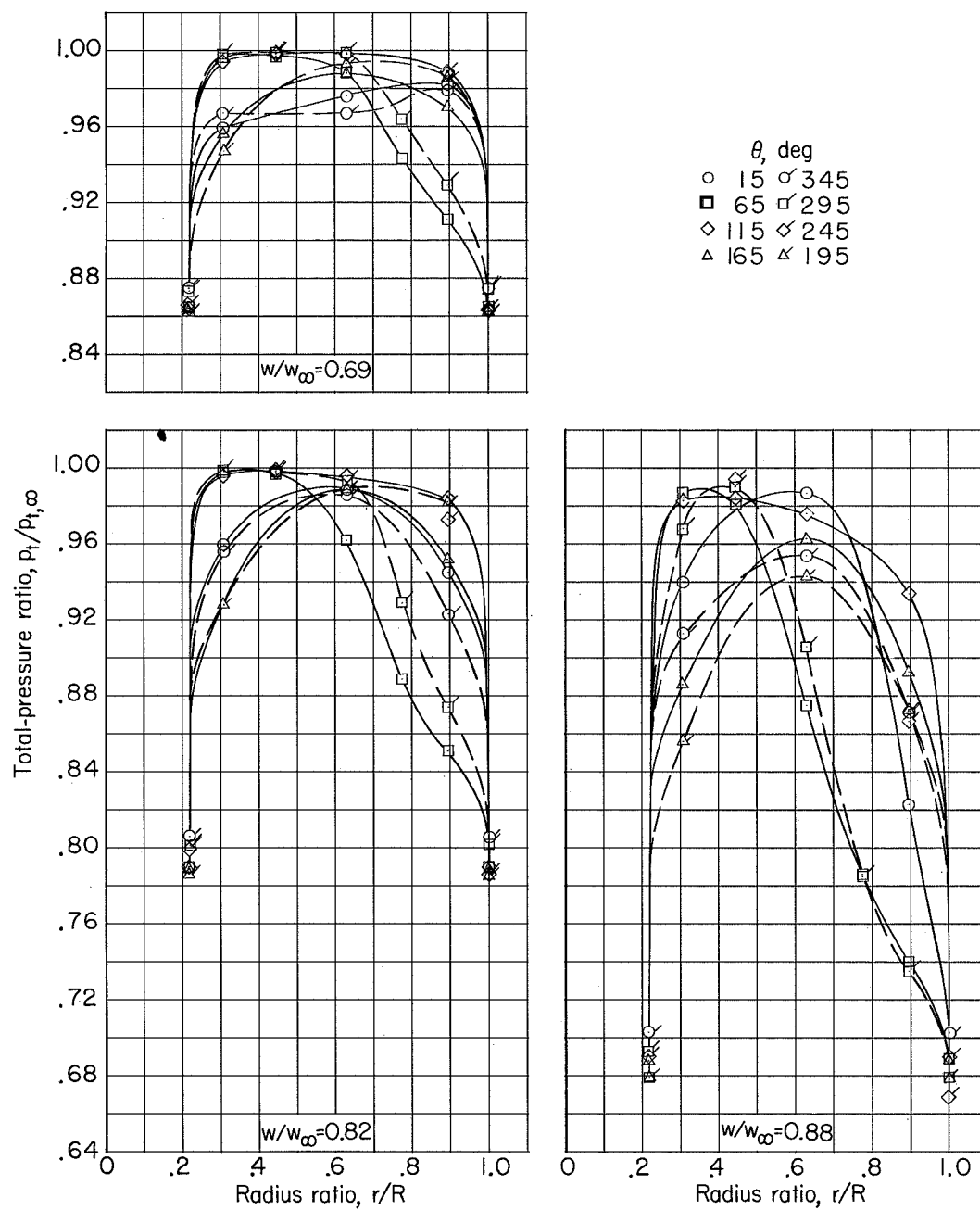
(e) $M = 0.90$; $\alpha = 10^\circ$.

Figure 6.- Continued.



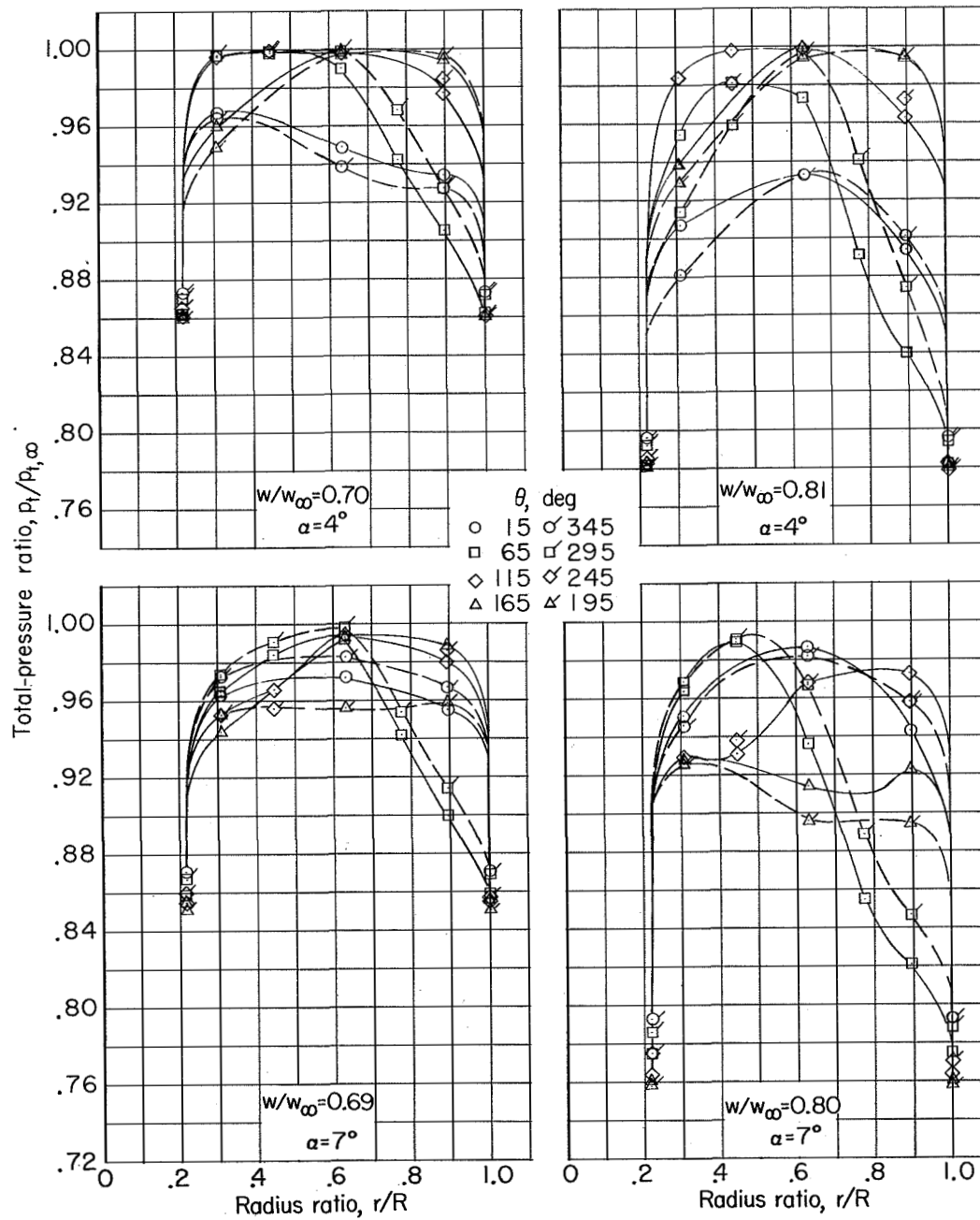
(f) $M = 0.95$; $\alpha = -4^\circ$ and 0° .

Figure 6.- Continued.



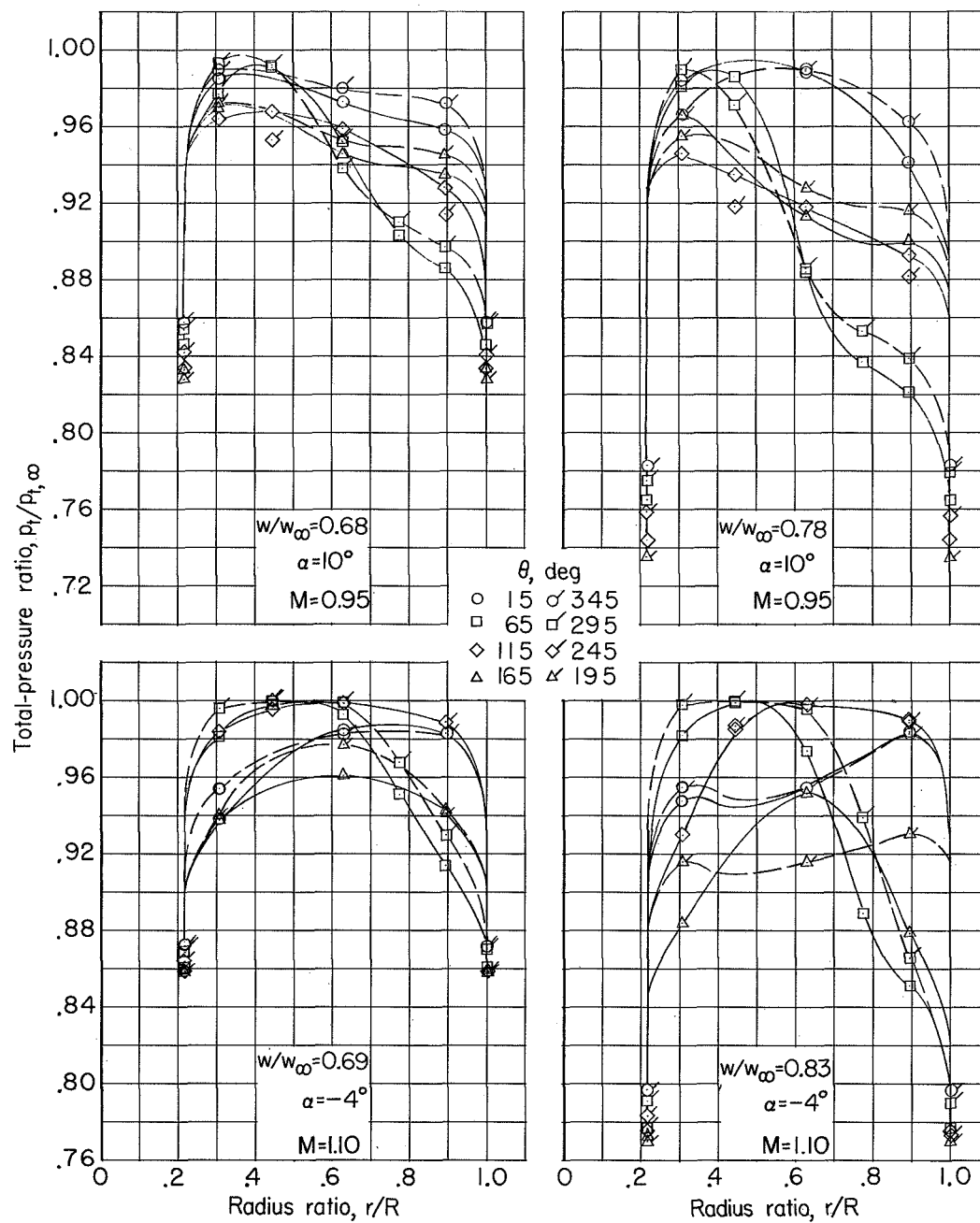
(g) $M = 0.95$; $\alpha = 0^\circ$.

Figure 6.- Continued.



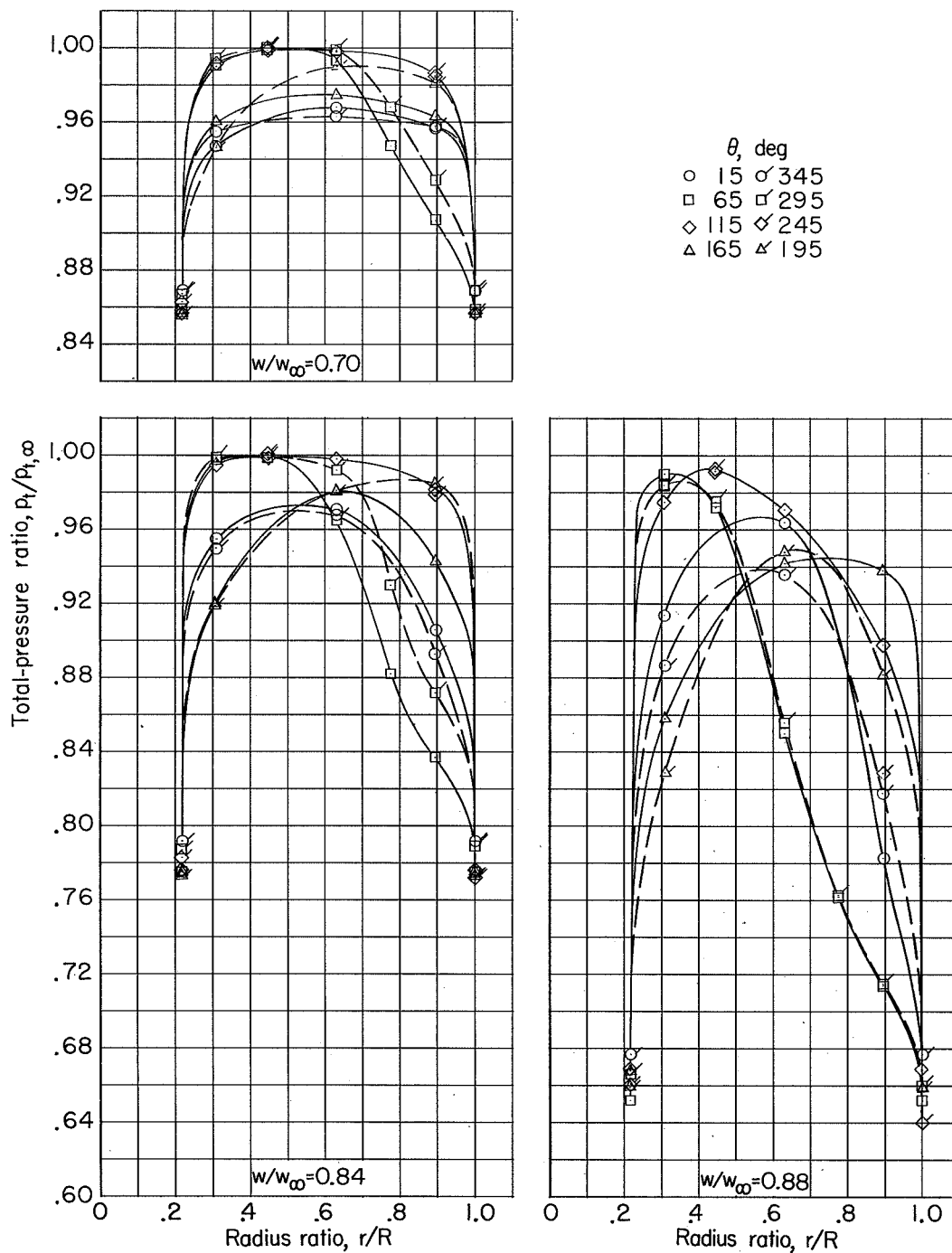
(h) $M = 0.95$; $\alpha = 4^\circ$ and 7° .

Figure 6.- Continued.



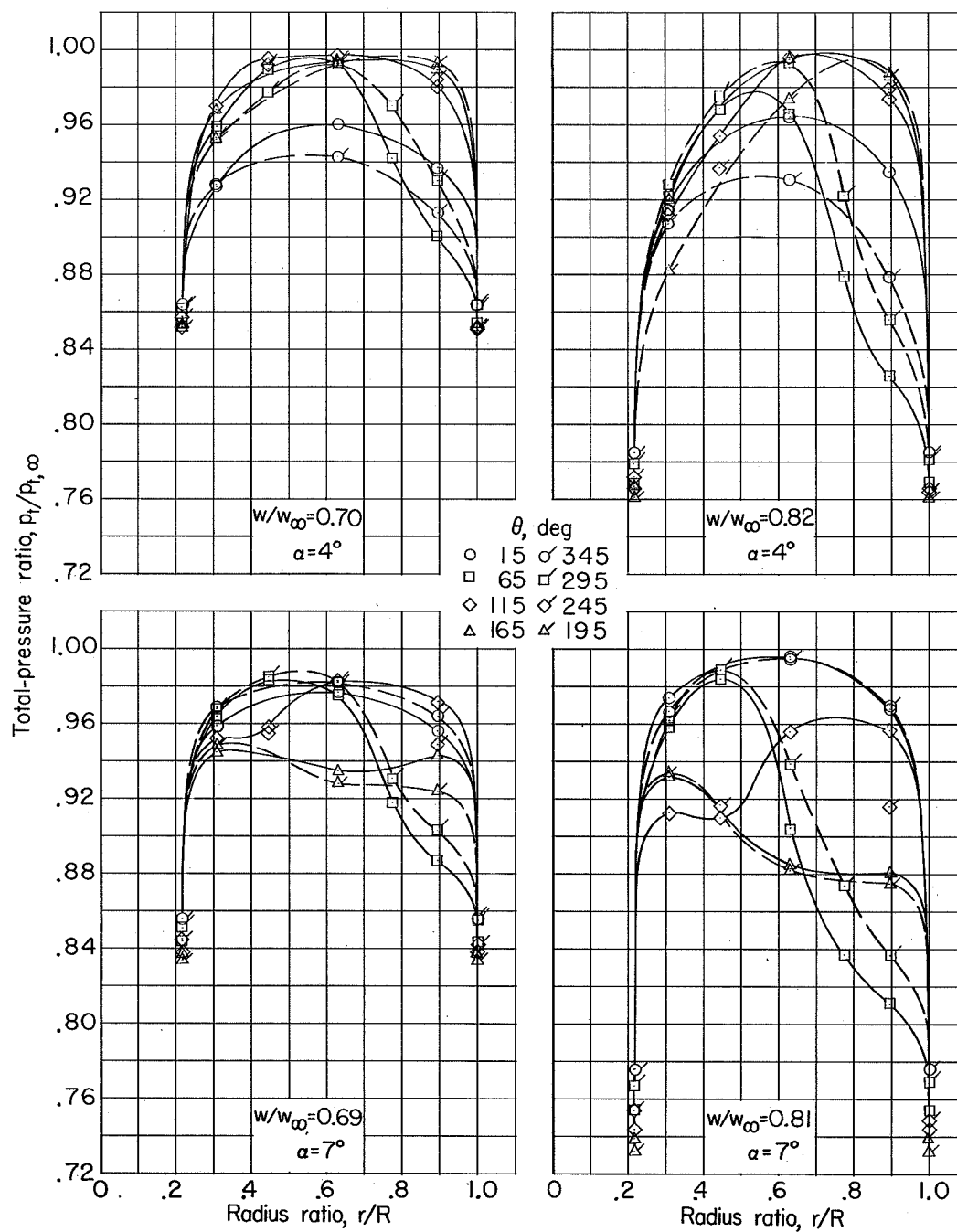
(i) $M = 0.95$ and 1.10 ; $\alpha = 10^\circ$ and -4° .

Figure 6.- Continued.



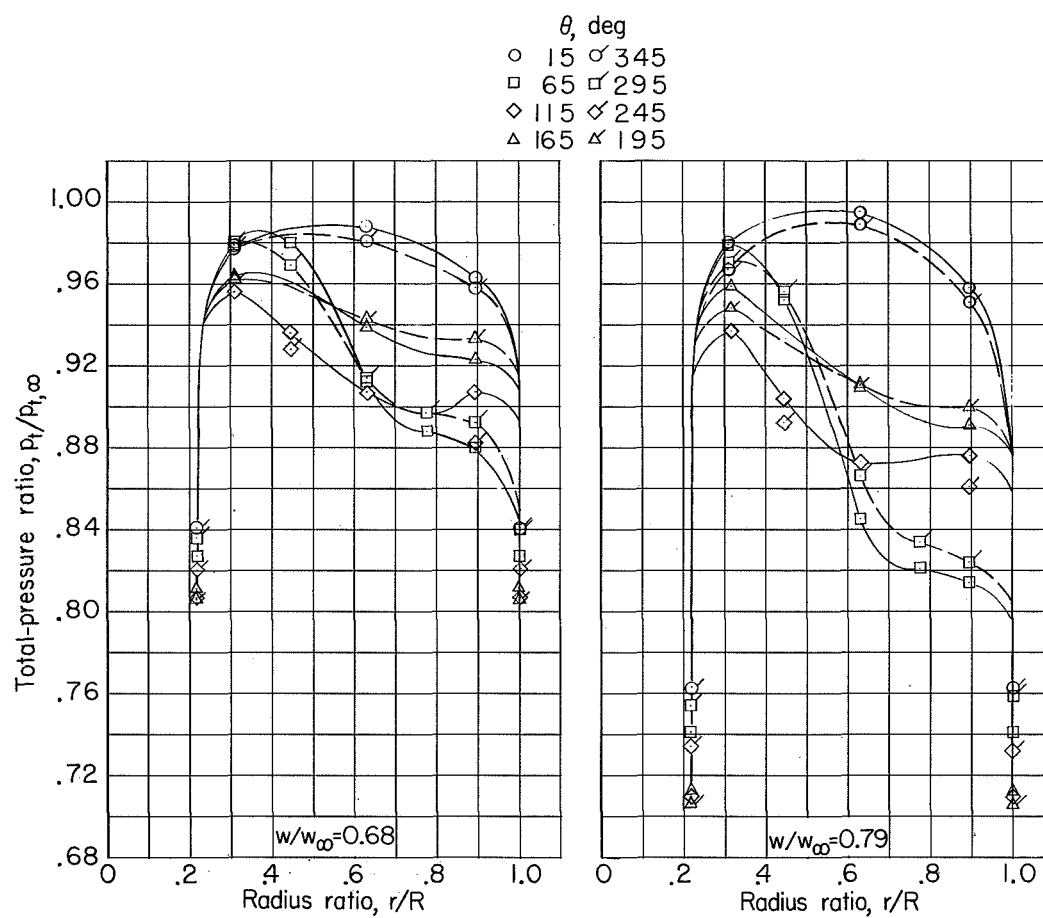
(j) $M = 1.10$; $\alpha = 0^\circ$.

Figure 6.- Continued.



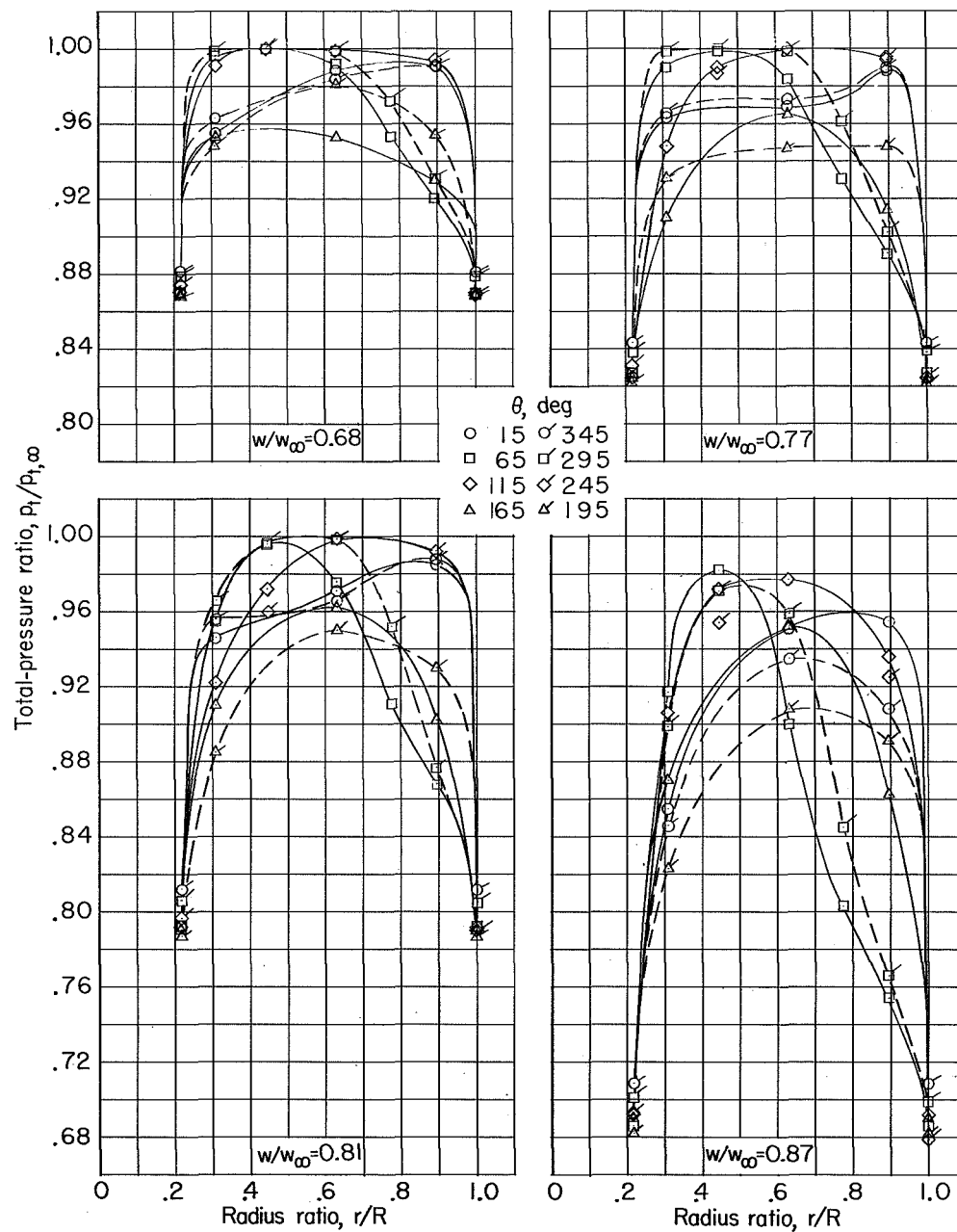
(k) $M = 1.10$; $\alpha = 4^\circ$ and 7° .

Figure 6.- Continued.



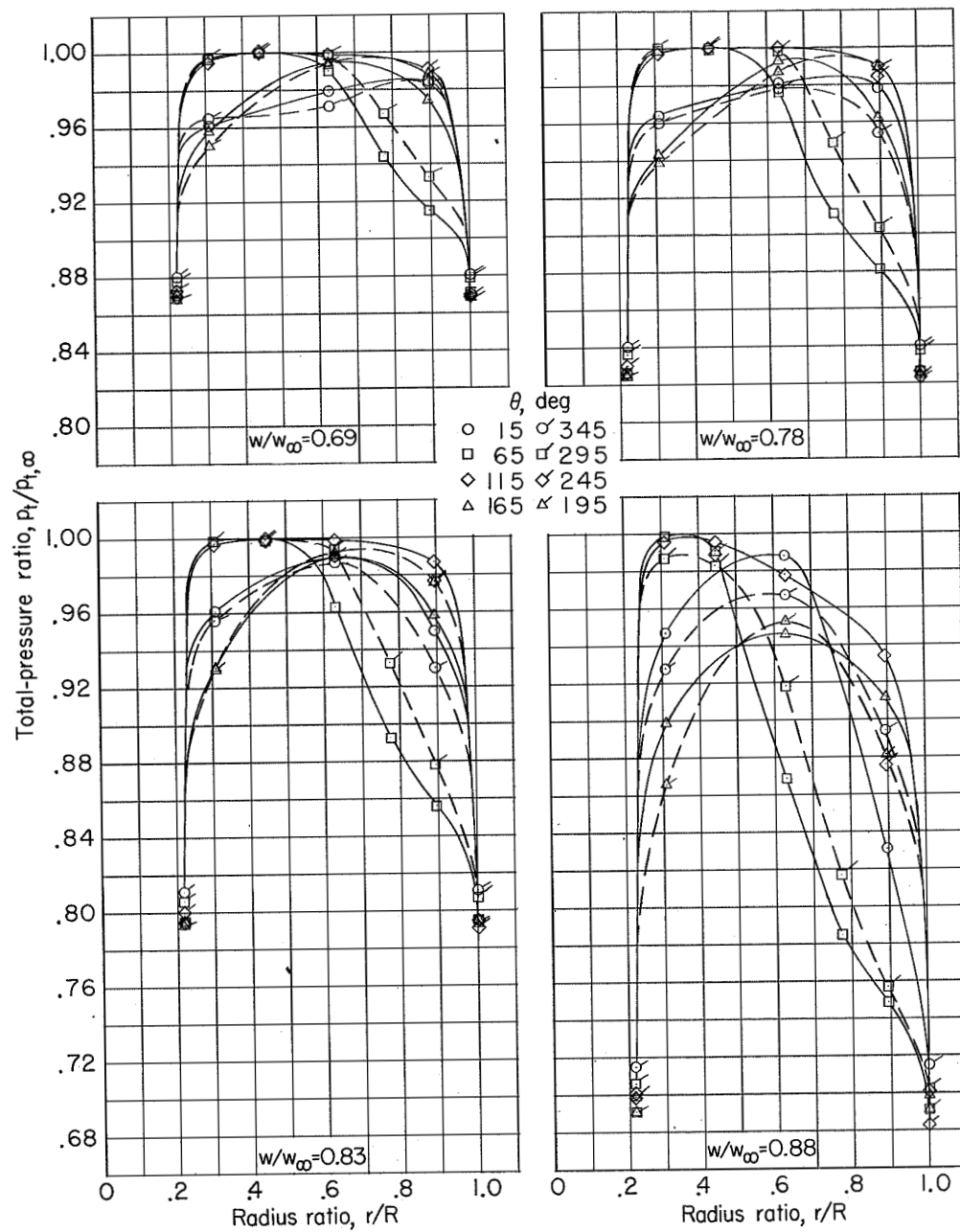
(1) $M = 1.10$; $\alpha = 10^\circ$.

Figure 6.- Concluded.



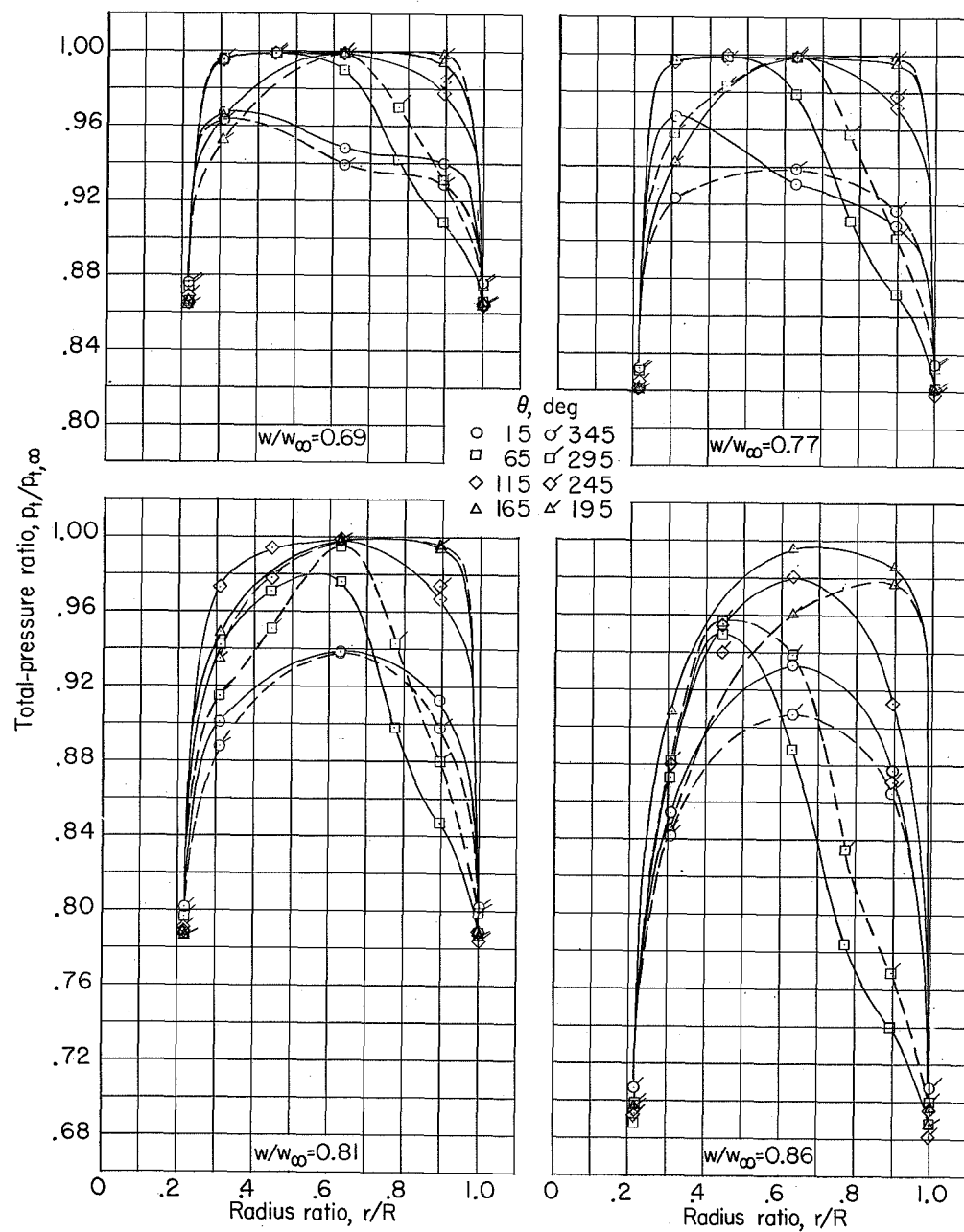
(a) $M = 0.90$; $\alpha = -4^\circ$.

Figure 7.- Radial variation of total-pressure ratio at various angles of attack, mass-flow ratios, and Mach numbers. Basic configuration with transition strip on fuselage. $\beta = 0^\circ$.



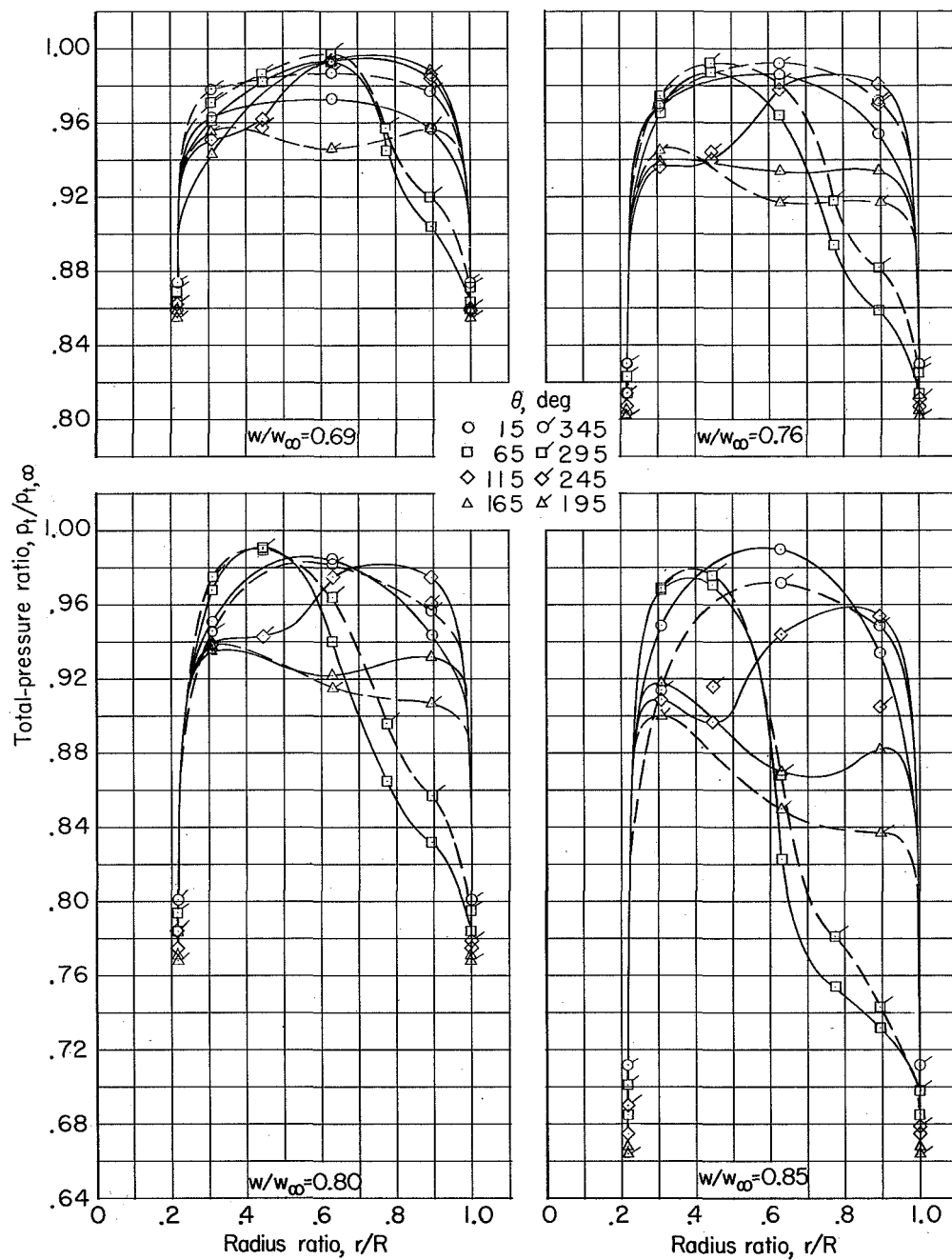
(b) $M = 0.90$; $\alpha = 0^\circ$.

Figure 7.- Continued.



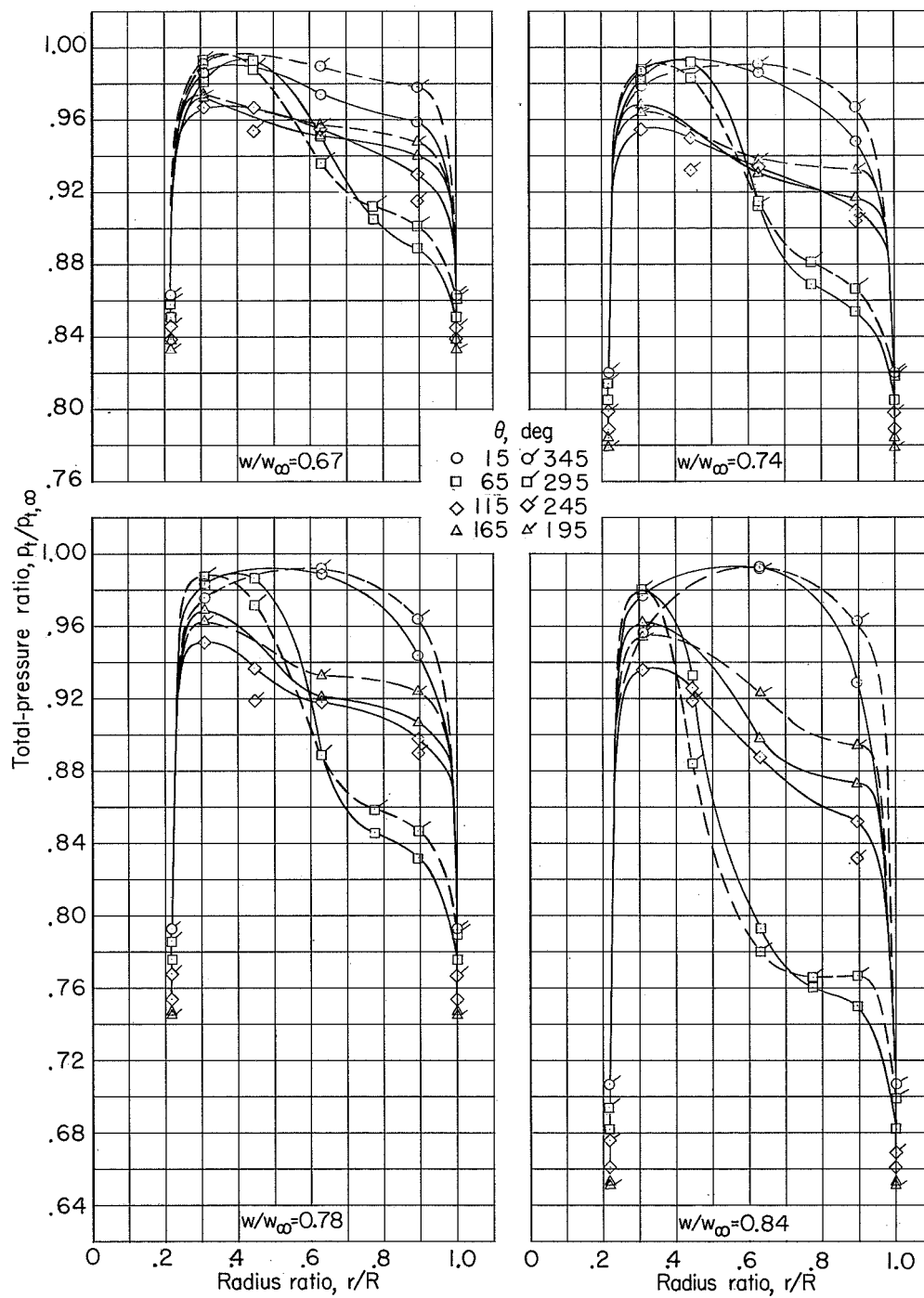
(c) $M = 0.90$; $\alpha = 4^\circ$.

Figure 7.- Continued.



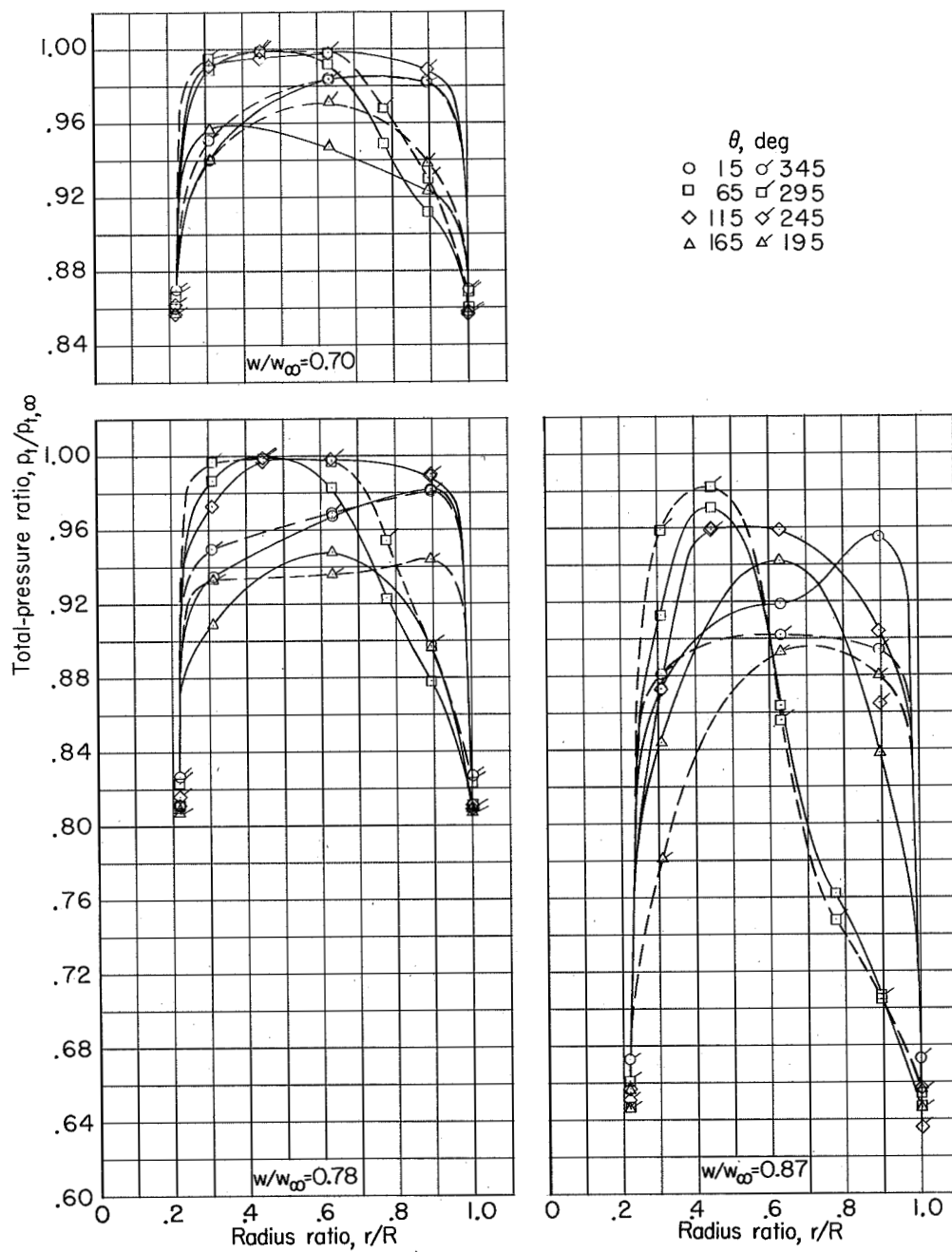
(d) $M = 0.90$; $\alpha = 7^\circ$.

Figure 7.- Continued.



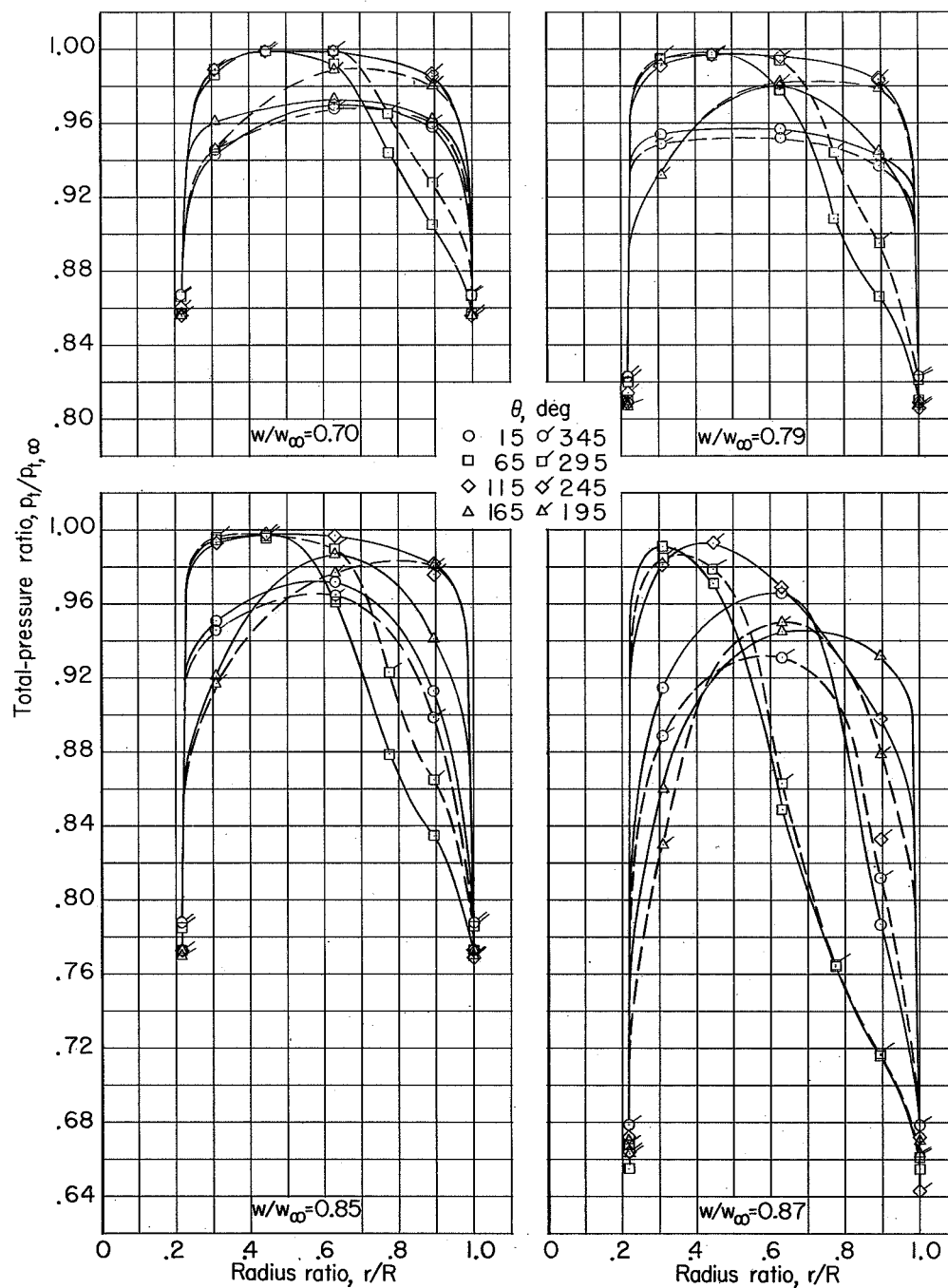
(e) $M = 0.90$; $\alpha = 10^\circ$.

Figure 7.- Continued.



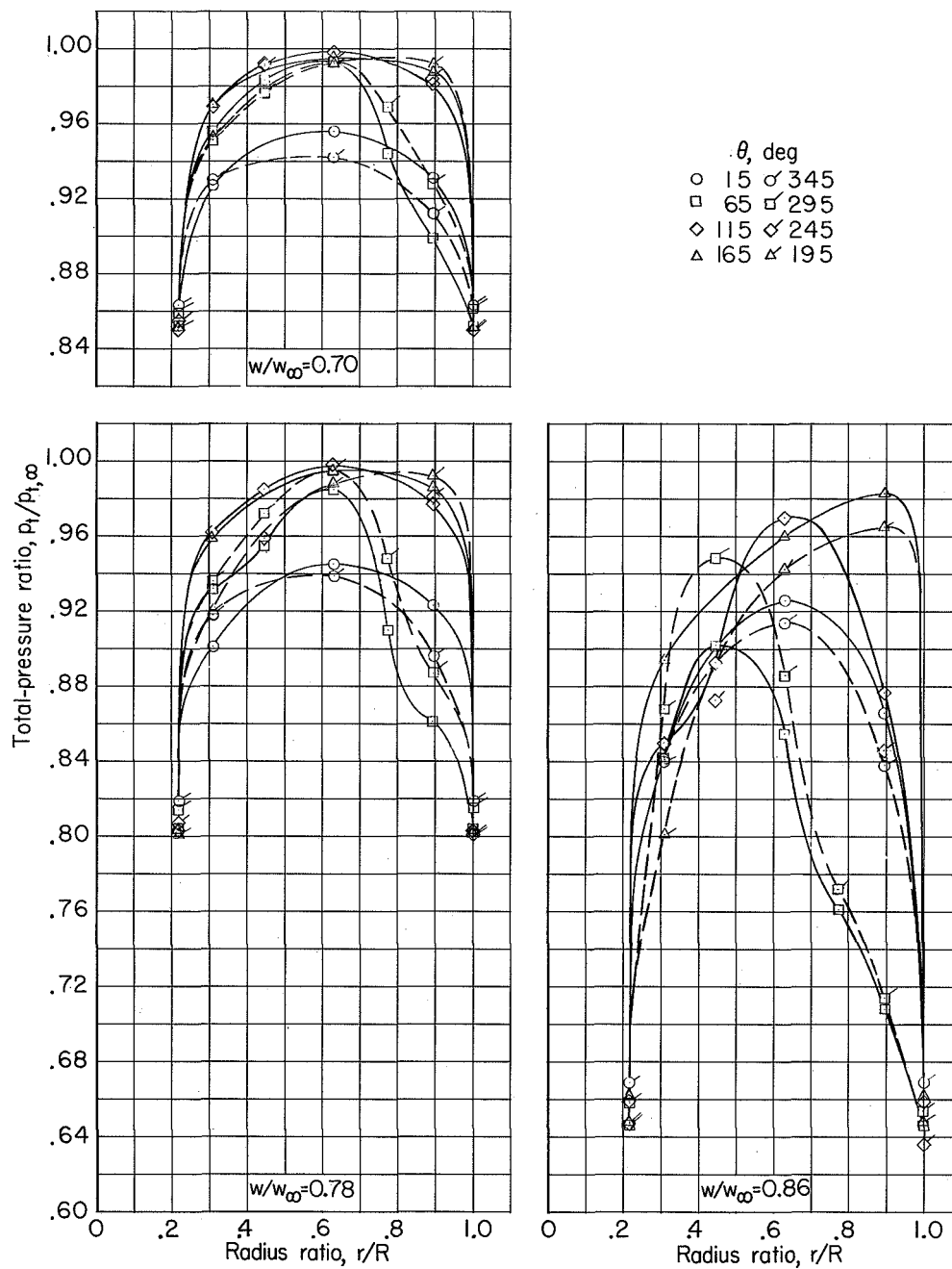
(f) $M = 1.10$; $\alpha = -4^\circ$.

Figure 7.- Continued.



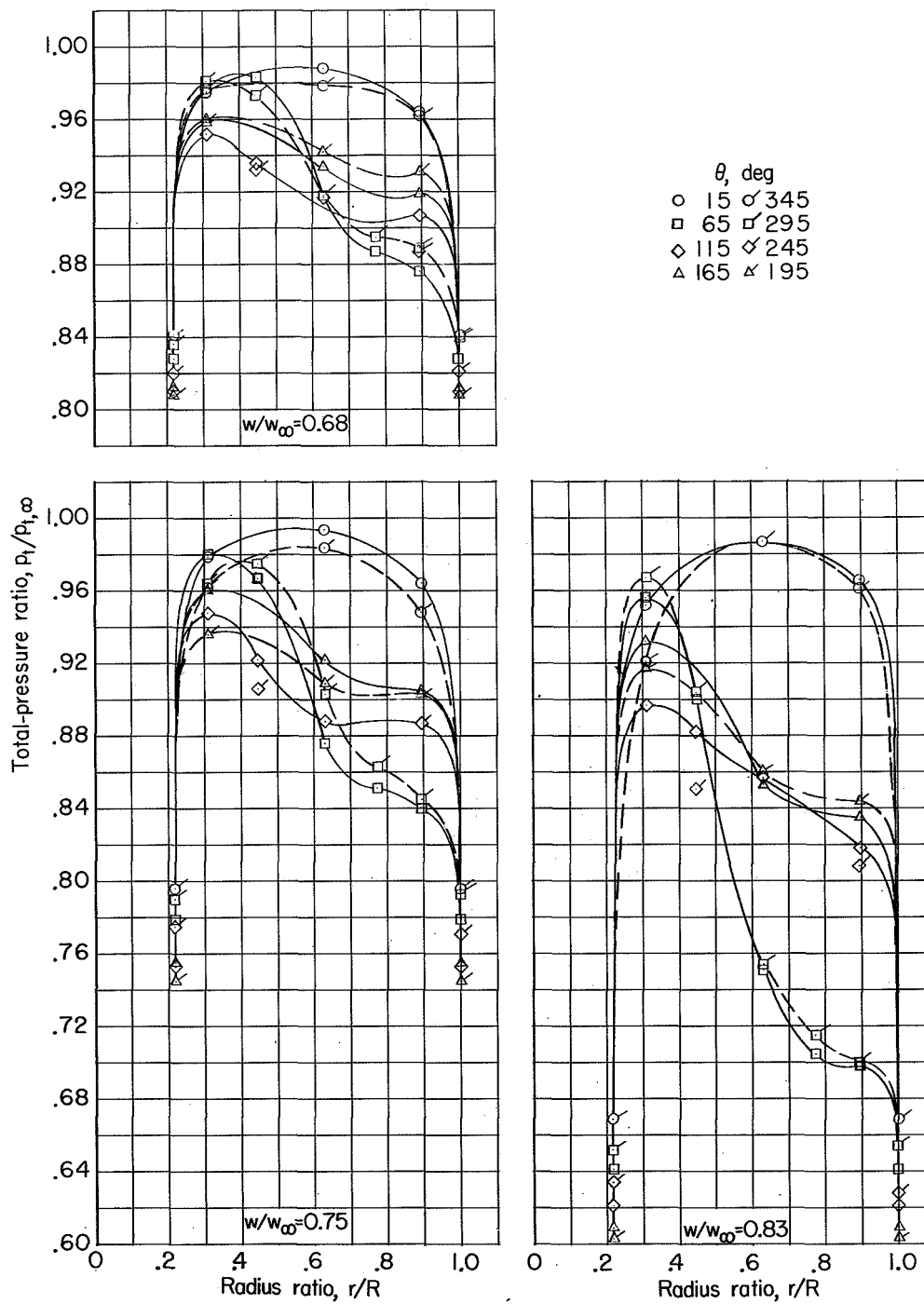
(g) $M = 1.10$; $\alpha = 0^\circ$.

Figure 7.- Continued.



(h) $M = 1.10$; $\alpha = 4^\circ$.

Figure 7.- Continued.



(i) $M = 1.10$; $\alpha = 10^\circ$.

Figure 7.- Concluded.

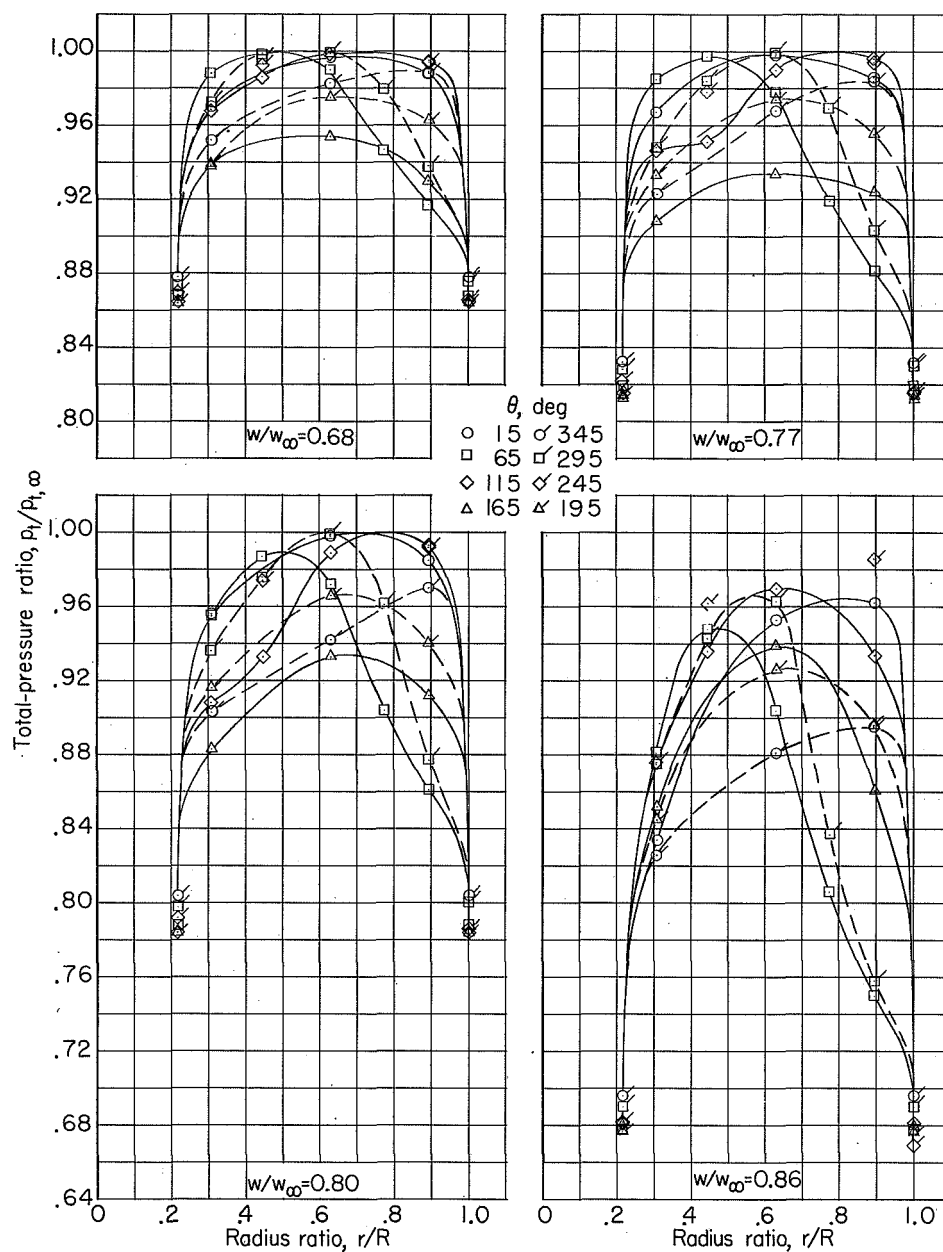
(a) $M = 0.90; \alpha = -4^\circ$.

Figure 8.- Radial variation of total-pressure ratio at various angles of attack, mass-flow ratios, and Mach numbers. Basic configuration. $\beta = -5.2^\circ$.

L-200

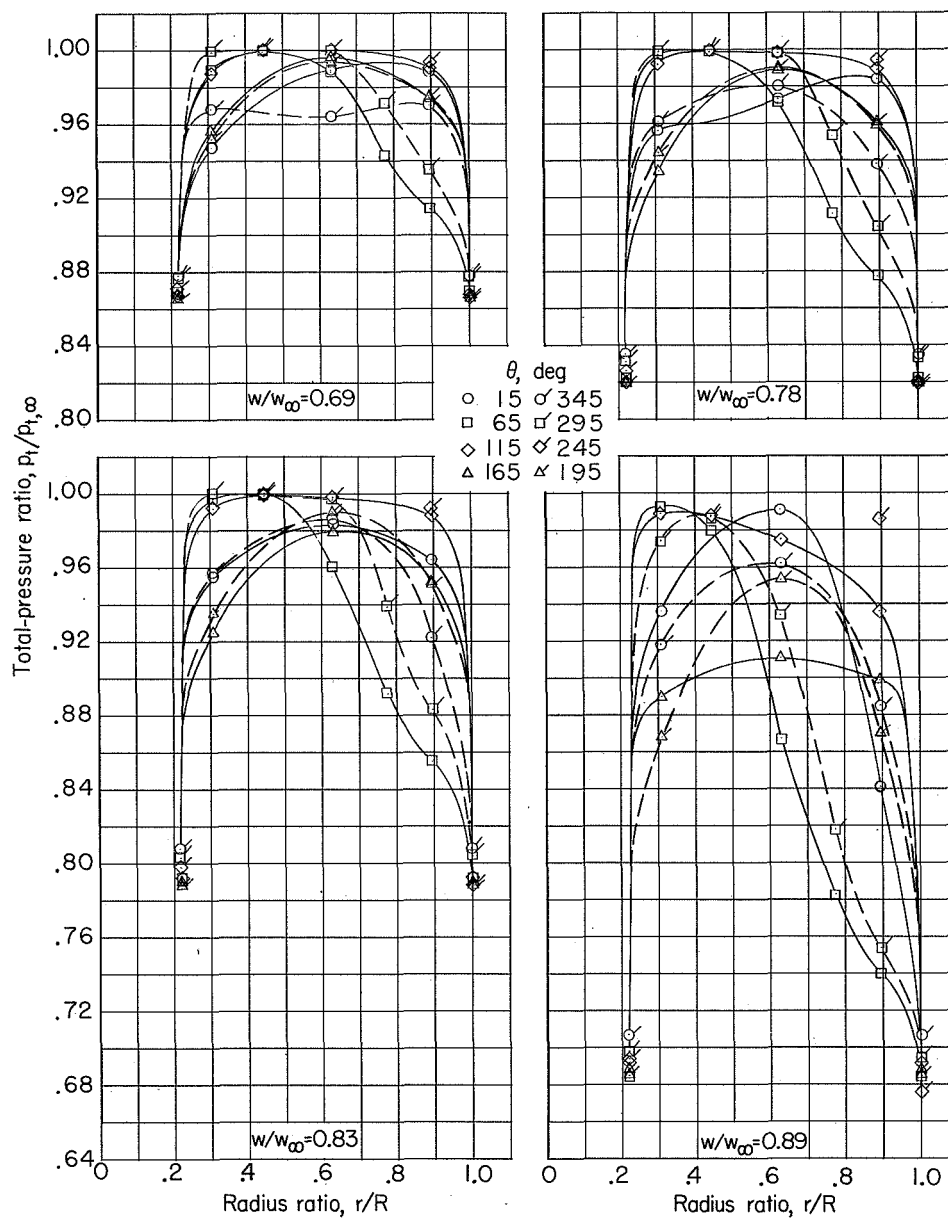
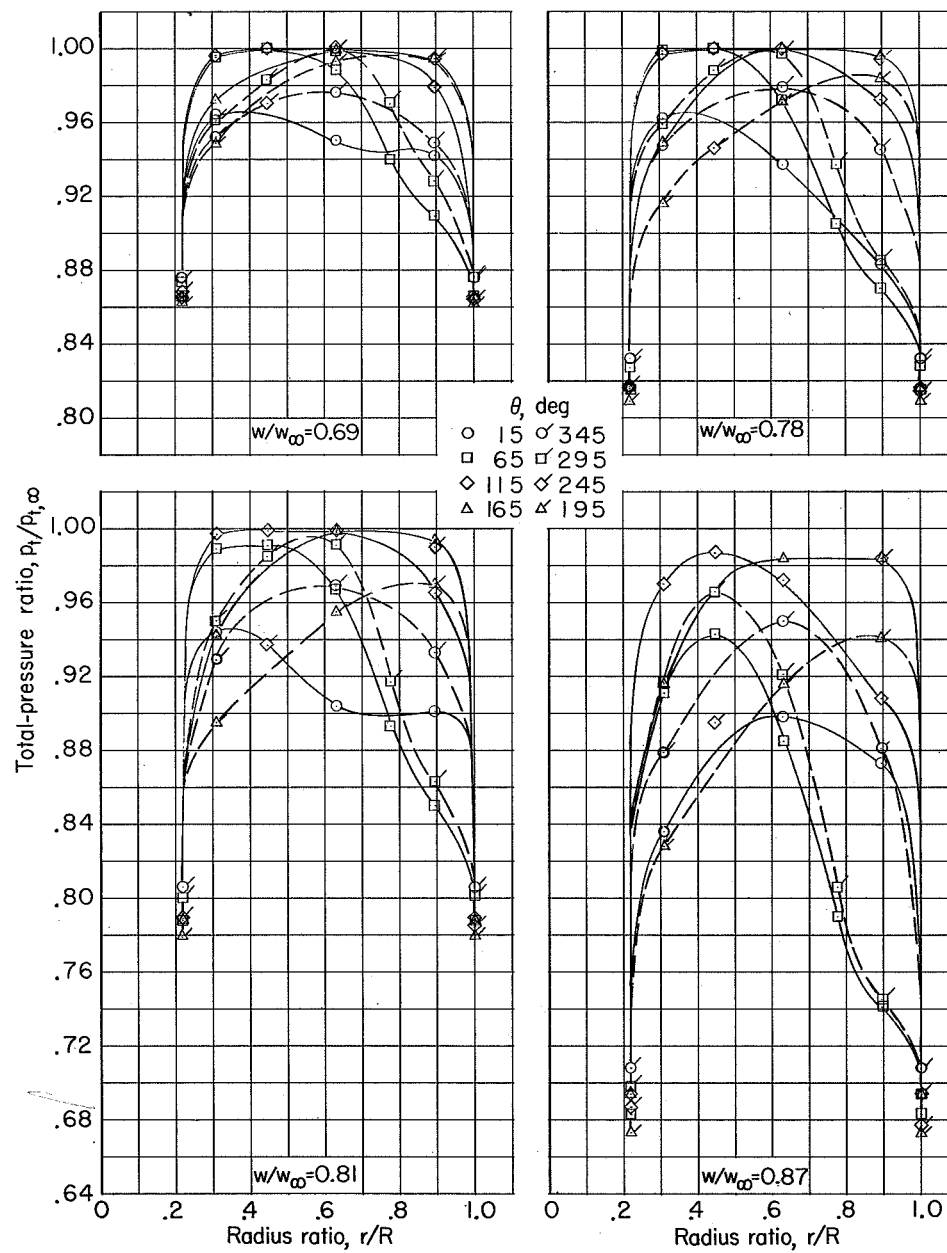
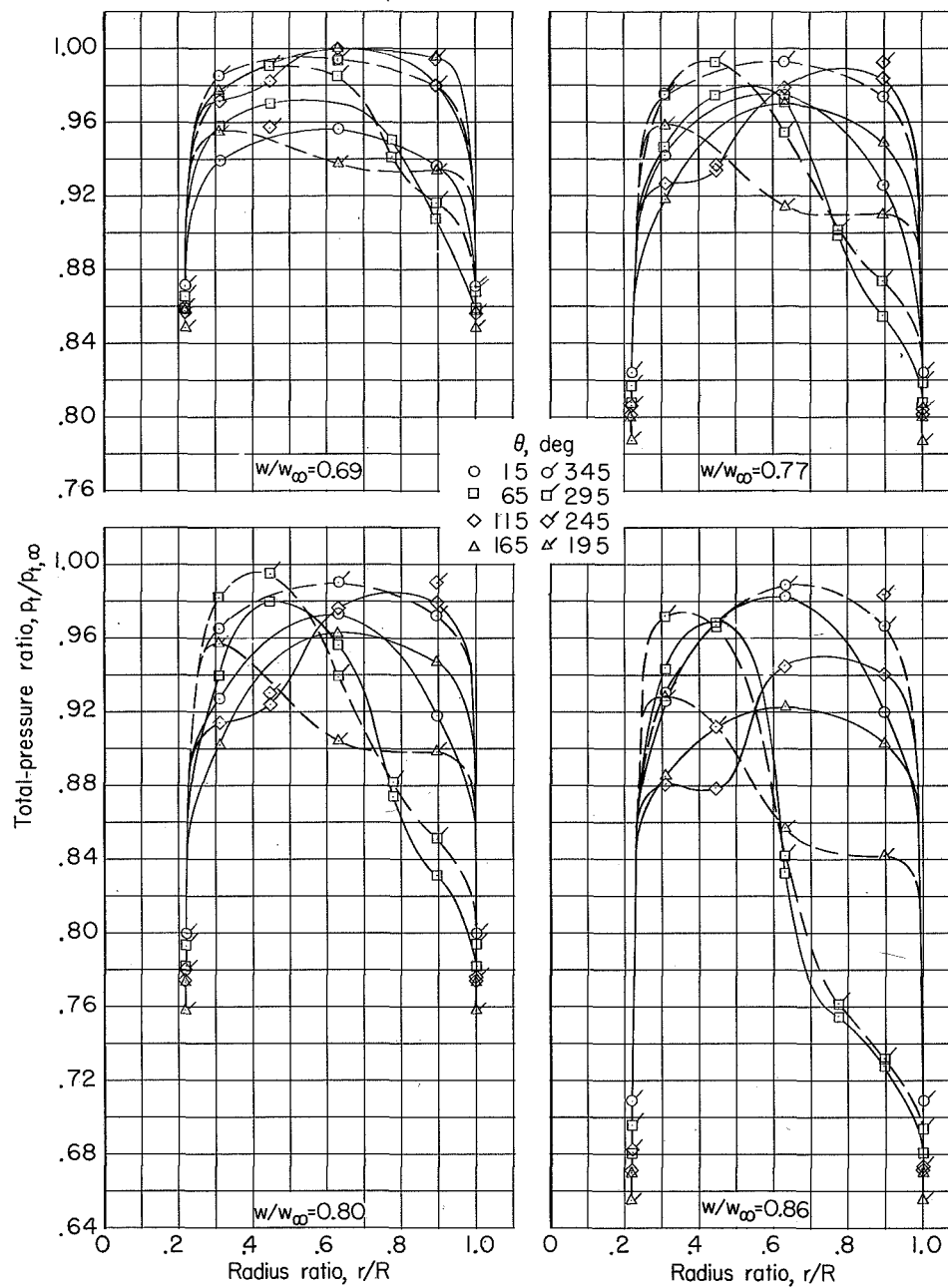
(b) $M = 0.90$; $\alpha = 0^\circ$.

Figure 8.- Continued.



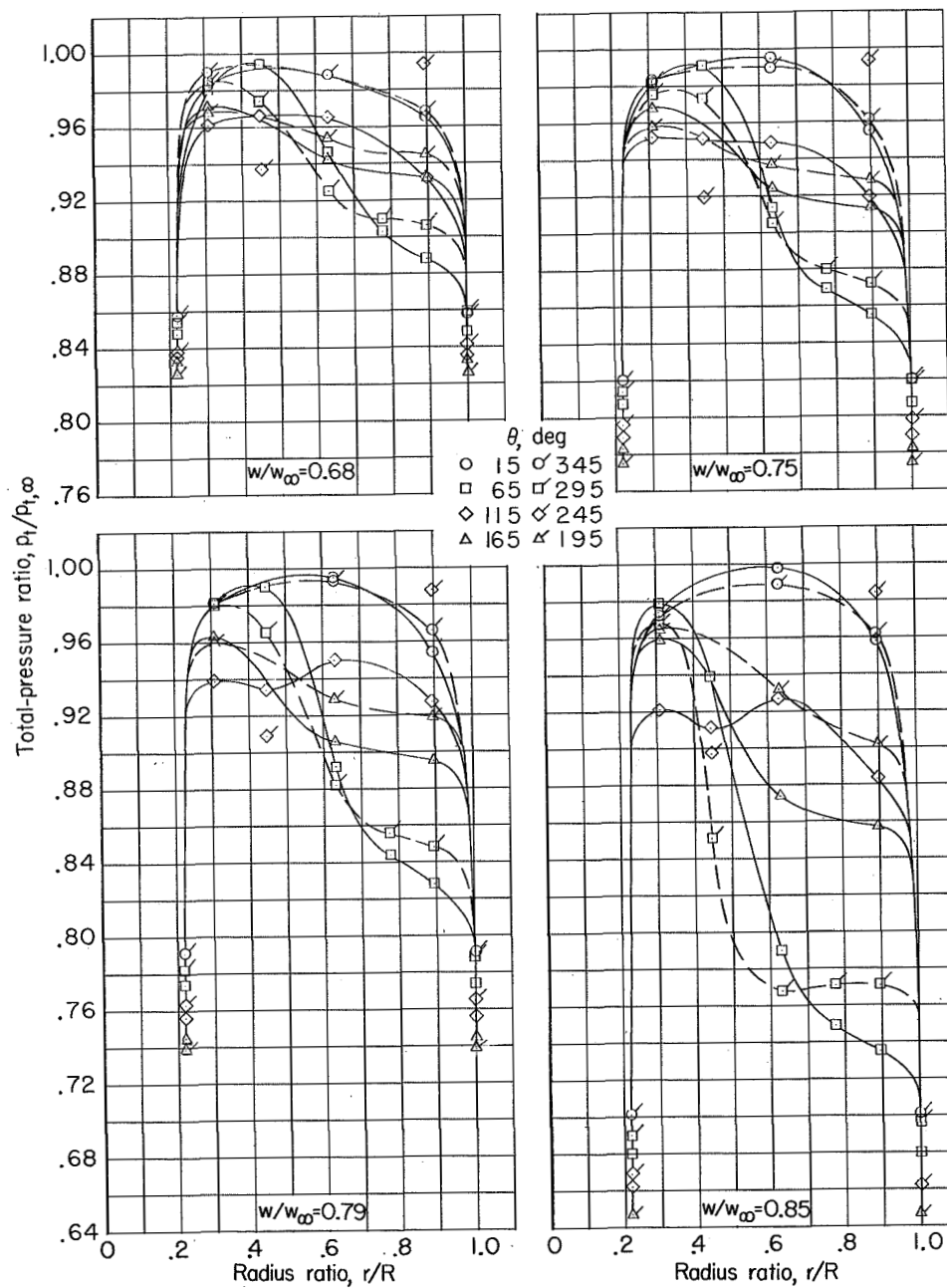
(c) $M = 0.90$; $\alpha = 4^\circ$.

Figure 8.- Continued.



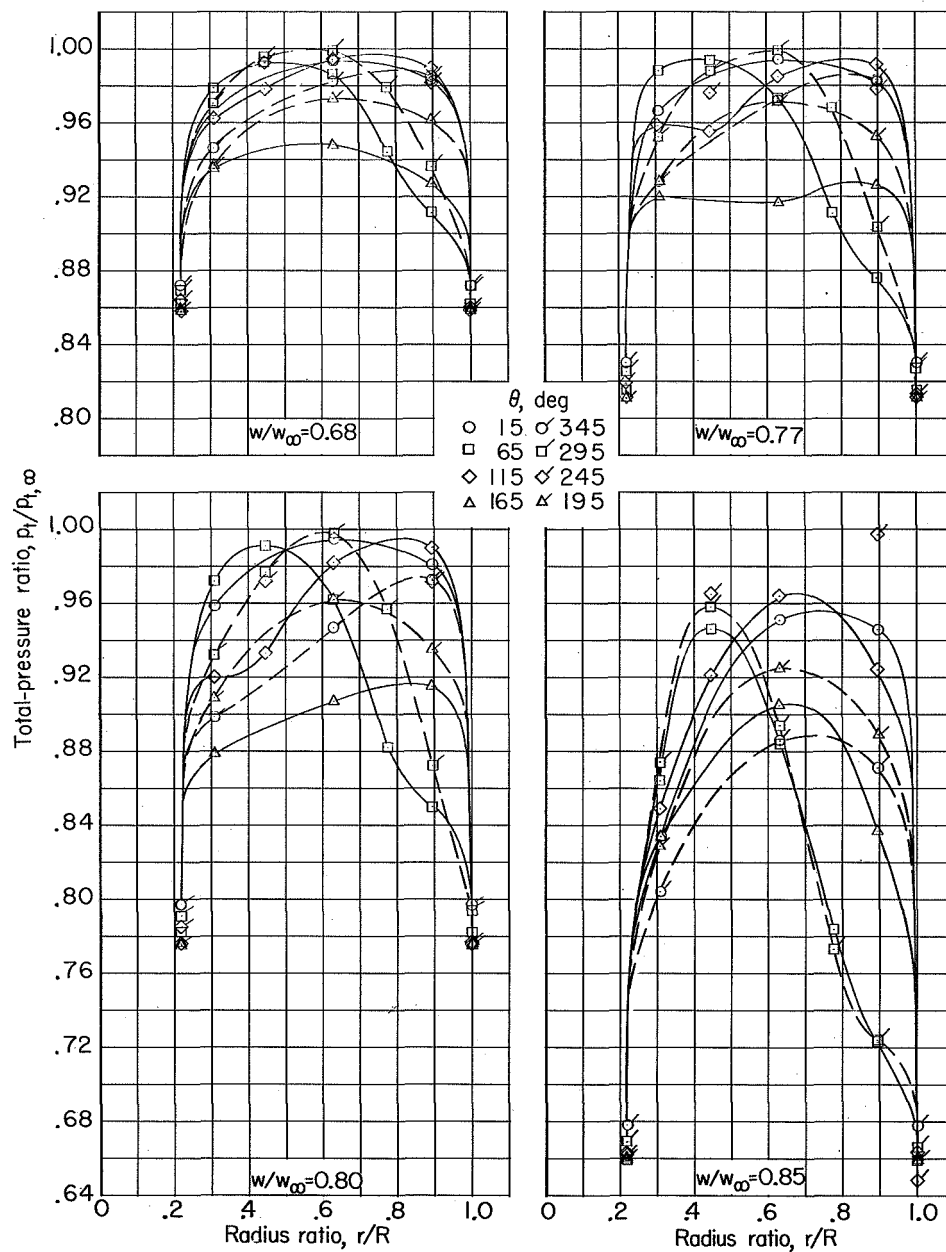
(d) $M = 0.90$; $\alpha = 7^\circ$.

Figure 8.- Continued.



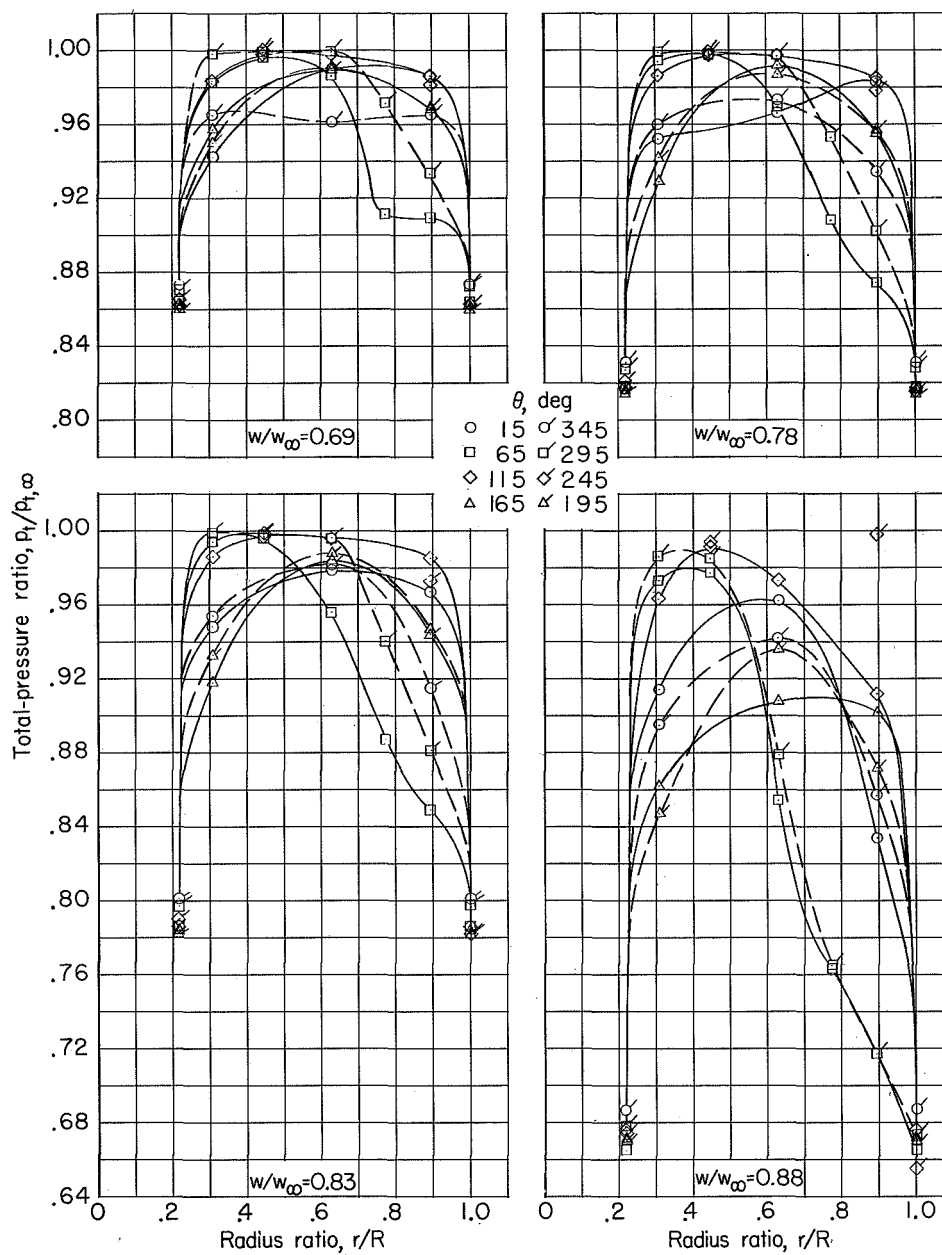
(e) $M = 0.90$; $\alpha = 10^\circ$.

Figure 8.- Continued.



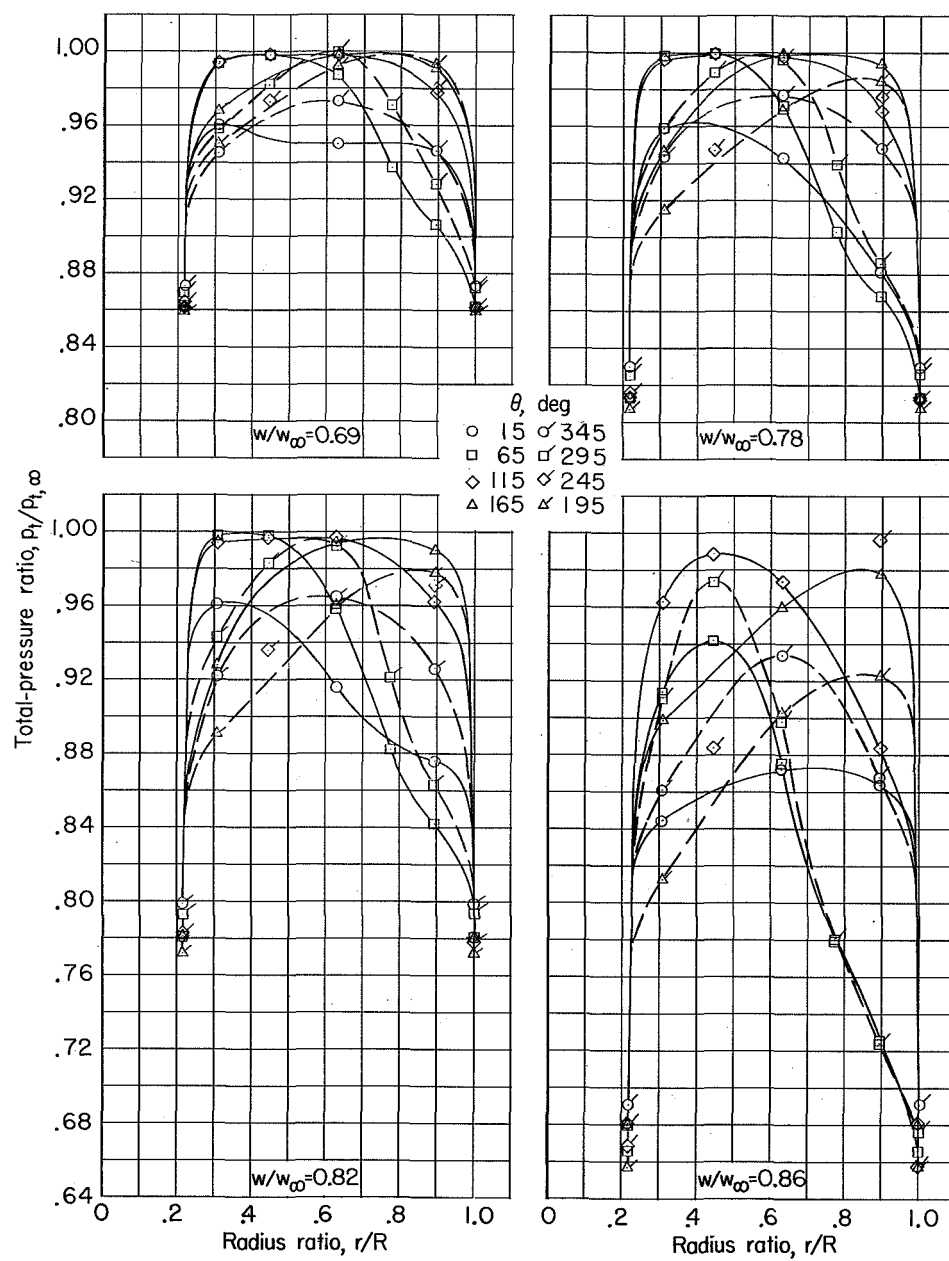
(f) $M = 0.95$; $\alpha = -4^\circ$.

Figure 8.- Continued.



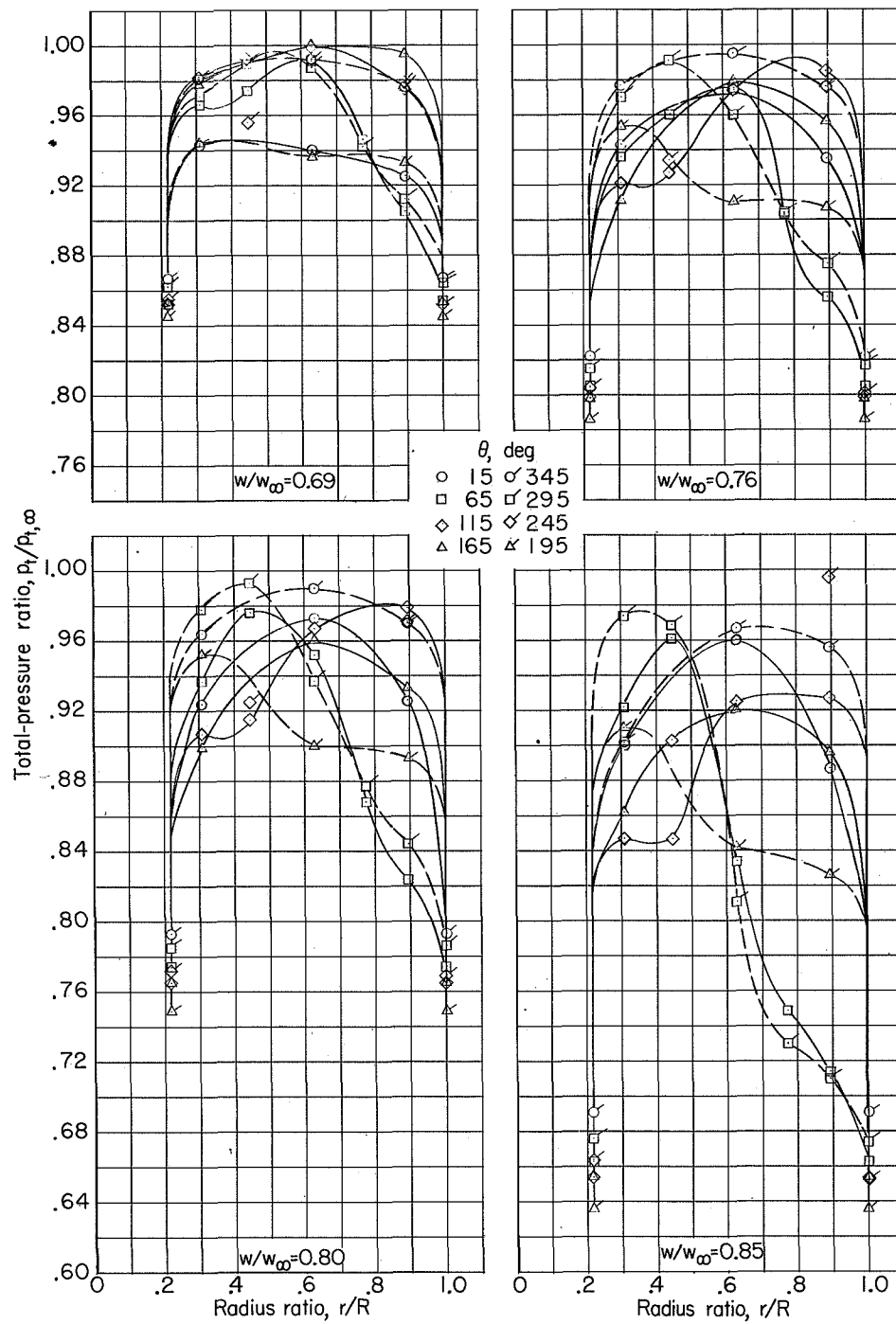
(g) $M = 0.95$; $\alpha = 0^\circ$.

Figure 8.- Continued.



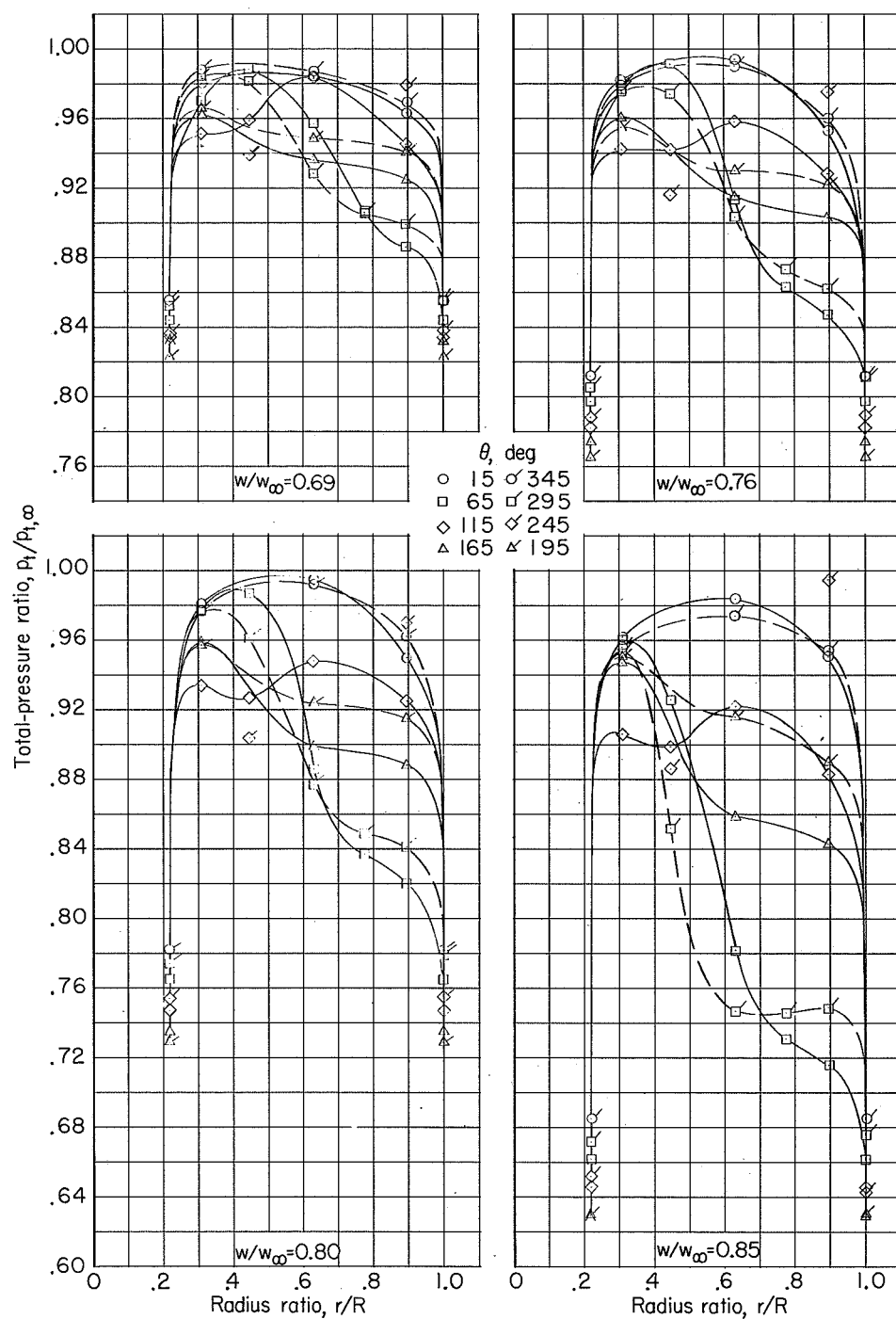
(h) $M = 0.95$; $\alpha = 4^\circ$.

Figure 8.- Continued.



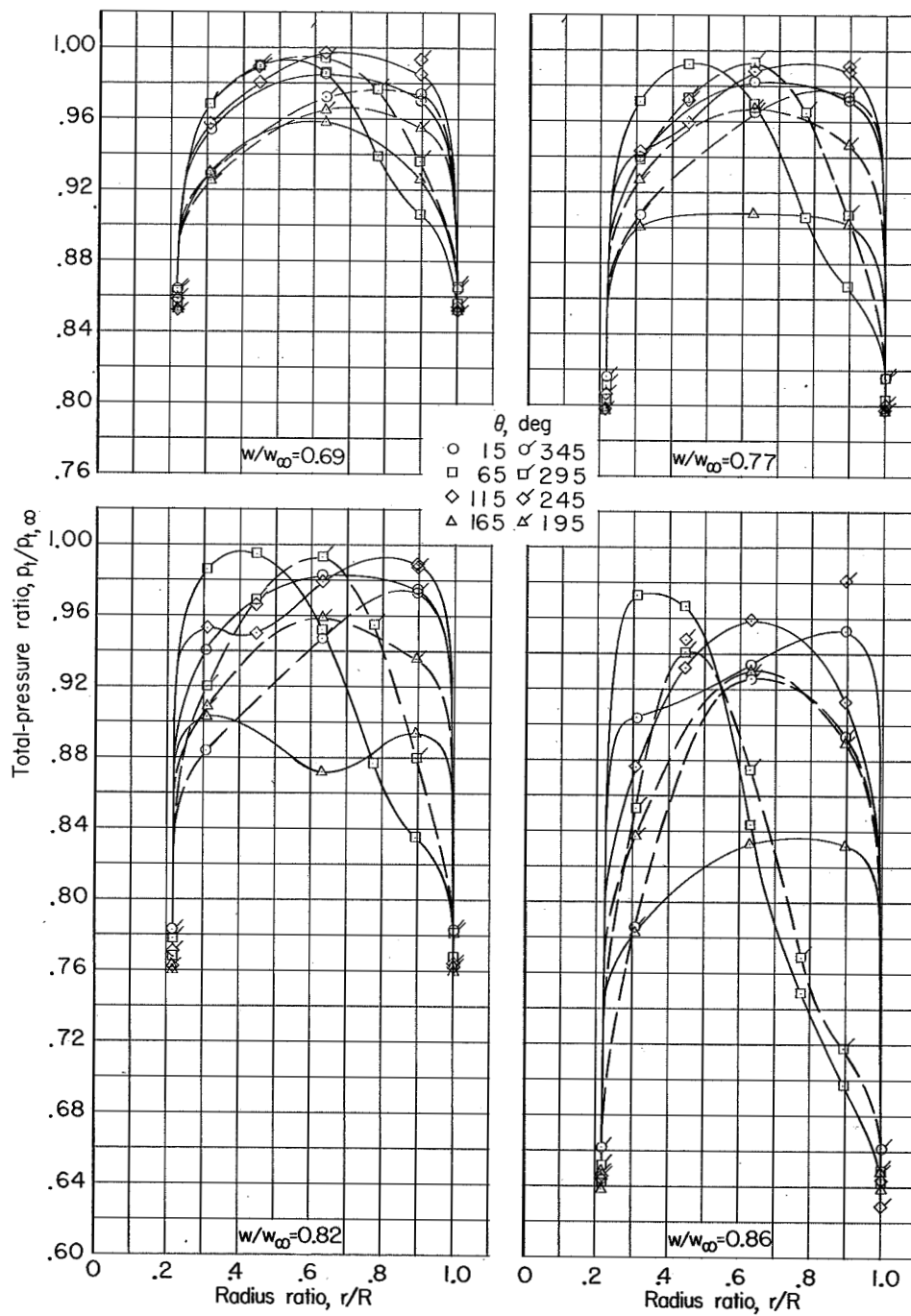
(i) $M = 0.95$; $\alpha = 7^\circ$.

Figure 8.- Continued.



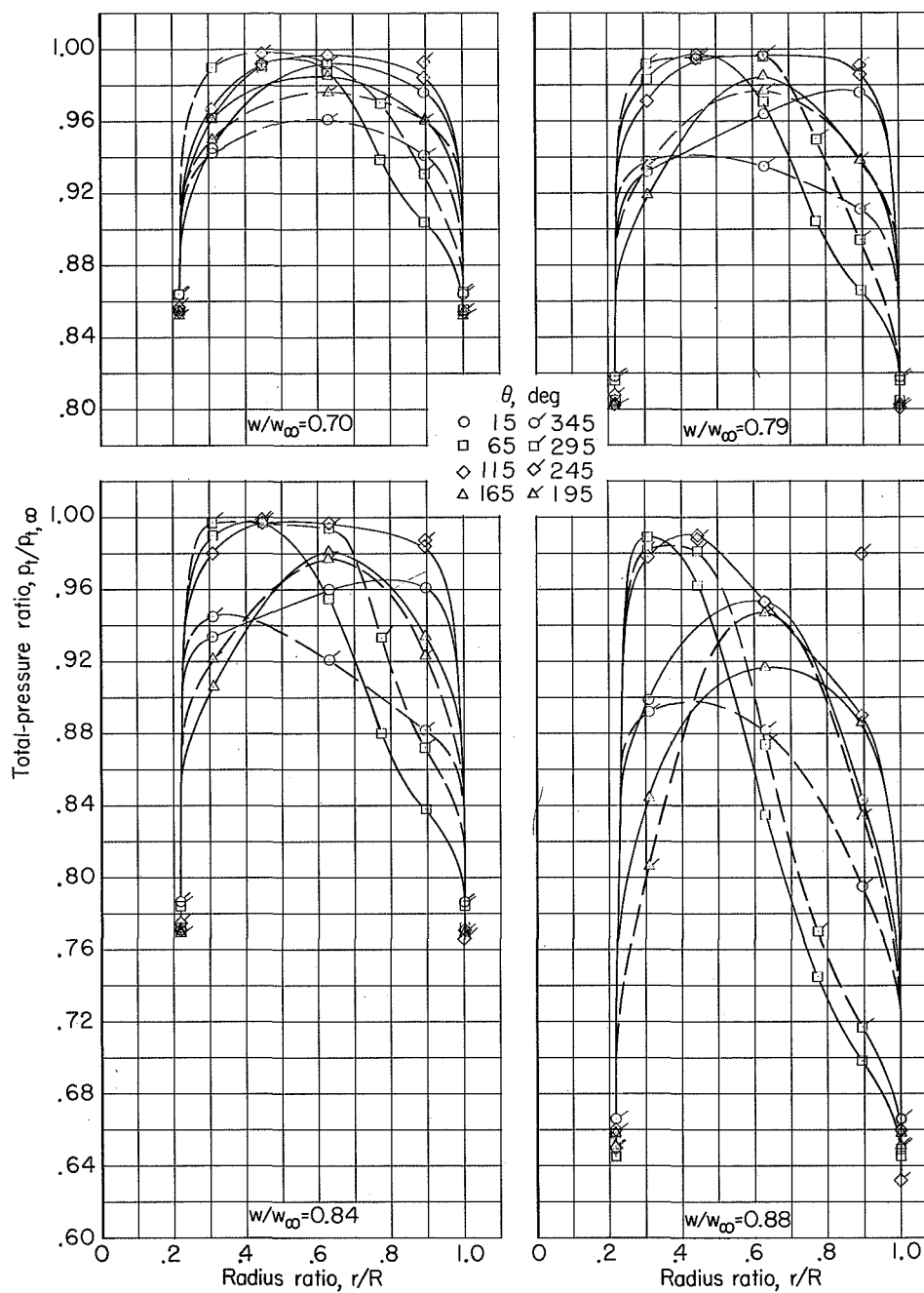
(j) $M = 0.95$; $\alpha = 10^\circ$.

Figure 8.- Continued.



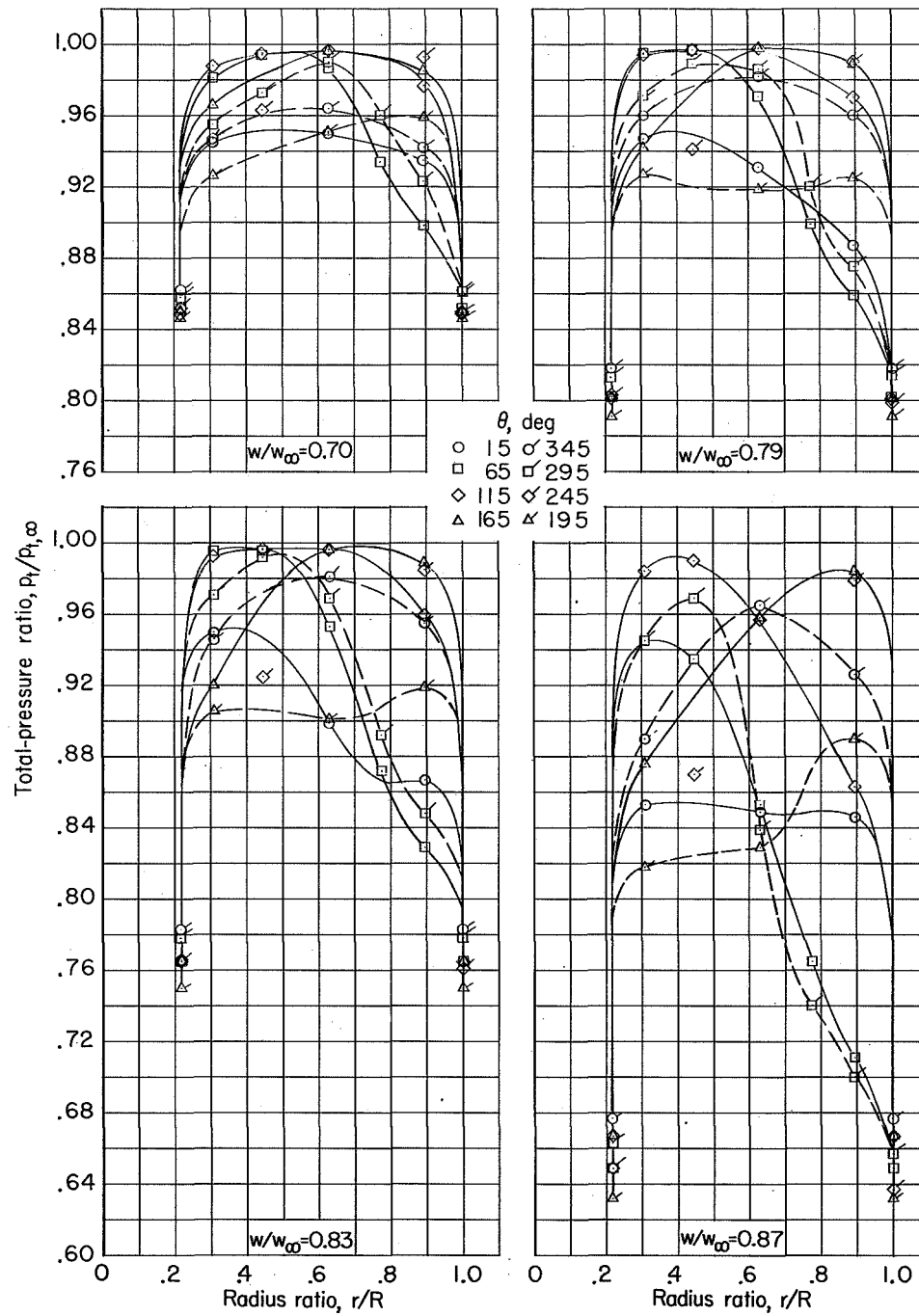
(k) $M = 1.10$; $\alpha = -4^\circ$.

Figure 8.- Continued.



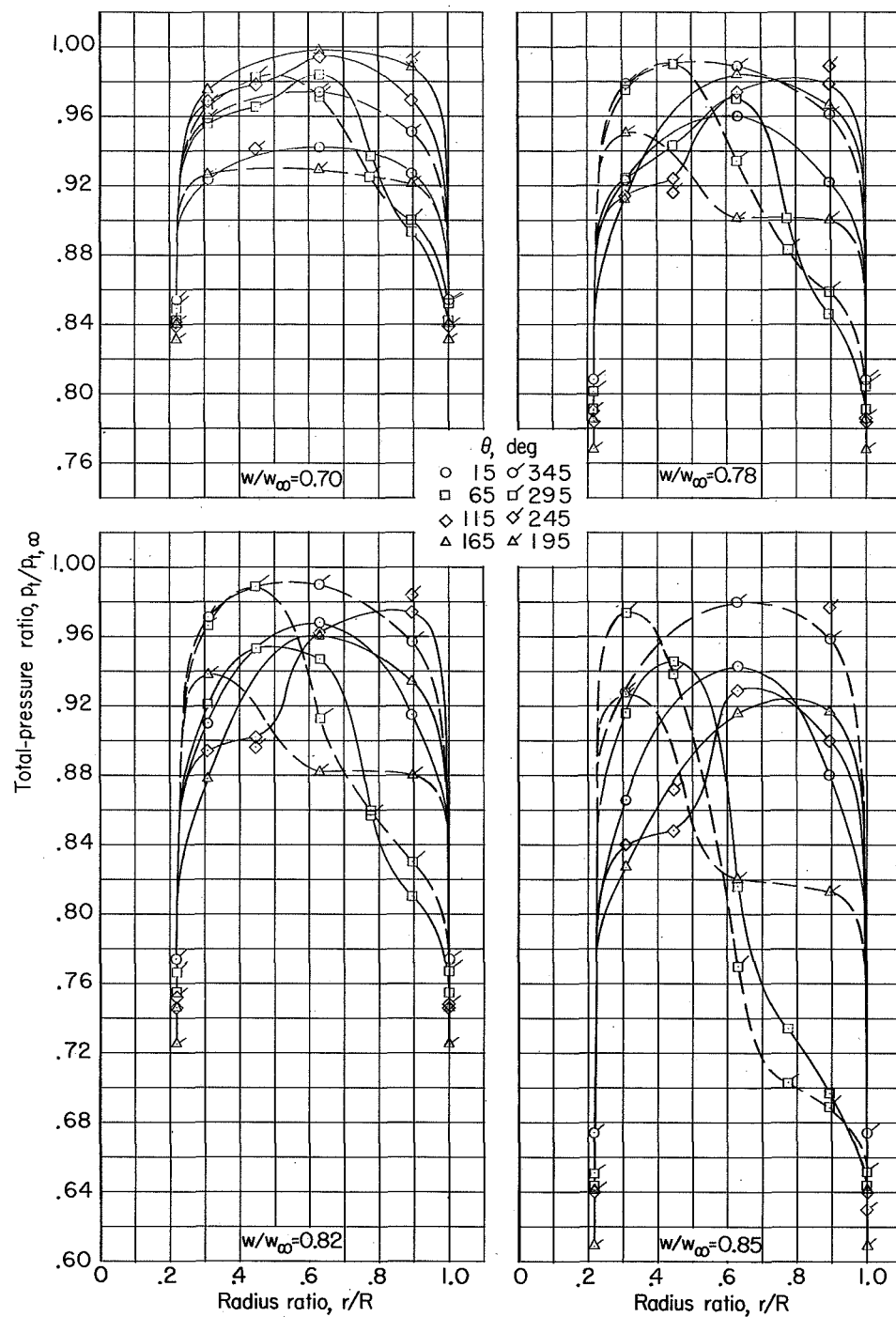
(1) $M = 1.10; \alpha = 0^\circ$.

Figure 8.- Continued.



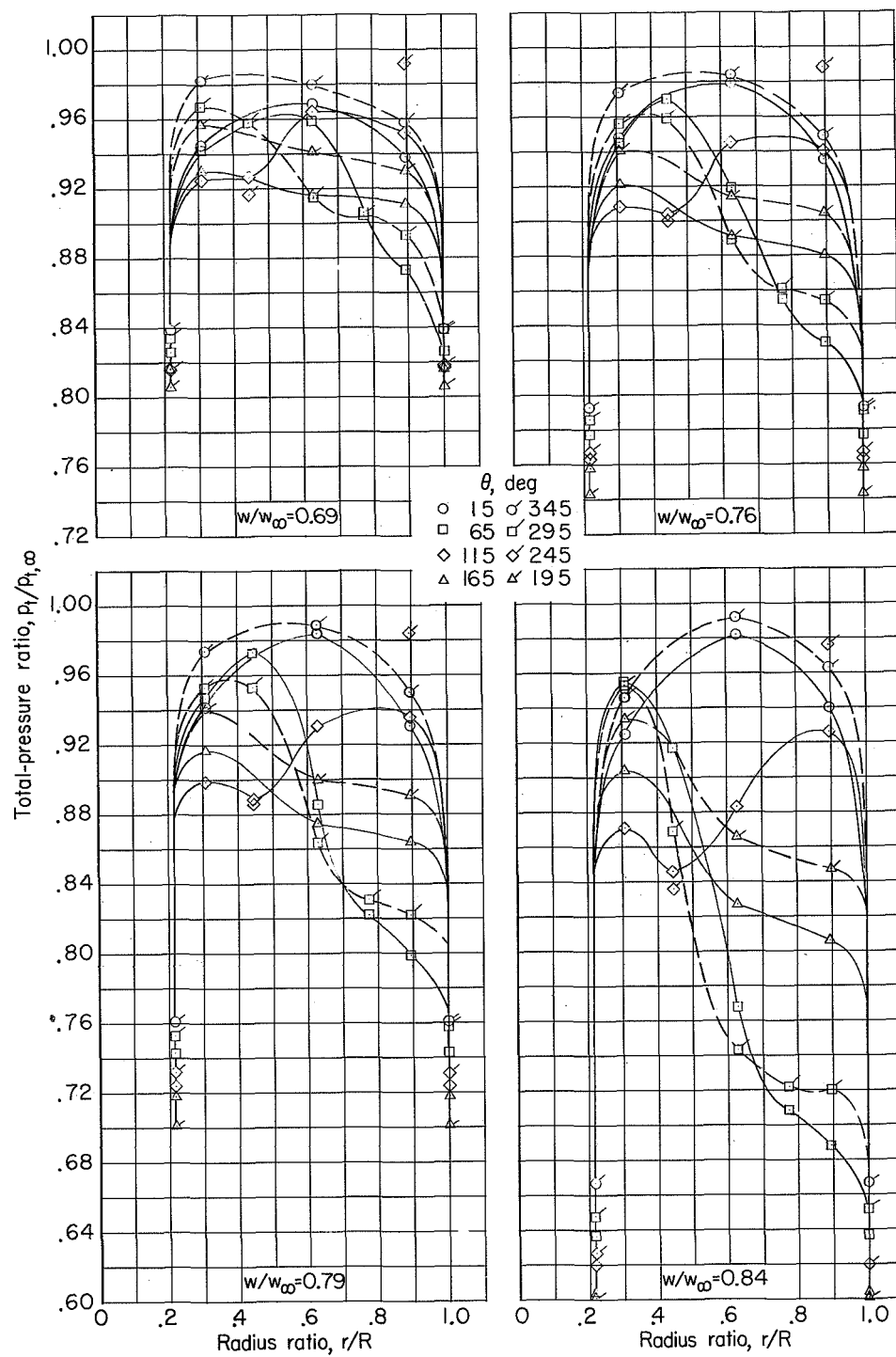
(m) $M = 1.10$; $\alpha = 4^\circ$.

Figure 8.- Continued.



(n) $M = 1.10$; $\alpha = 7^\circ$.

Figure 8.- Continued.



(o) $M = 1.10; \alpha = 10^\circ$.

Figure 8.- Concluded.

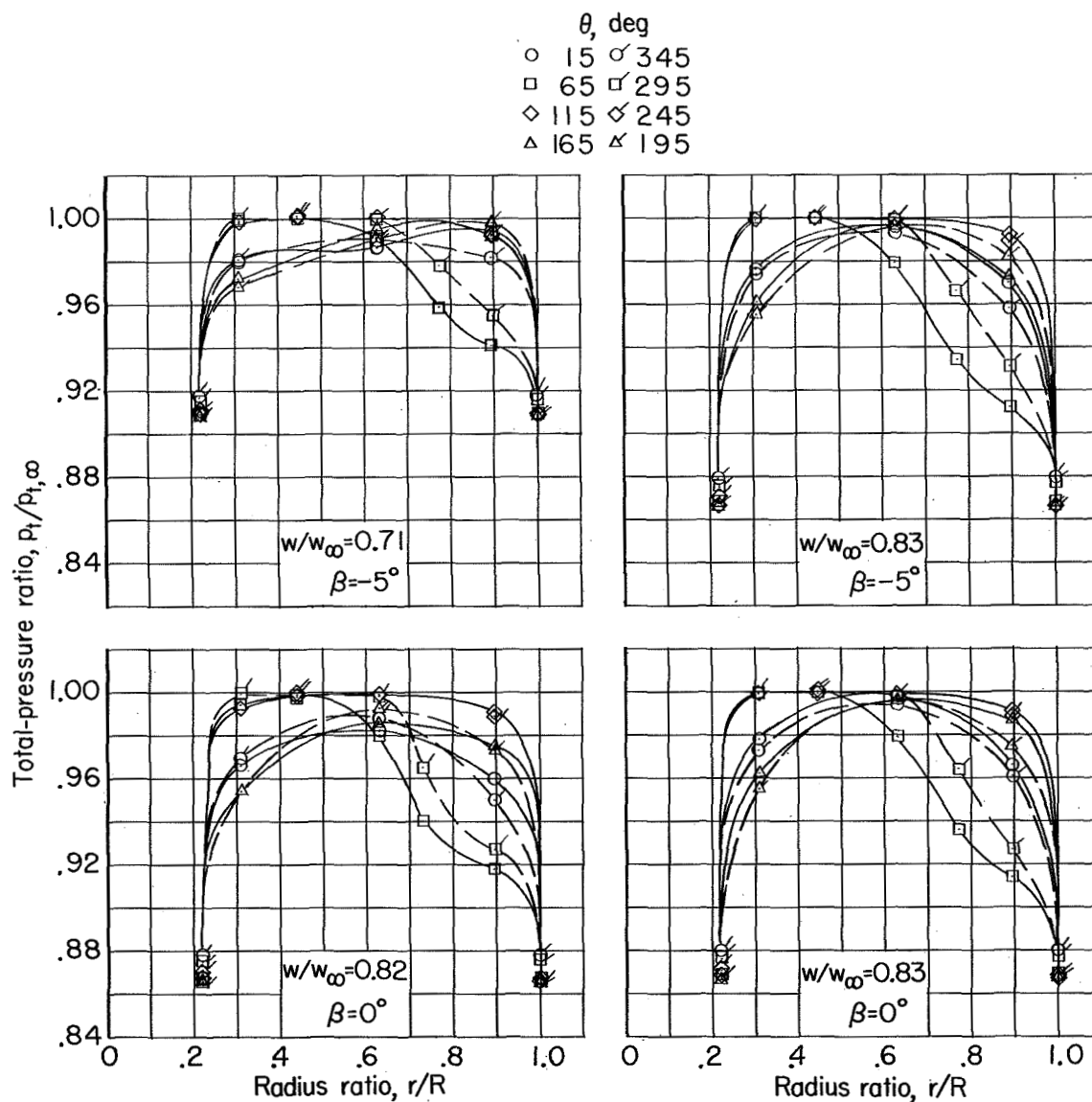
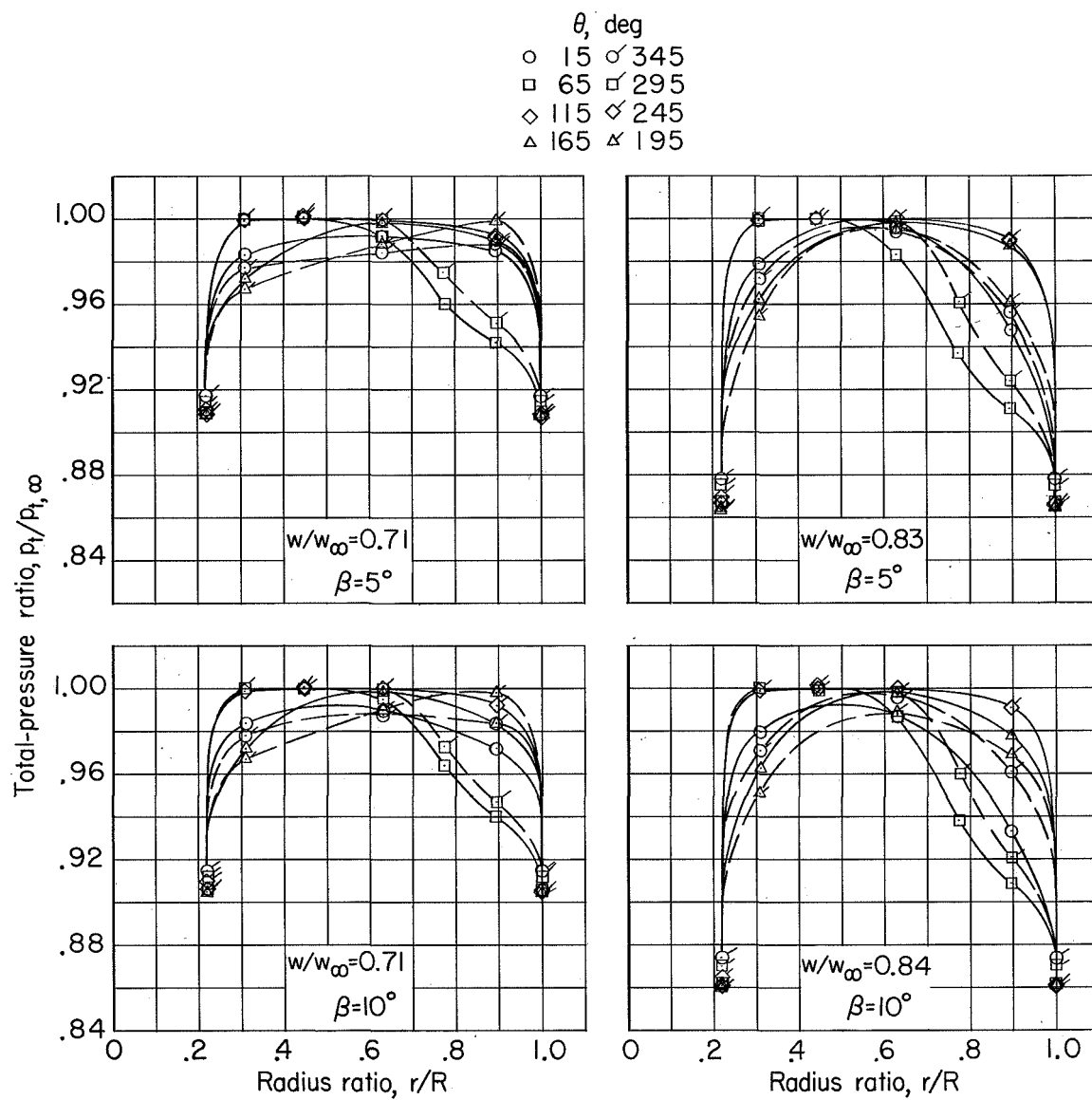
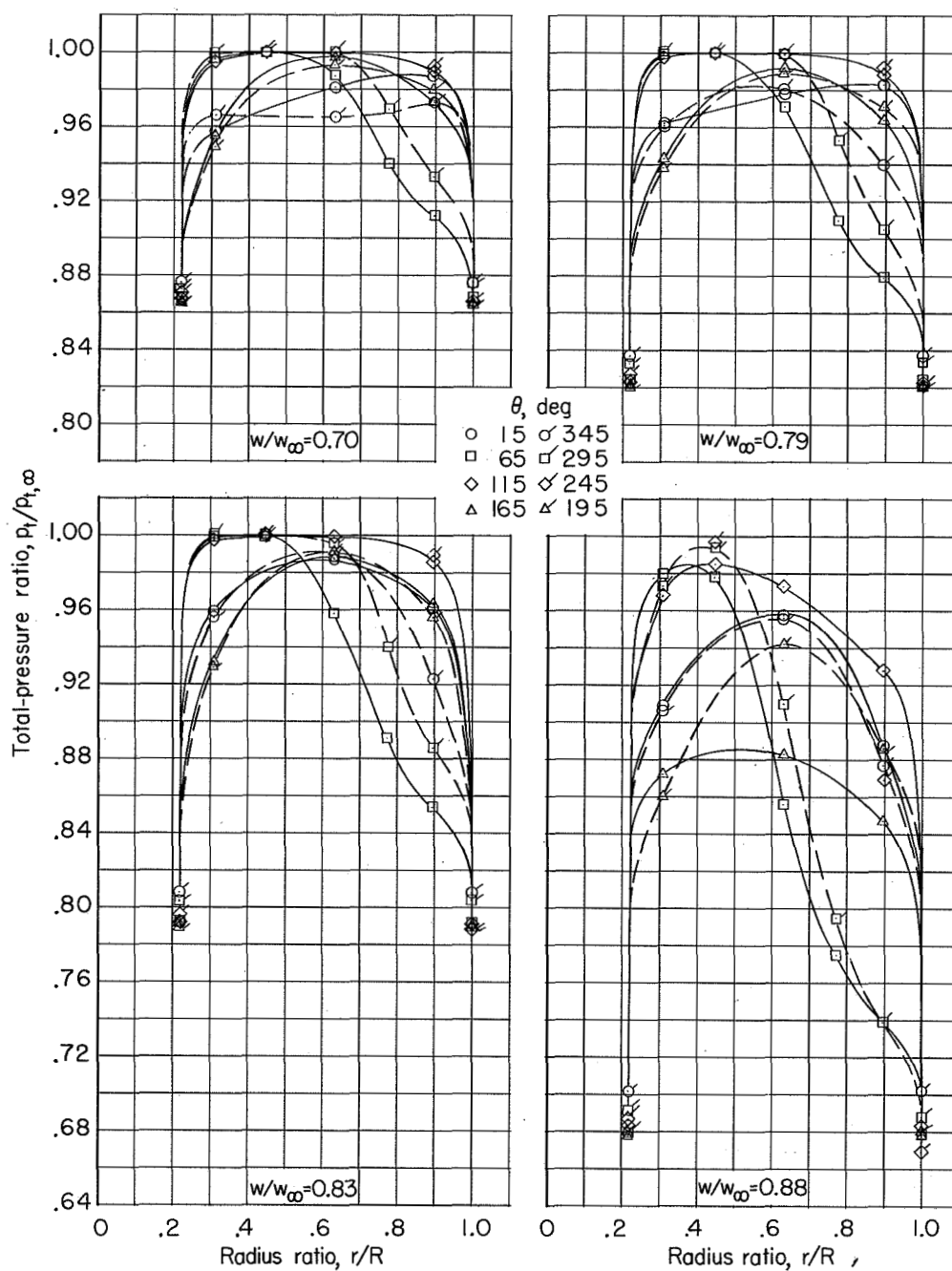


Figure 9.- Radial variation of total-pressure ratio at various angles of sideslip, mass-flow ratios, and Mach numbers. Basic configuration. $\alpha = 0^\circ$.



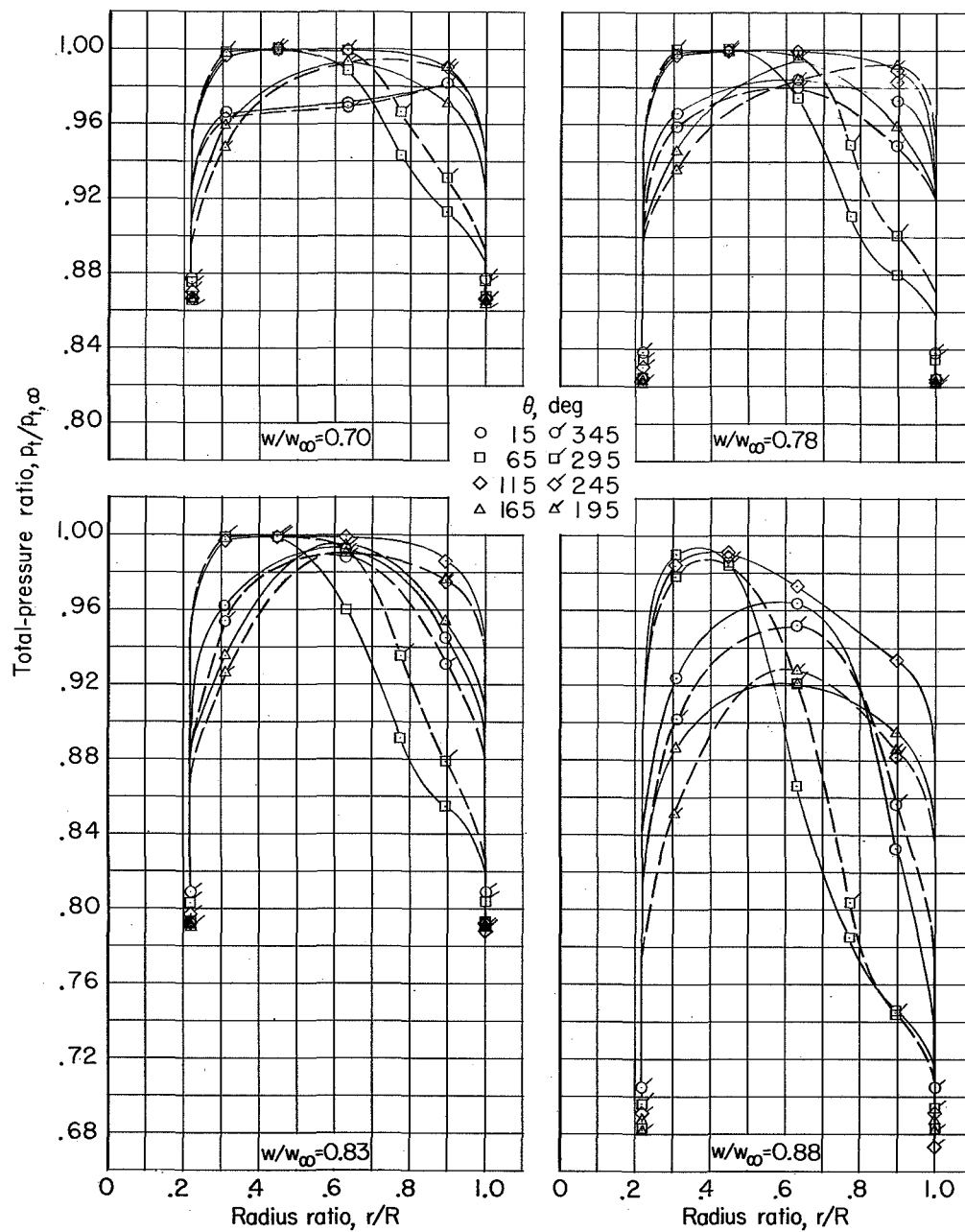
(b) $M = 0.60$; $\beta = 5^{\circ}$ and 10° .

Figure 9.- Continued.



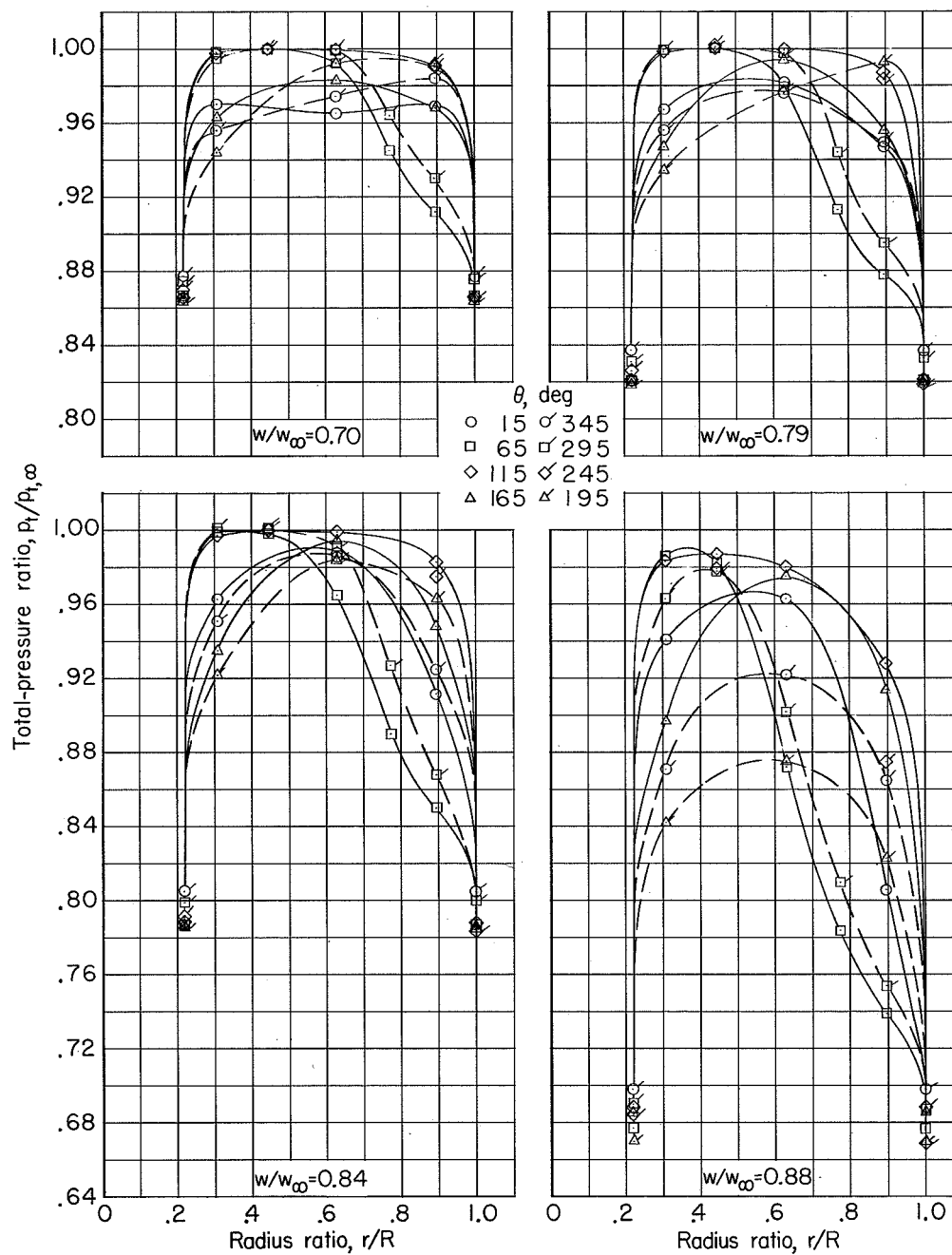
(c) $M = 0.90$; $\beta = -5^\circ$.

Figure 9.- Continued.



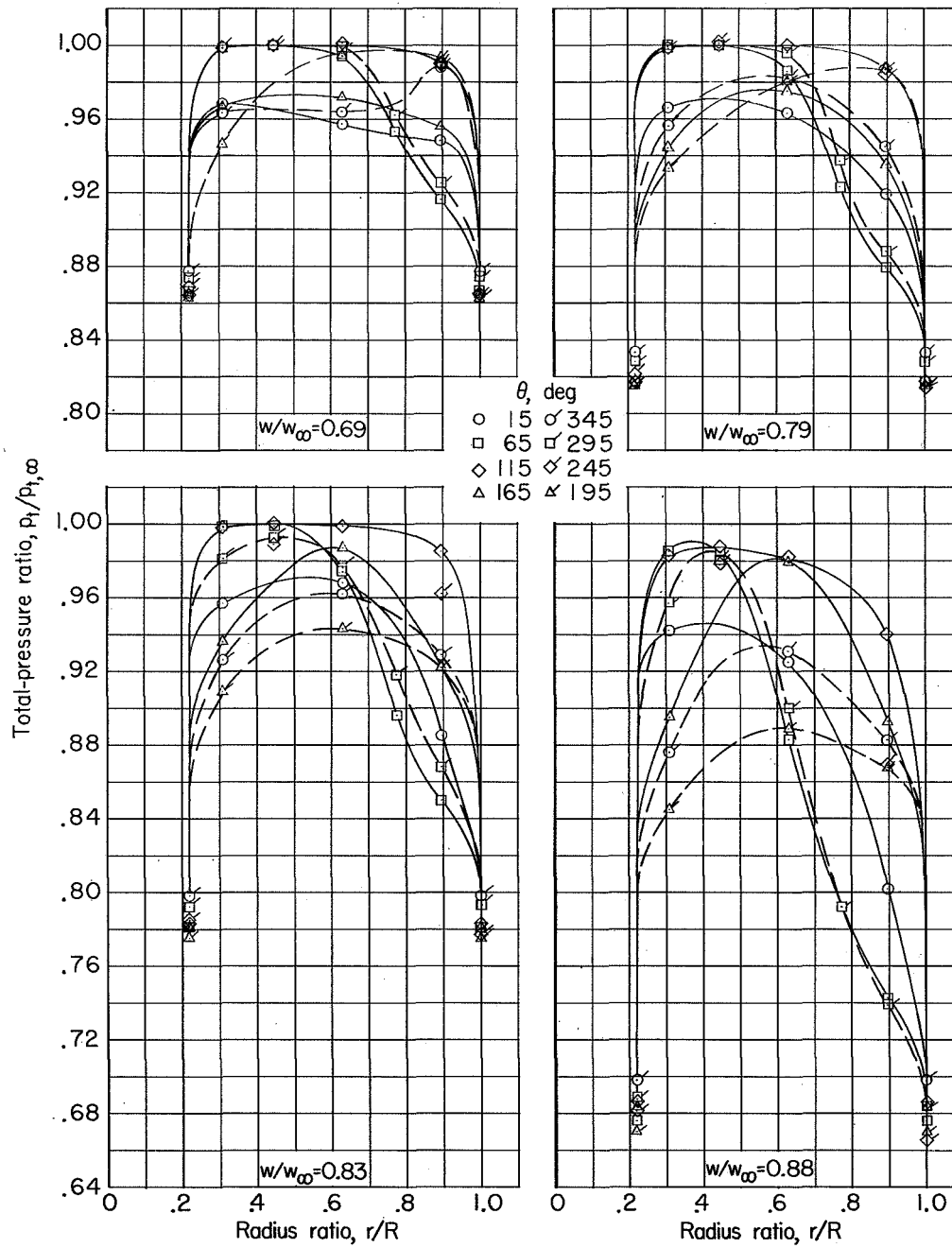
(d) $M = 0.90$; $\beta = 0^\circ$.

Figure 9.- Continued.



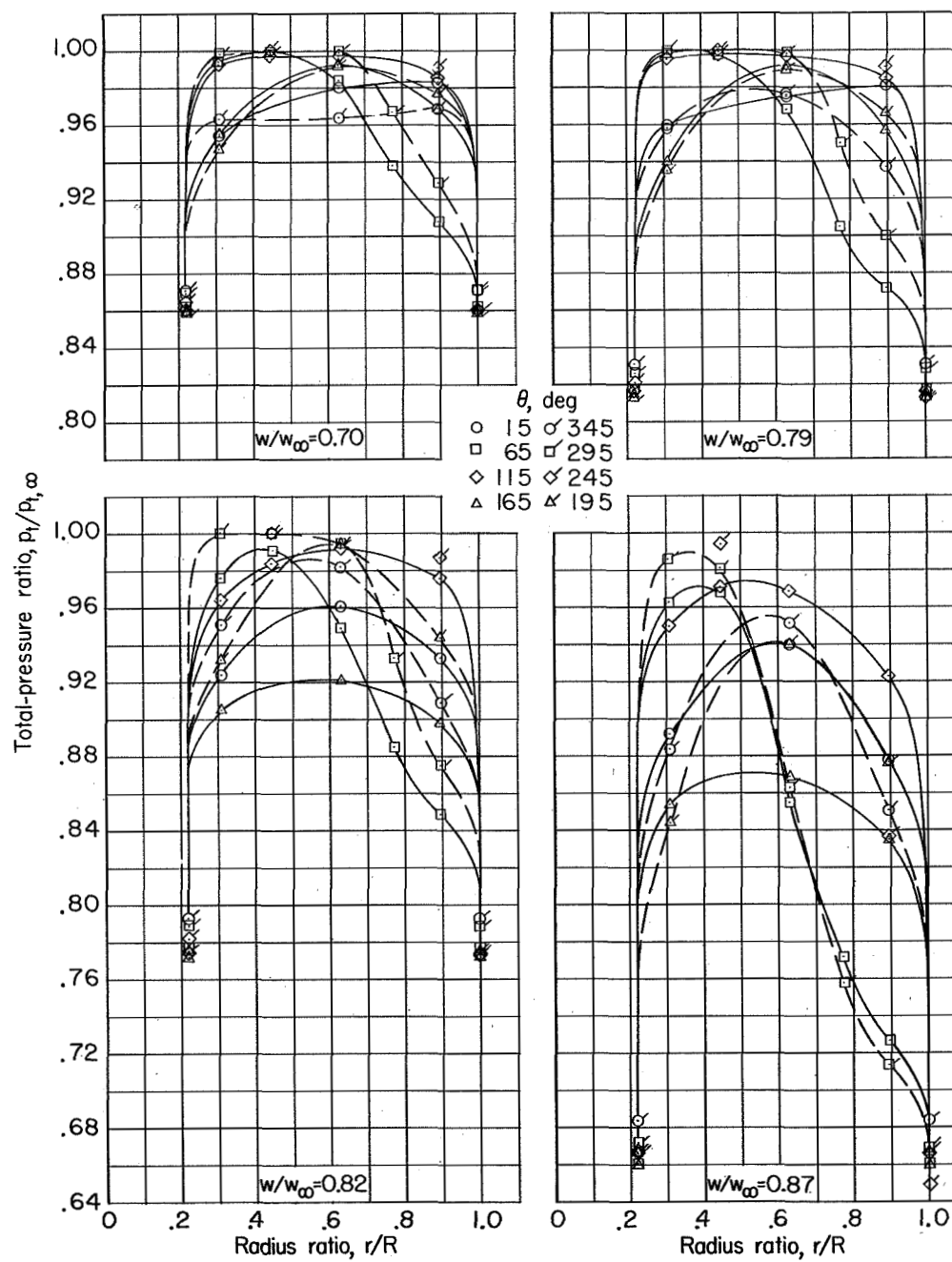
(e) $M = 0.90$; $\beta = 5^\circ$.

Figure 9.- Continued.



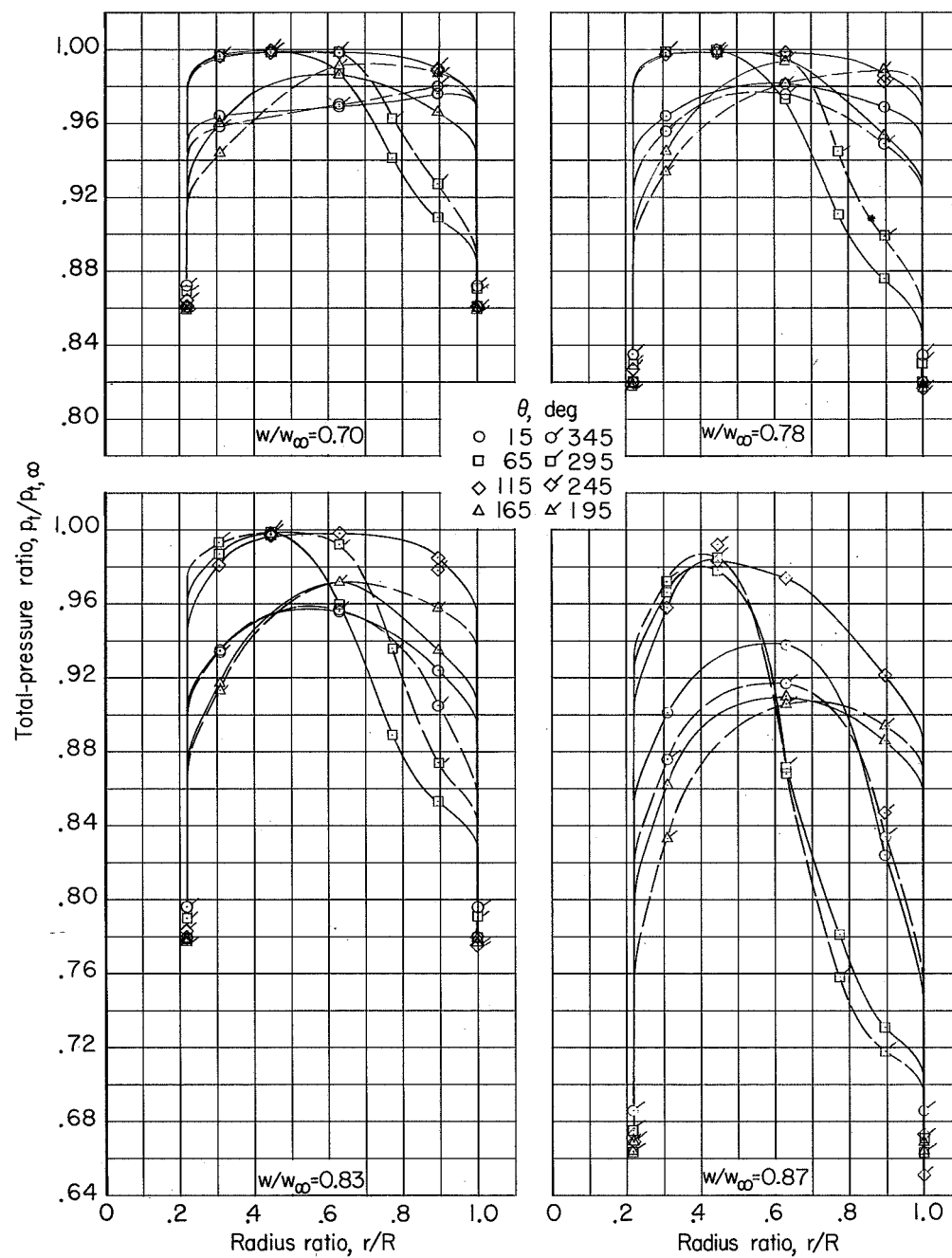
(f) $M = 0.90$; $\beta = 10^\circ$.

Figure 9.- Continued.



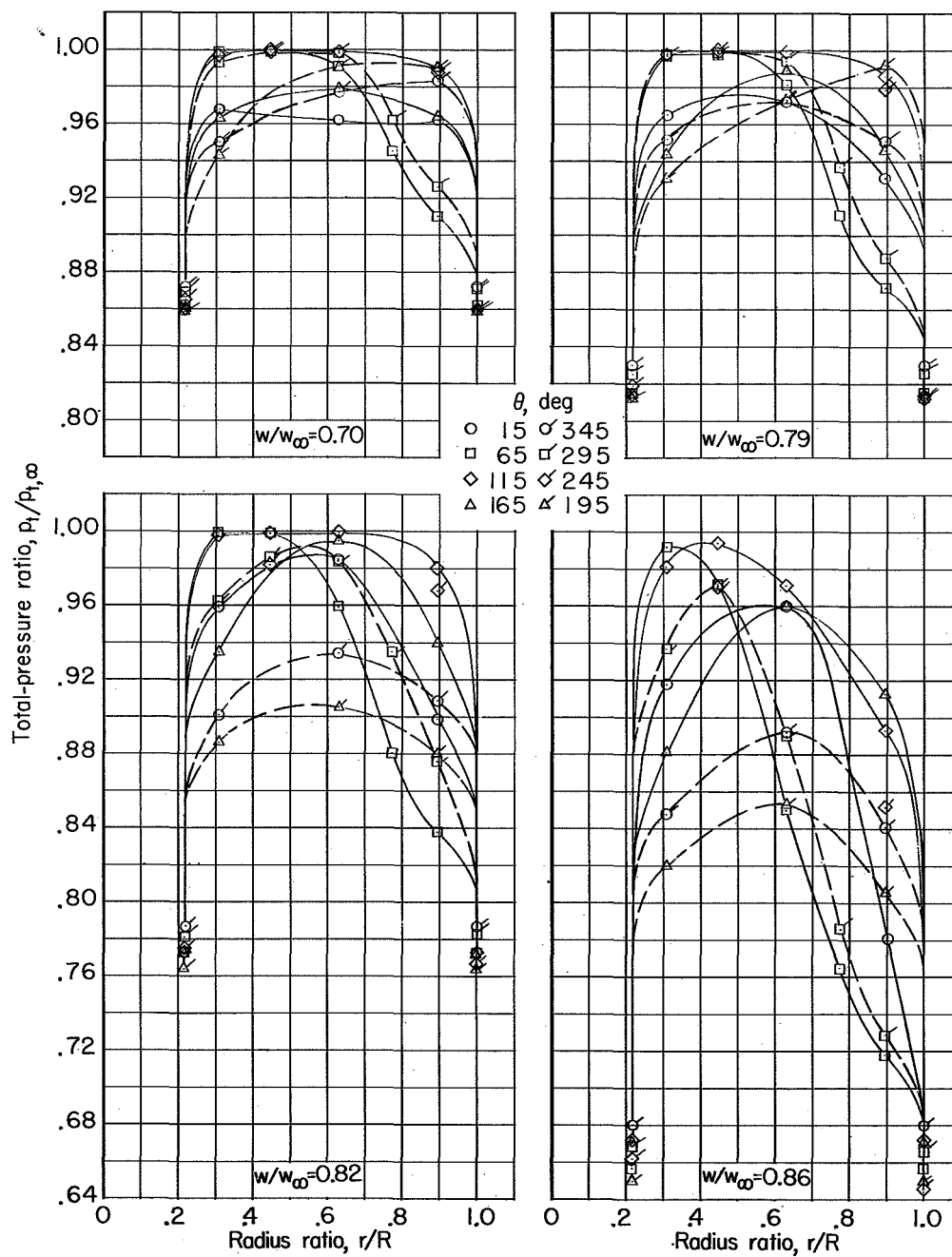
(g) $M = 0.95$; $\beta = -5^\circ$.

Figure 9.- Continued.



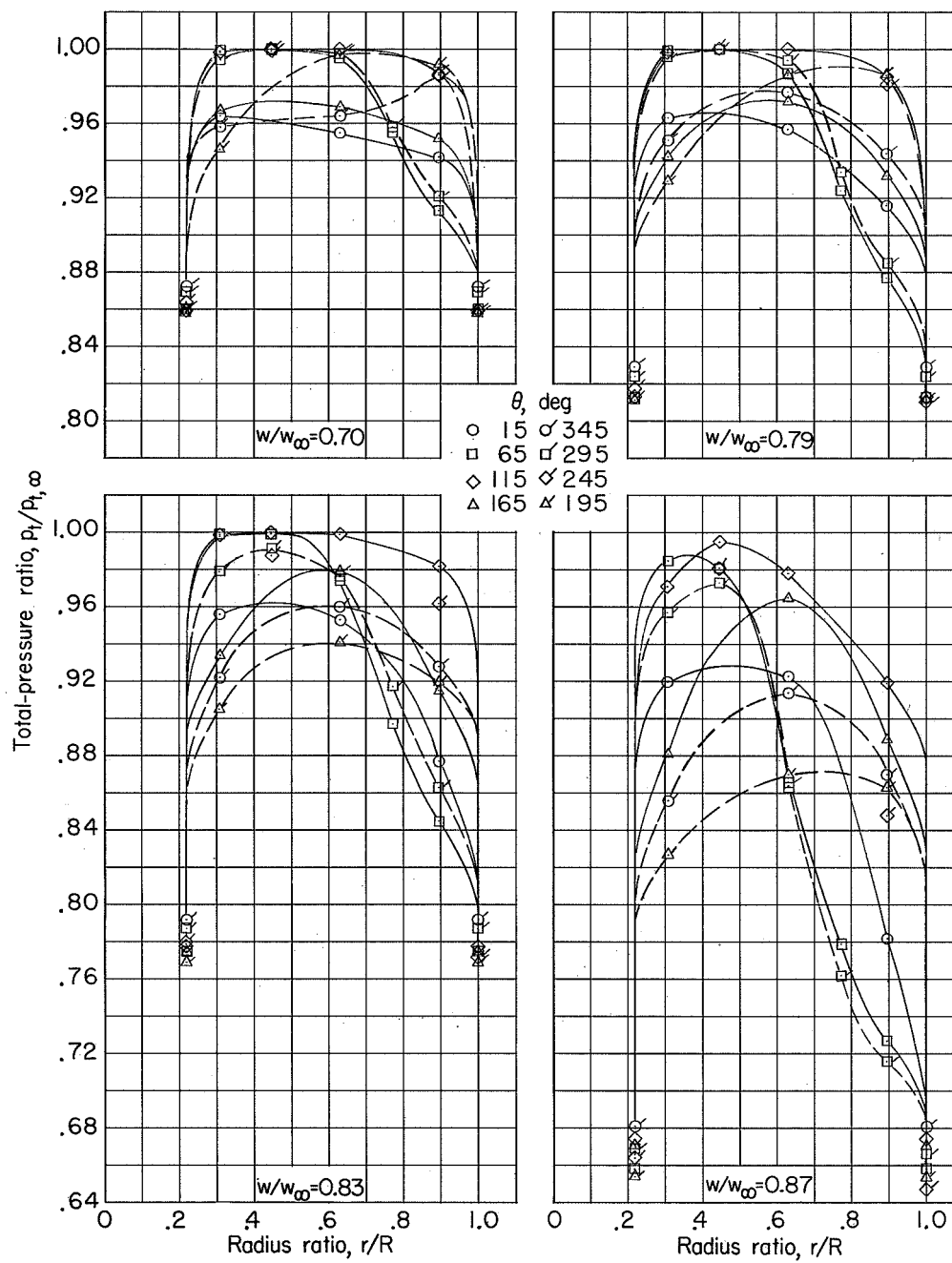
(h) $M = 0.95$; $\beta = 0^\circ$.

Figure 9.- Continued.



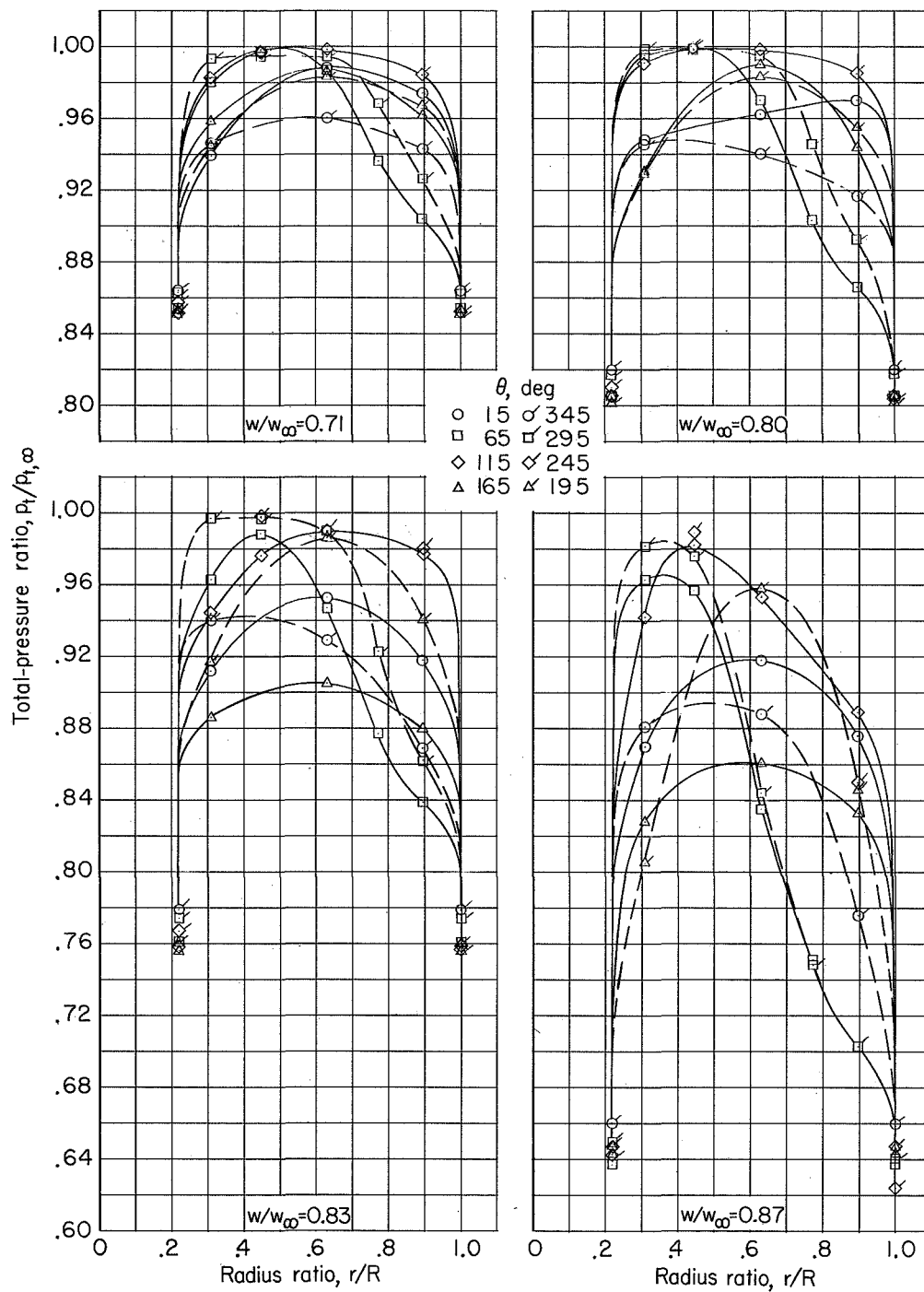
(i) $M = 0.95$; $\beta = 5^\circ$.

Figure 9.- Continued.



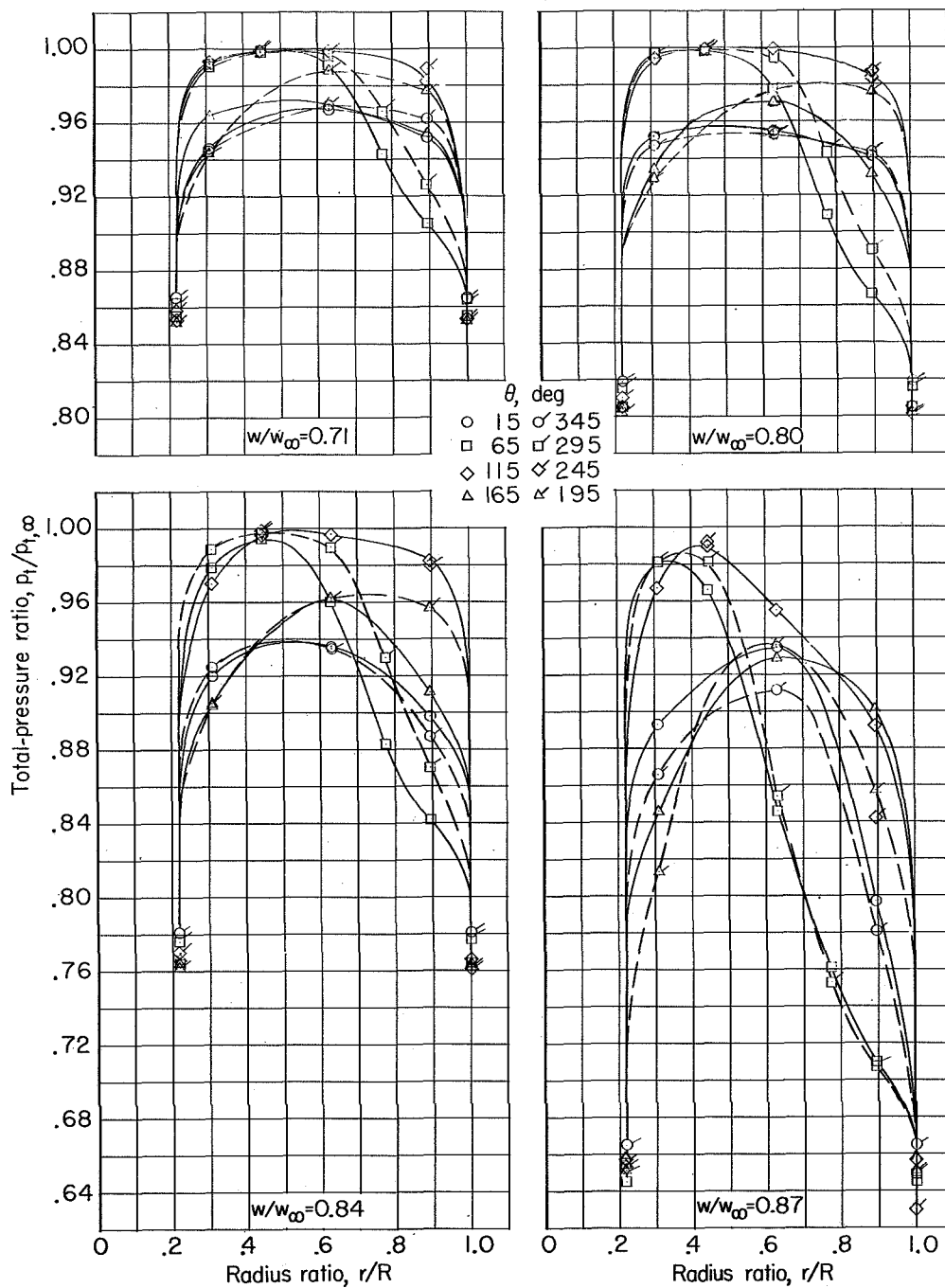
(j) $M = 0.95$; $\beta = 10^\circ$.

Figure 9.- Continued.



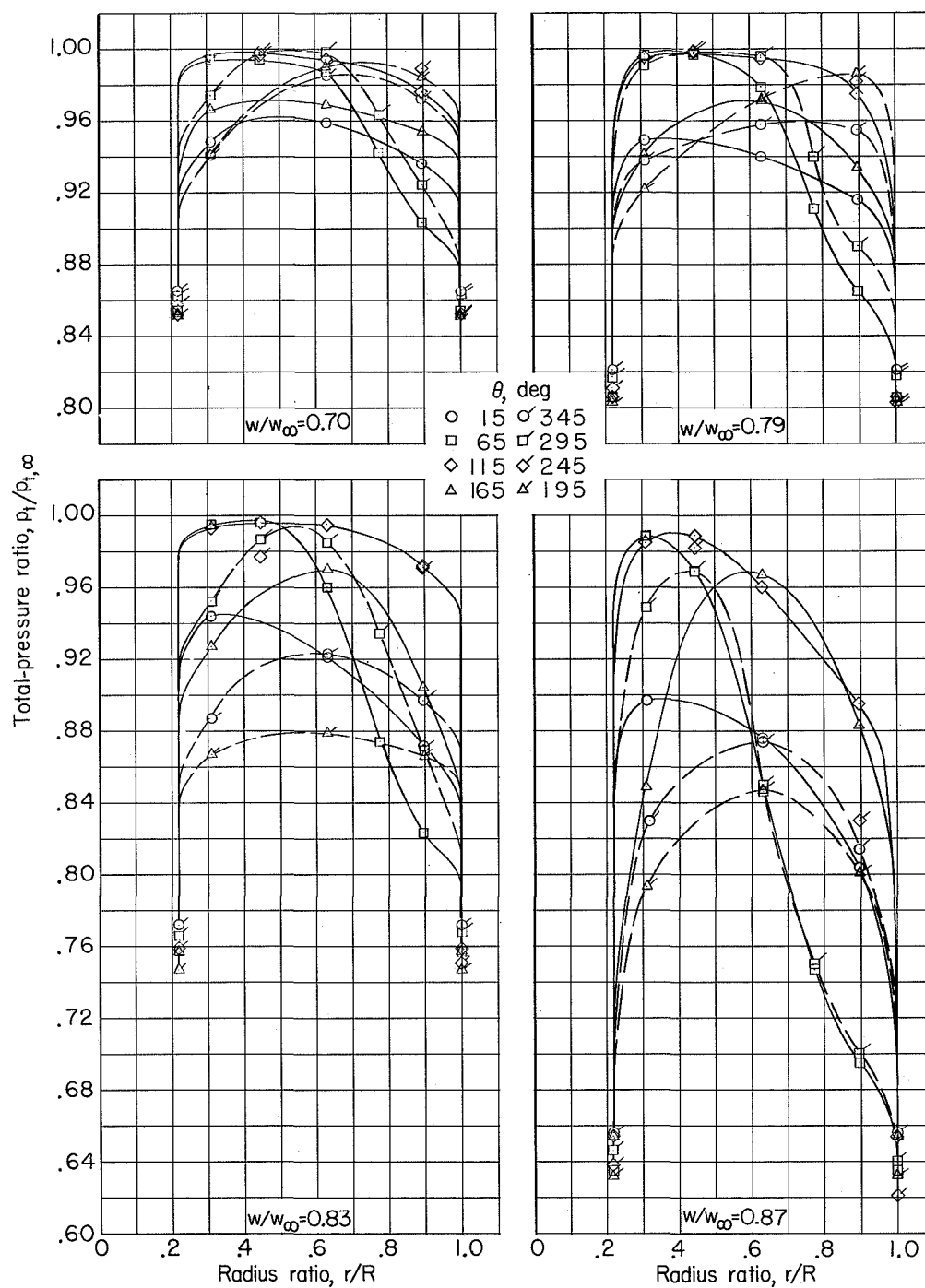
(k) $M = 1.10$; $\beta = -5^\circ$.

Figure 9.- Continued.



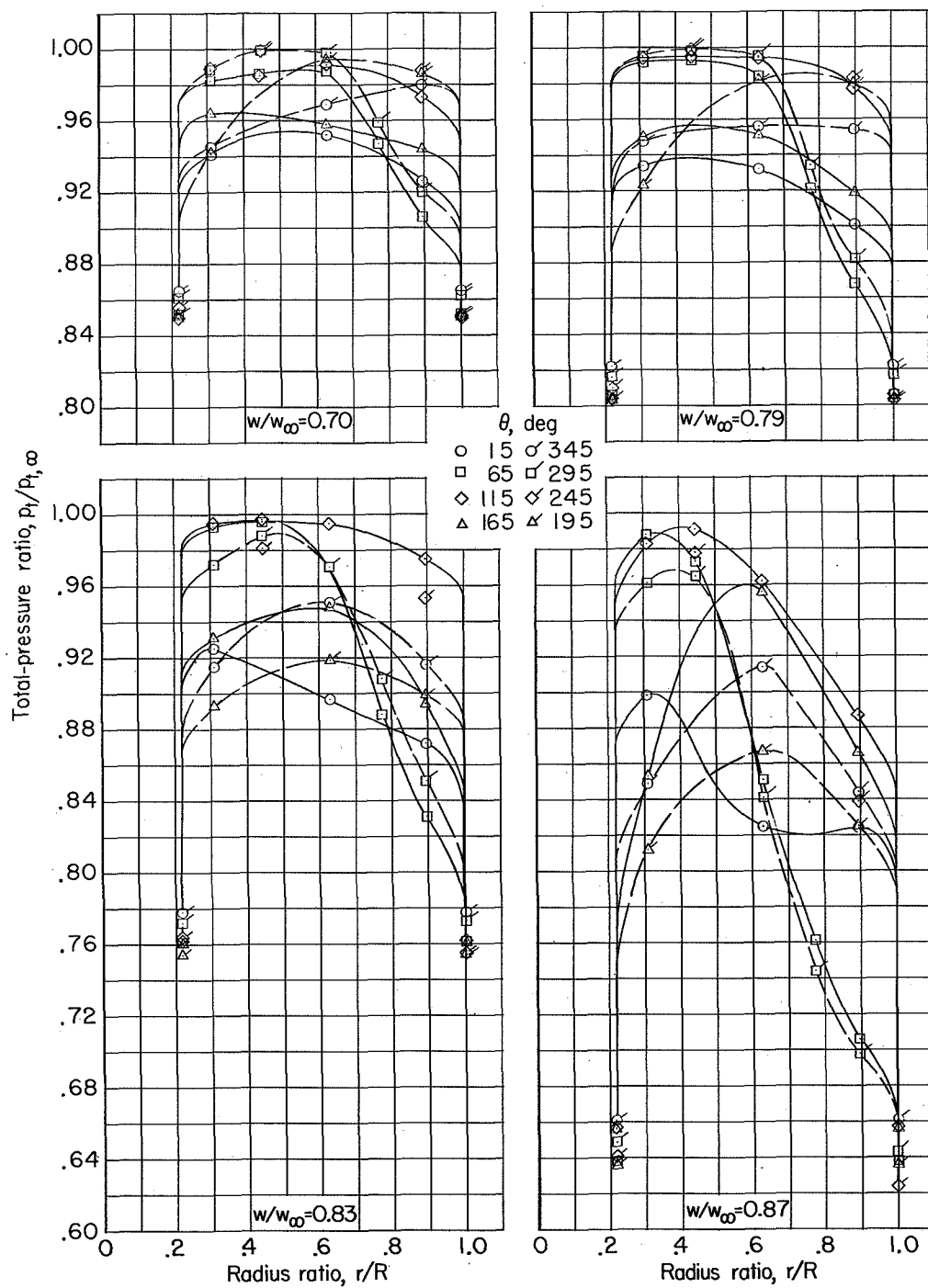
(1) $M = 1.10$; $\beta = 0^\circ$.

Figure 9.- Continued.



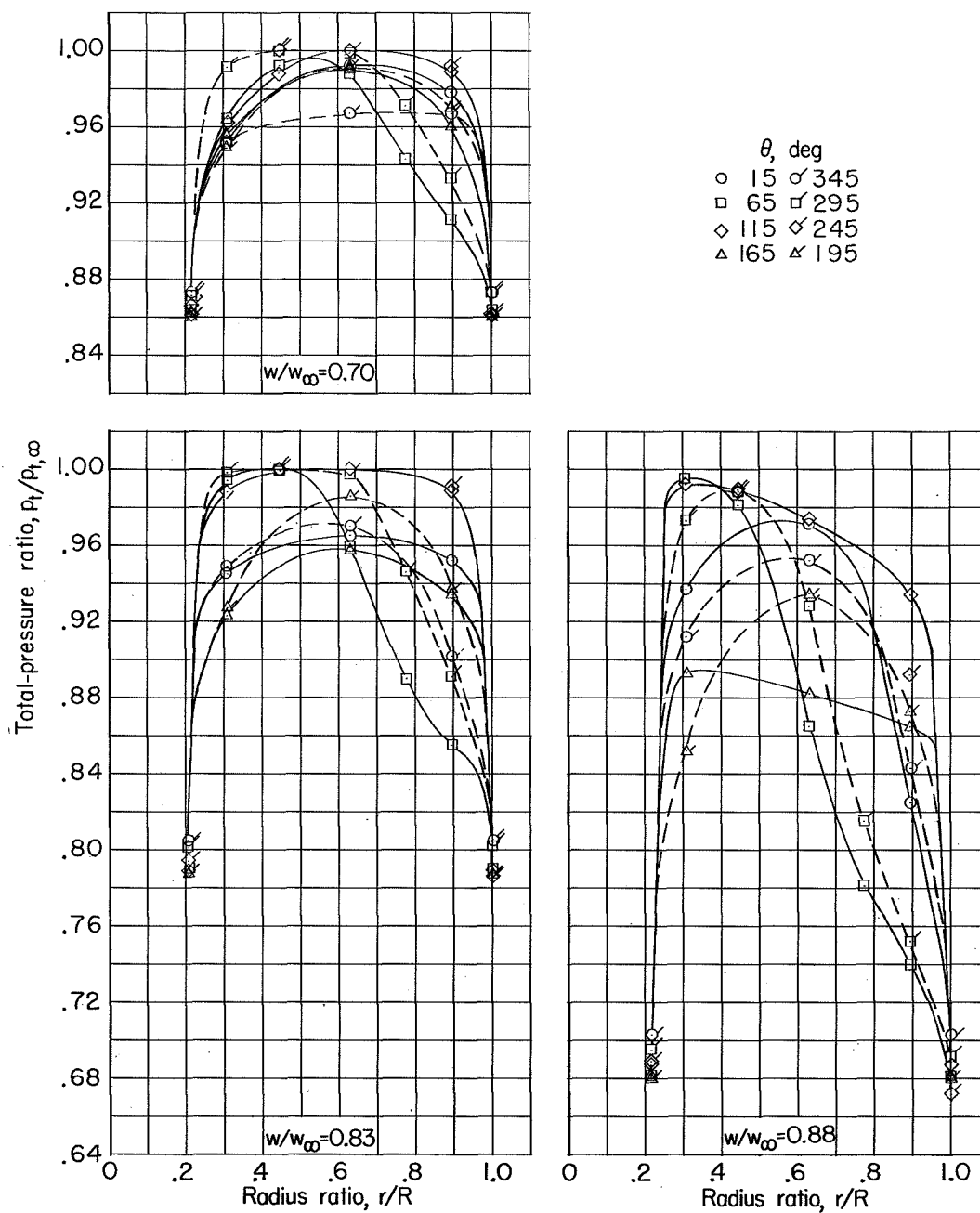
(m) $M = 1.10$; $\beta = 5^\circ$.

Figure 9.- Continued.



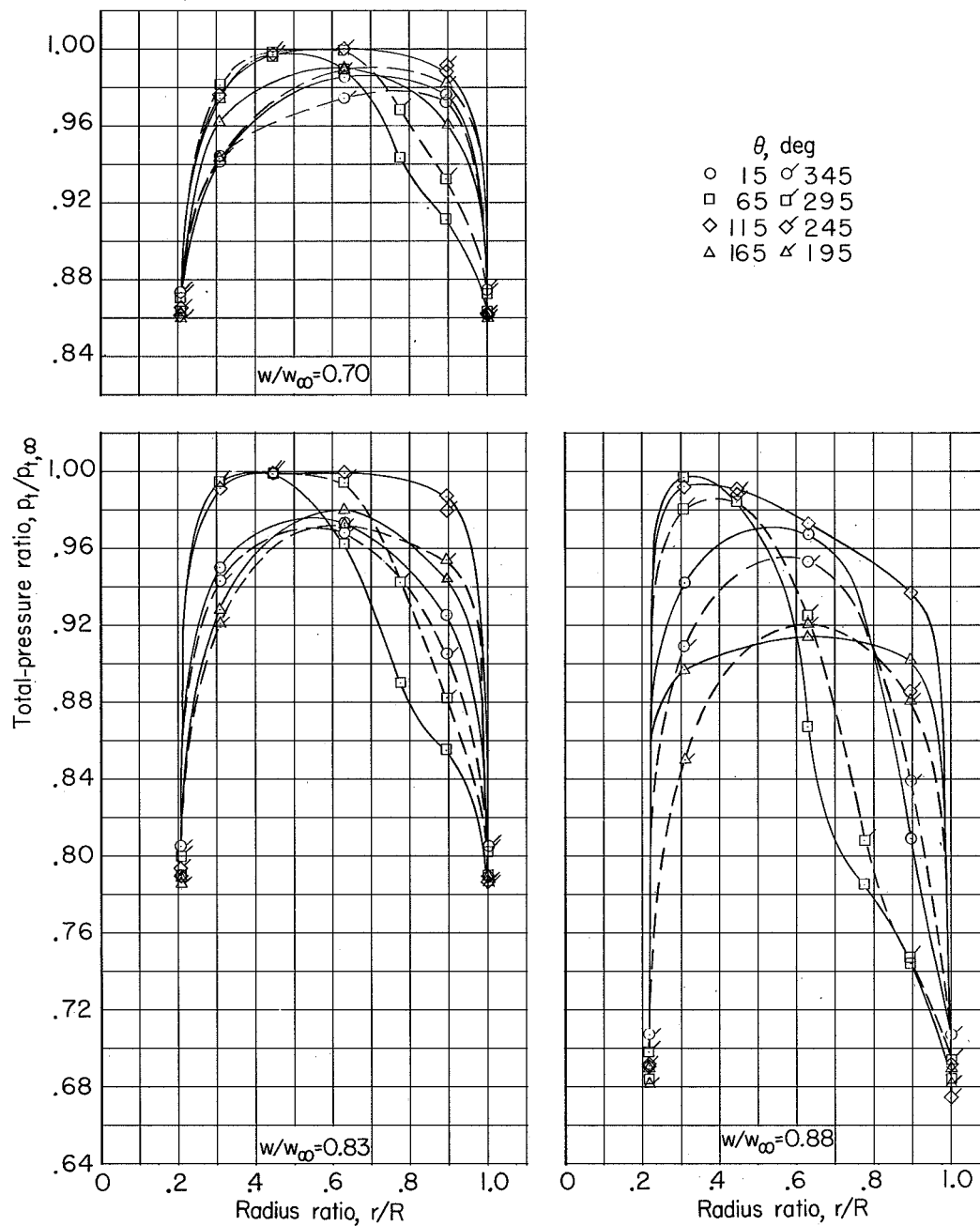
(n) $M = 1.10$; $\beta = 10^\circ$.

Figure 9.- Concluded.



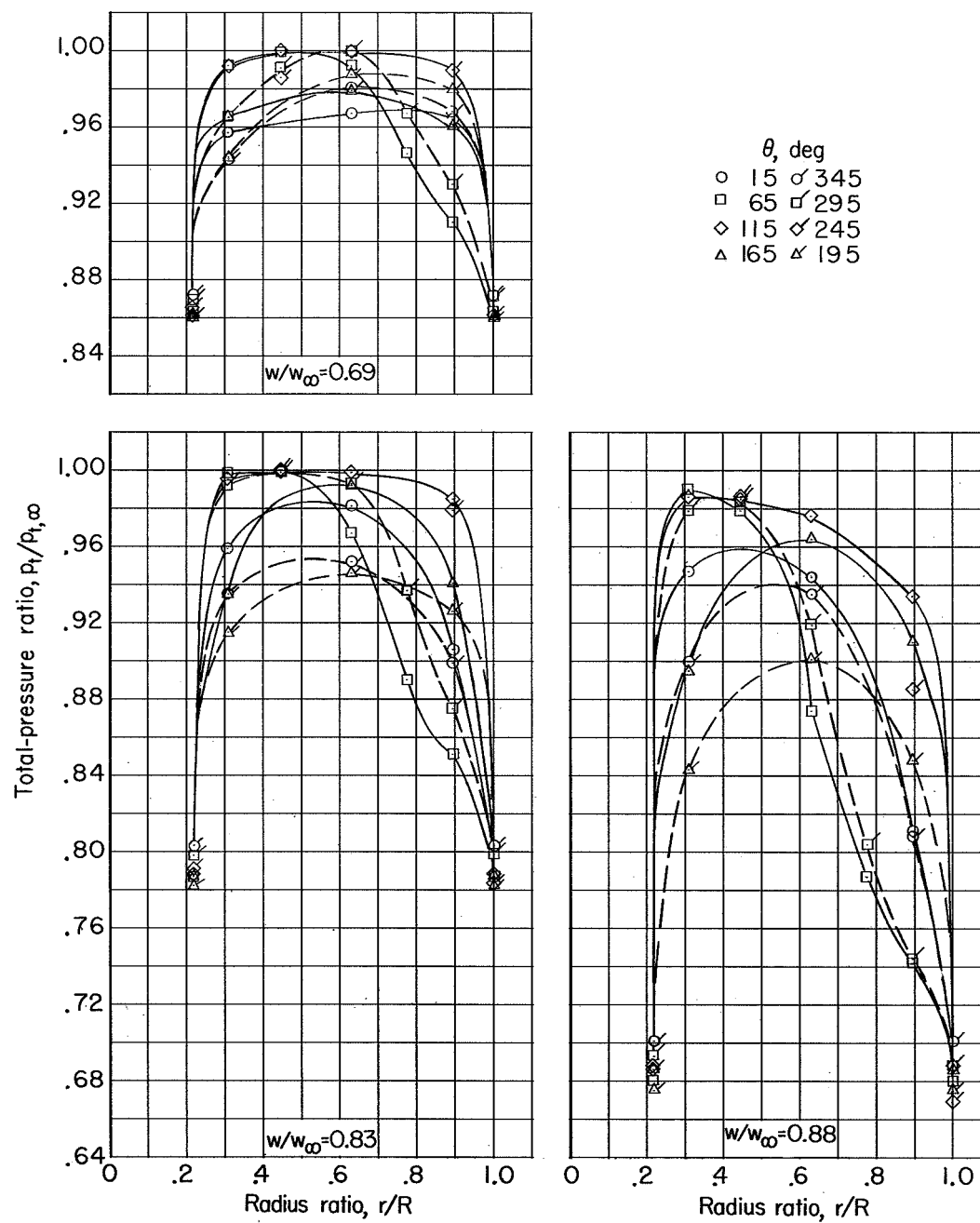
(a) $M = 0.90$; $\beta = -5^\circ$.

Figure 10.- Radial variation of total-pressure ratio at various angles of sideslip, mass-flow ratios, and Mach numbers. Basic configuration with fuselage gloves. $\alpha = 0^\circ$.



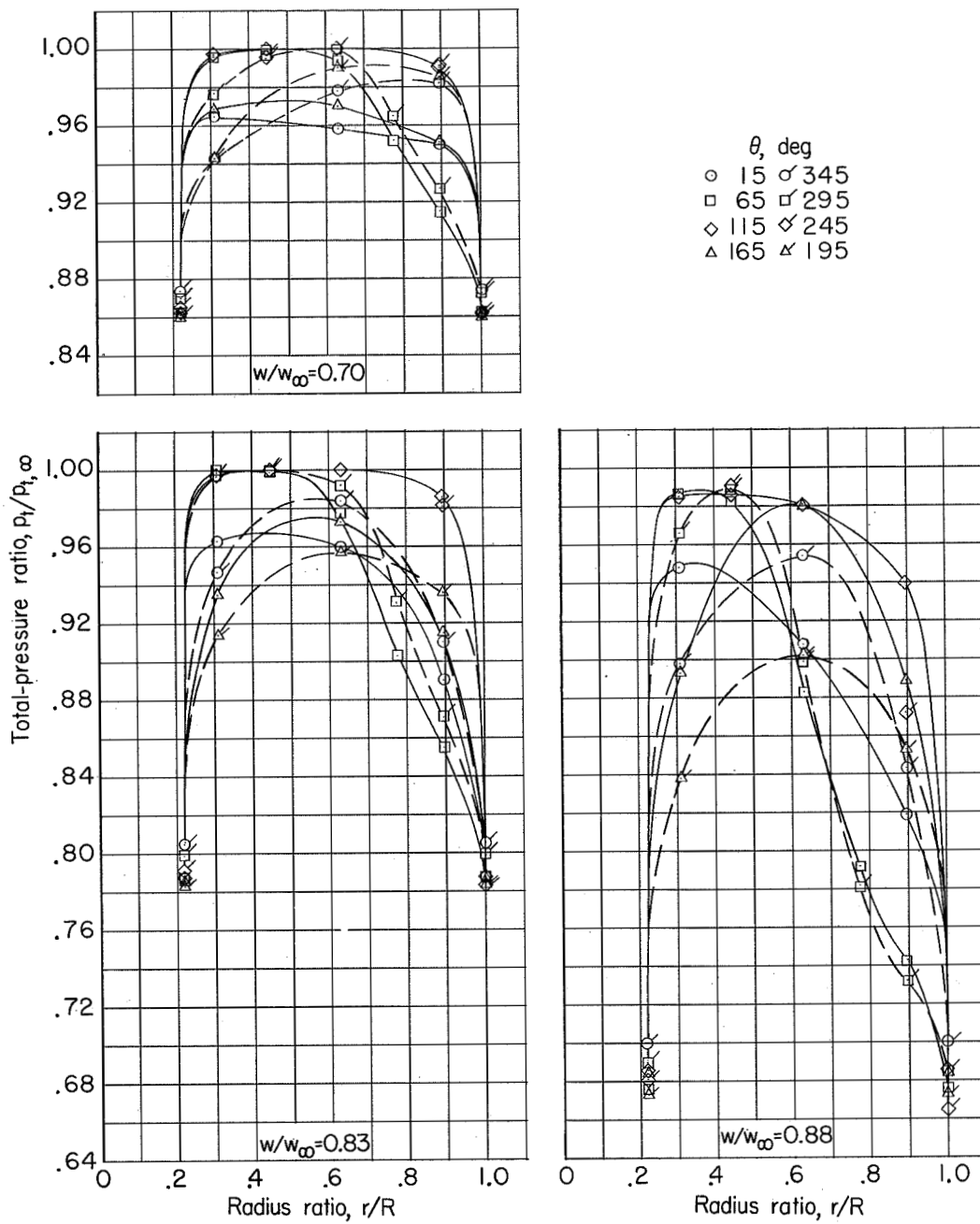
(b) $M = 0.90$; $\beta = 0^\circ$.

Figure 10.- Continued.



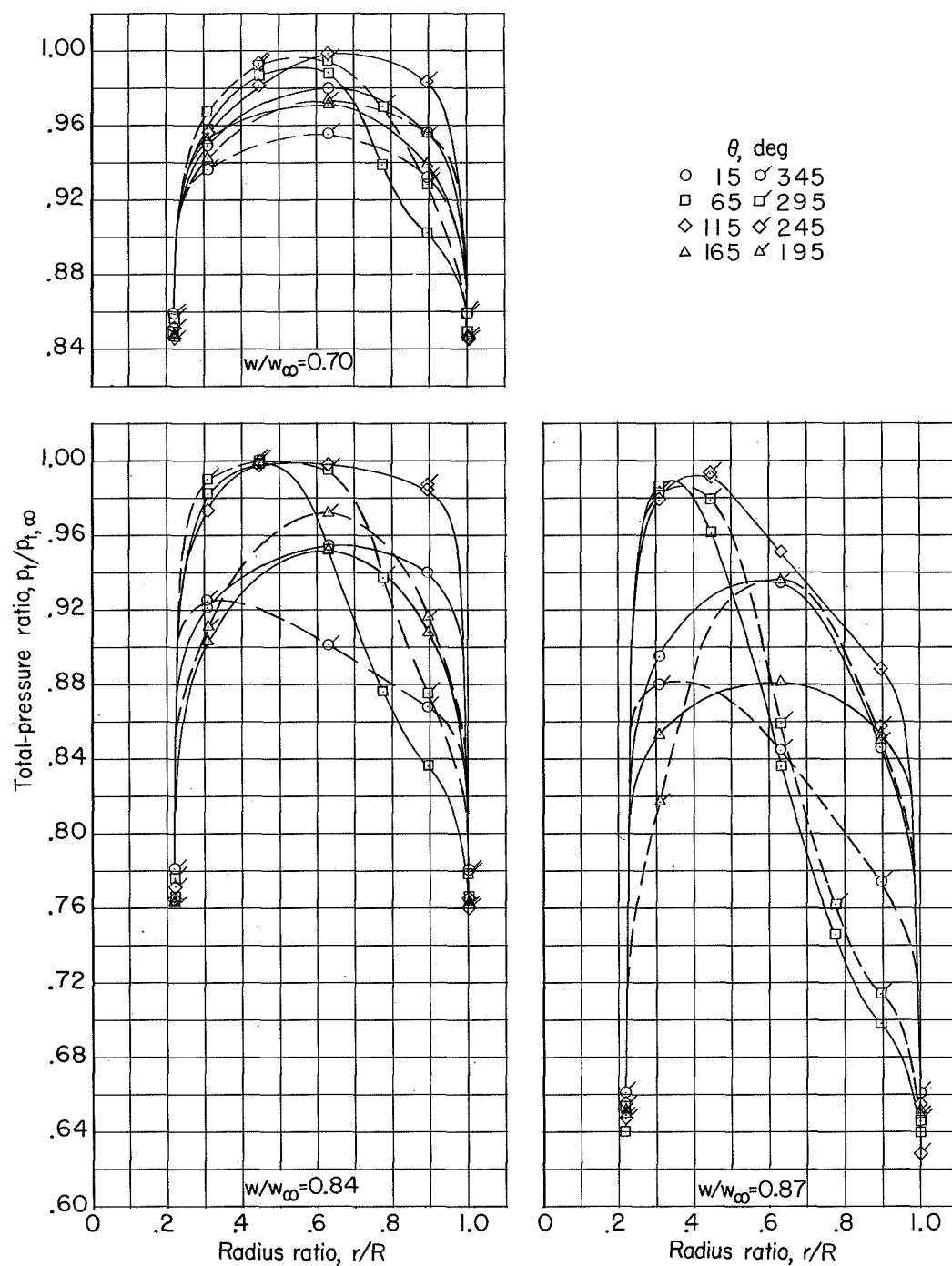
(c) $M = 0.90$; $\beta = 5^\circ$.

Figure 10.- Continued.



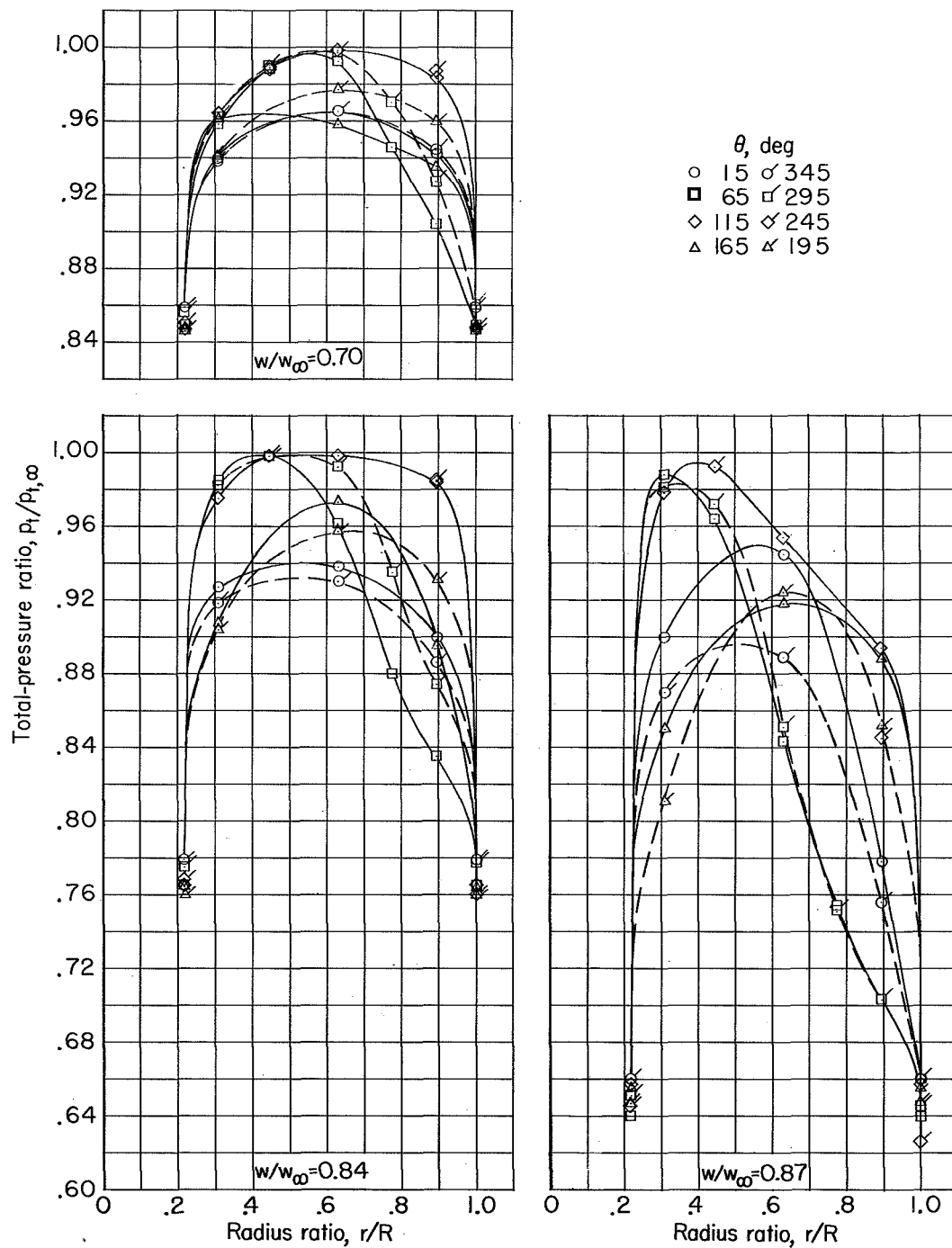
(d) $M = 0.90$; $\beta = 10^\circ$.

Figure 10.- Continued.



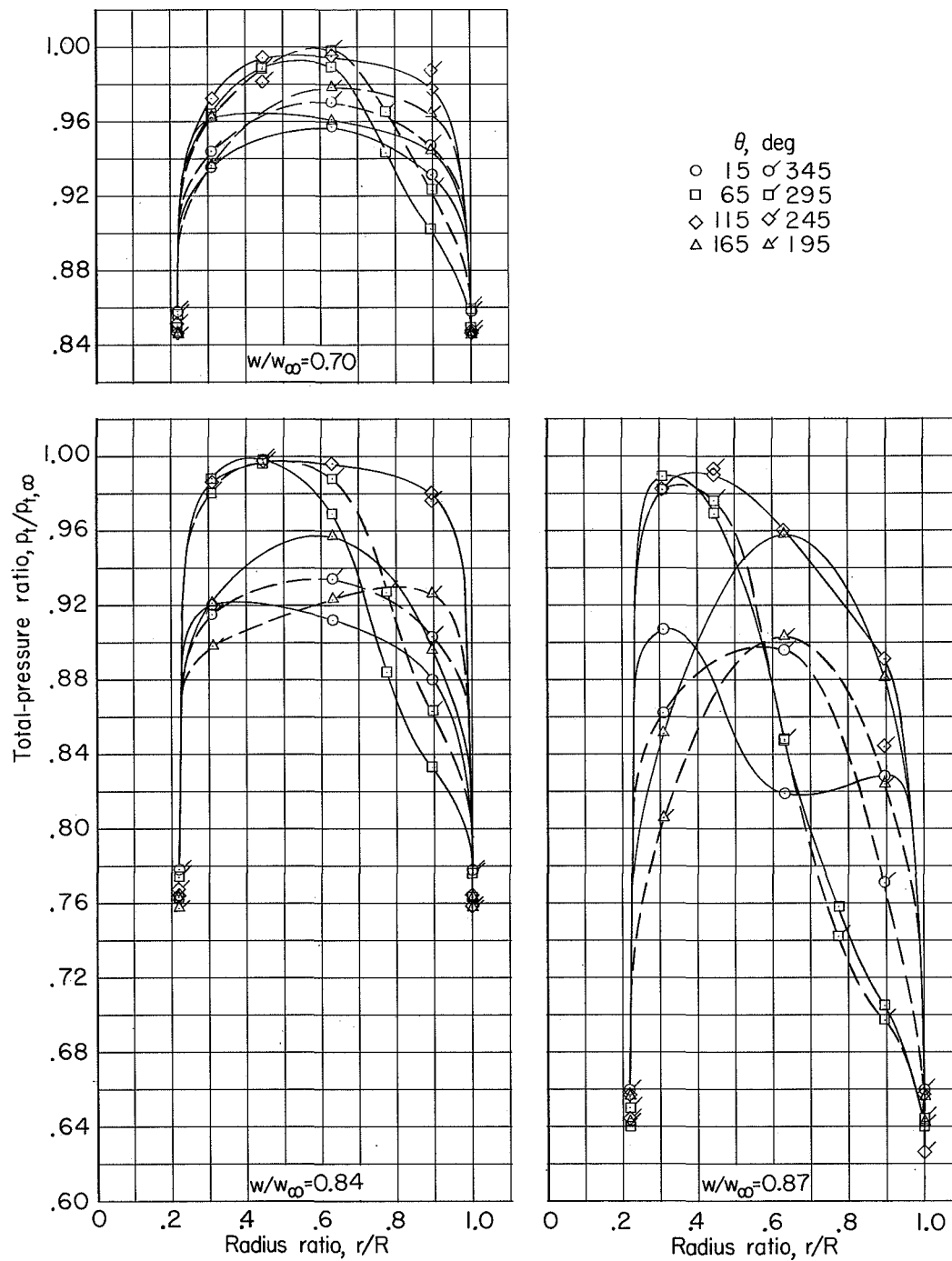
(e) $M = 1.10$; $\beta = -5^\circ$.

Figure 10.- Continued.



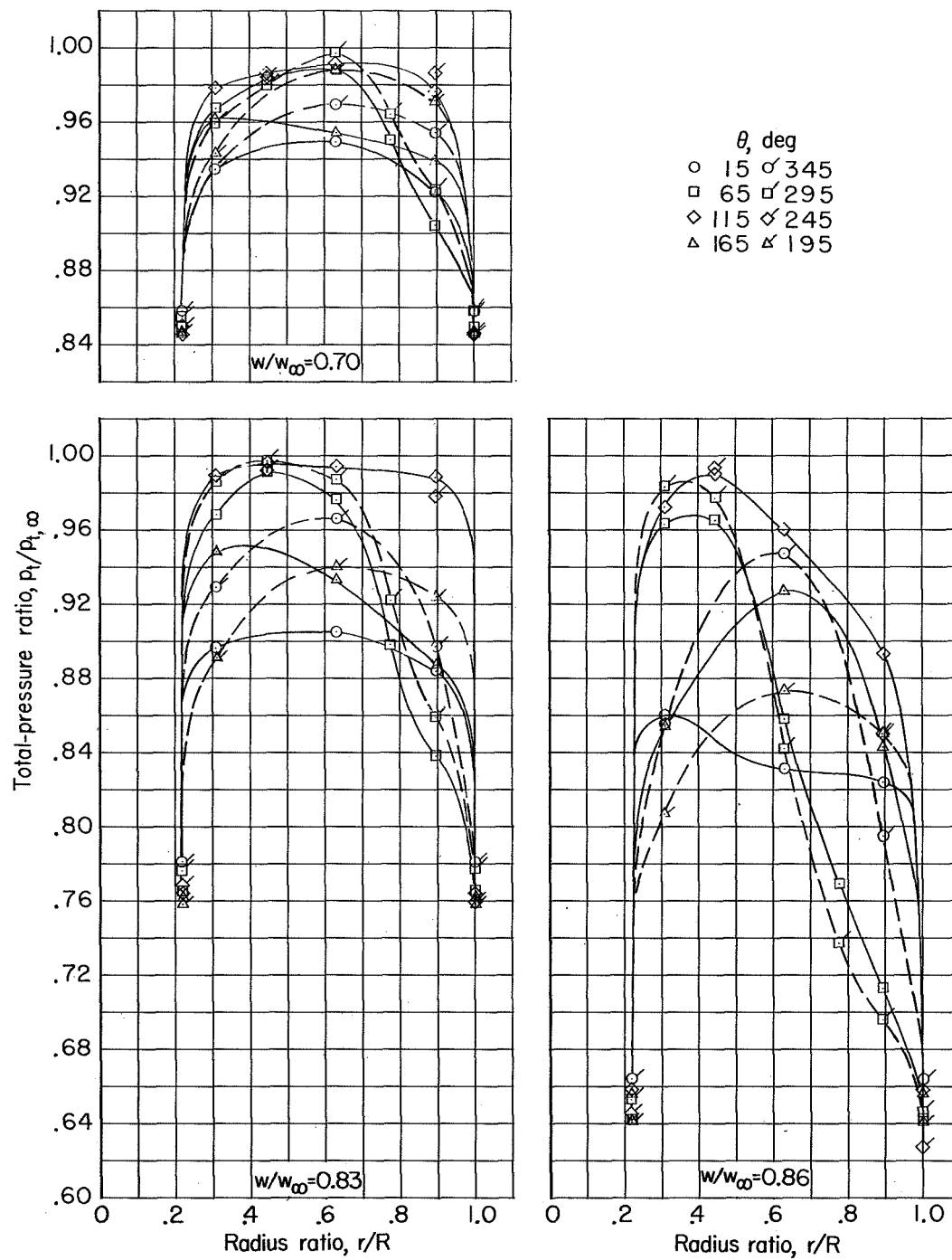
(f) $M = 1.10$; $\beta = 0^\circ$.

Figure 10.- Continued.



(g) $M = 1.10$; $\beta = 5^\circ$.

Figure 10.- Continued.



(h) $M = 1.10$; $\beta = 10^\circ$.

Figure 10.- Concluded.

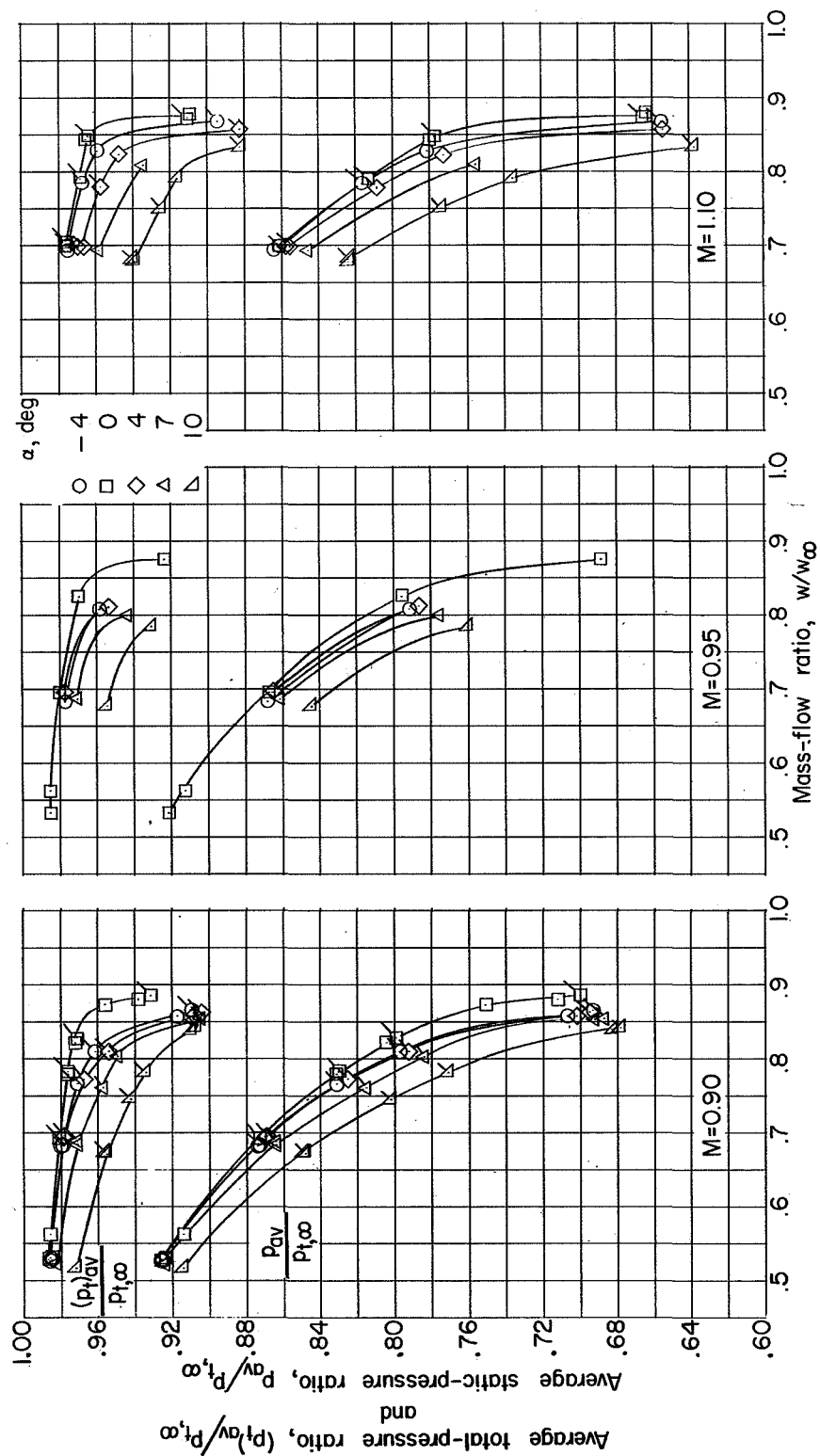


Figure 11.- Variation of average total-pressure and static-pressure ratios with mass-flow ratio at various angles of attack and Mach numbers. Basic configuration. $\beta = 0^\circ$. Flagged symbols indicate test points for model with transition strip on fuselage.

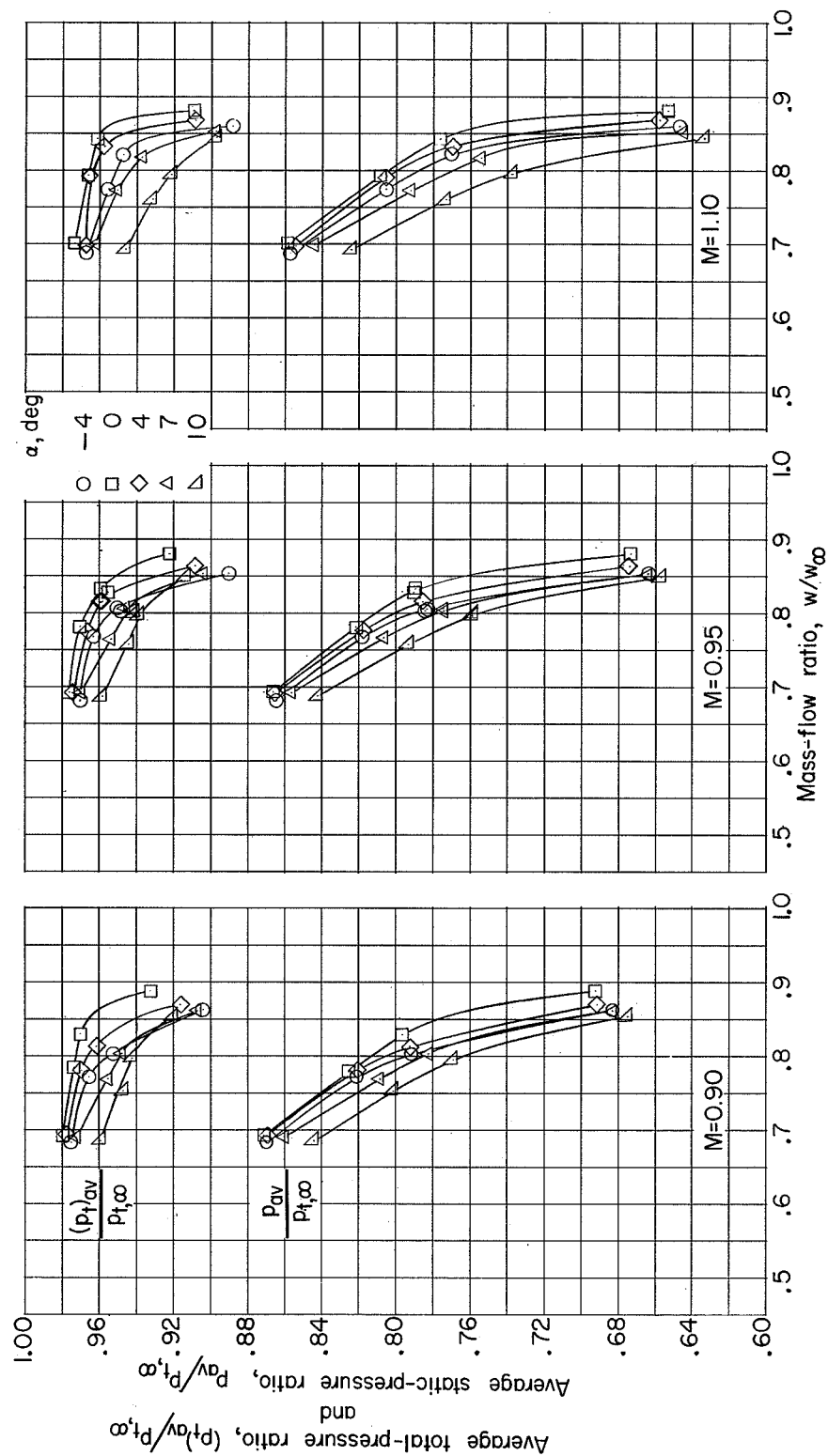


Figure 12.- Variation of average total-pressure and static-pressure ratios with mass-flow ratio at various angles of attack and Mach numbers. Basic configuration. $\beta = 5.2^\circ$.

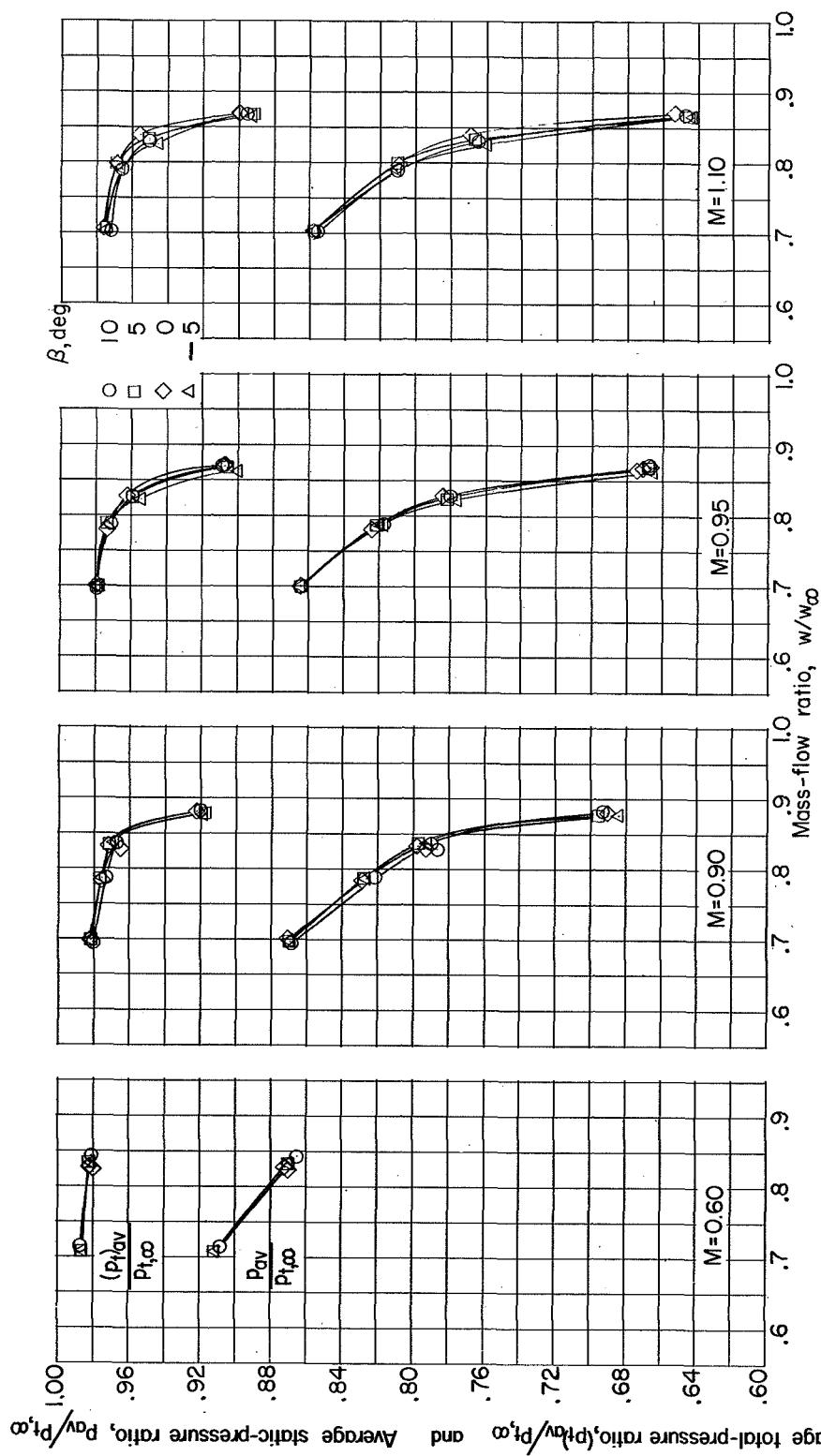


Figure 13.- Variation of average total-pressure and static-pressure ratios with mass-flow ratio at various angles of sideslip and Mach numbers. Basic configuration. $\alpha = 0^\circ$.

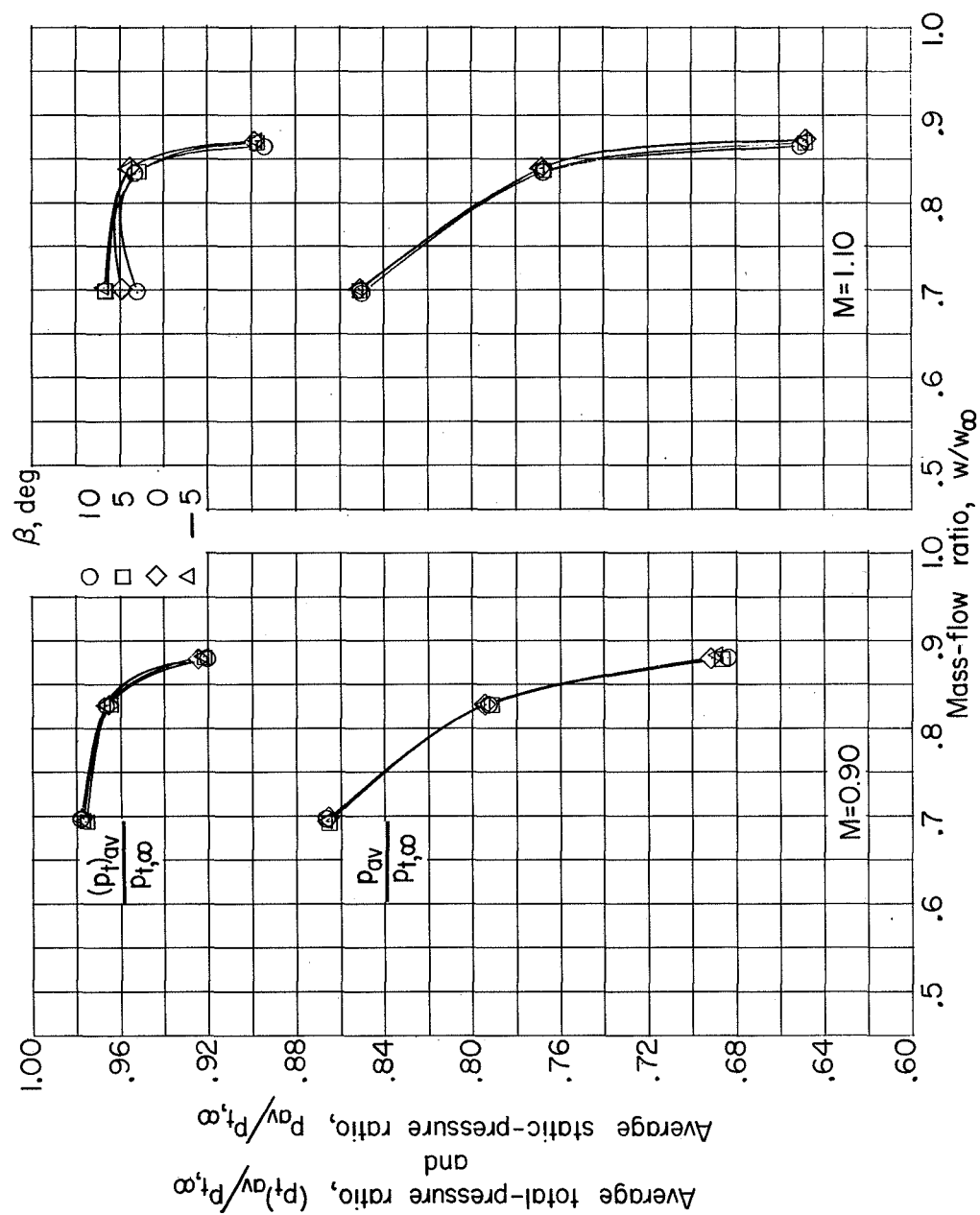


Figure 14.- Variation of average total-pressure and static-pressure ratios with mass-flow ratio at various angles of sideslip and Mach numbers. Basic configuration with fuselage gloves. $\alpha = 0^\circ$.

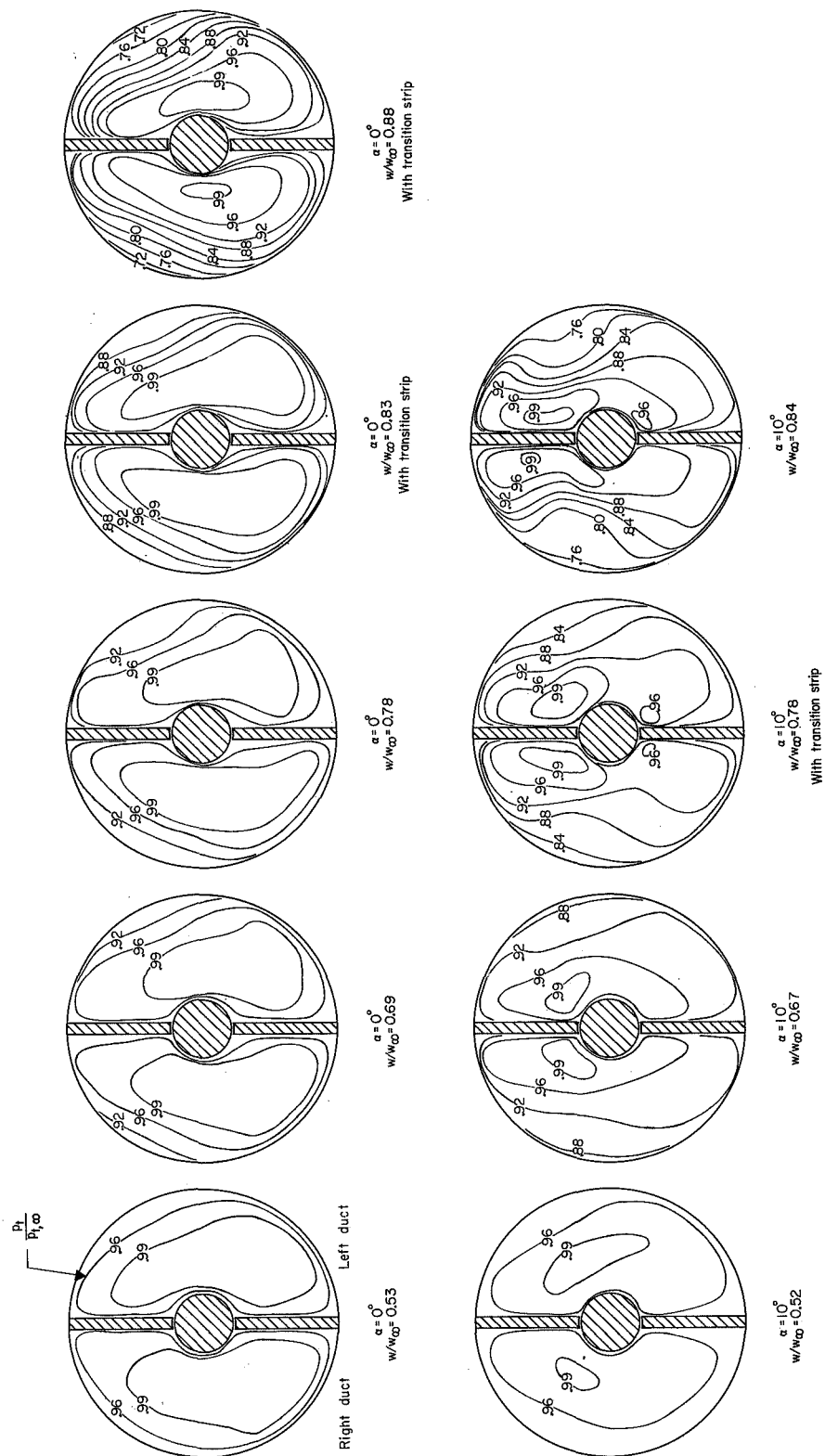
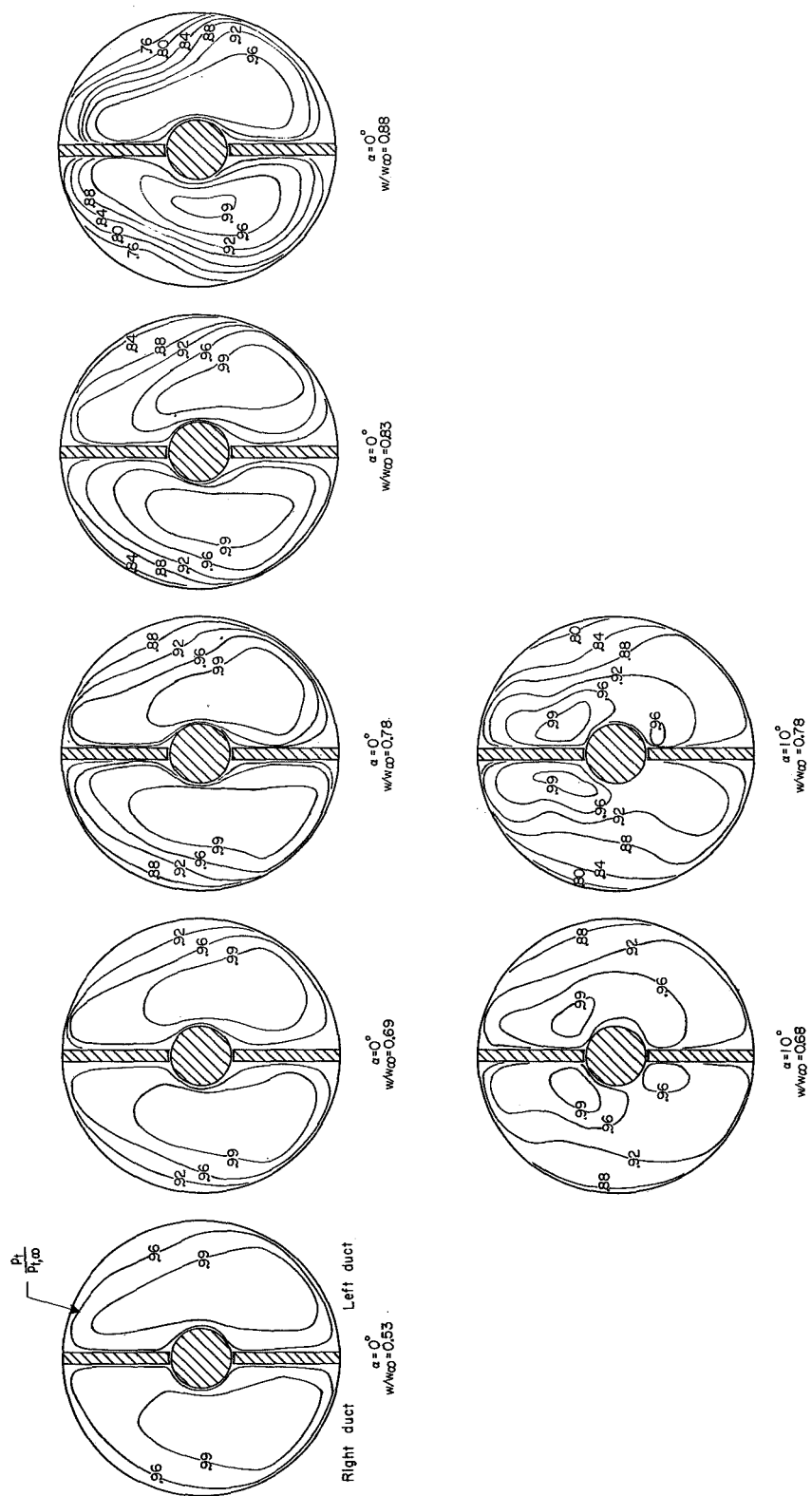
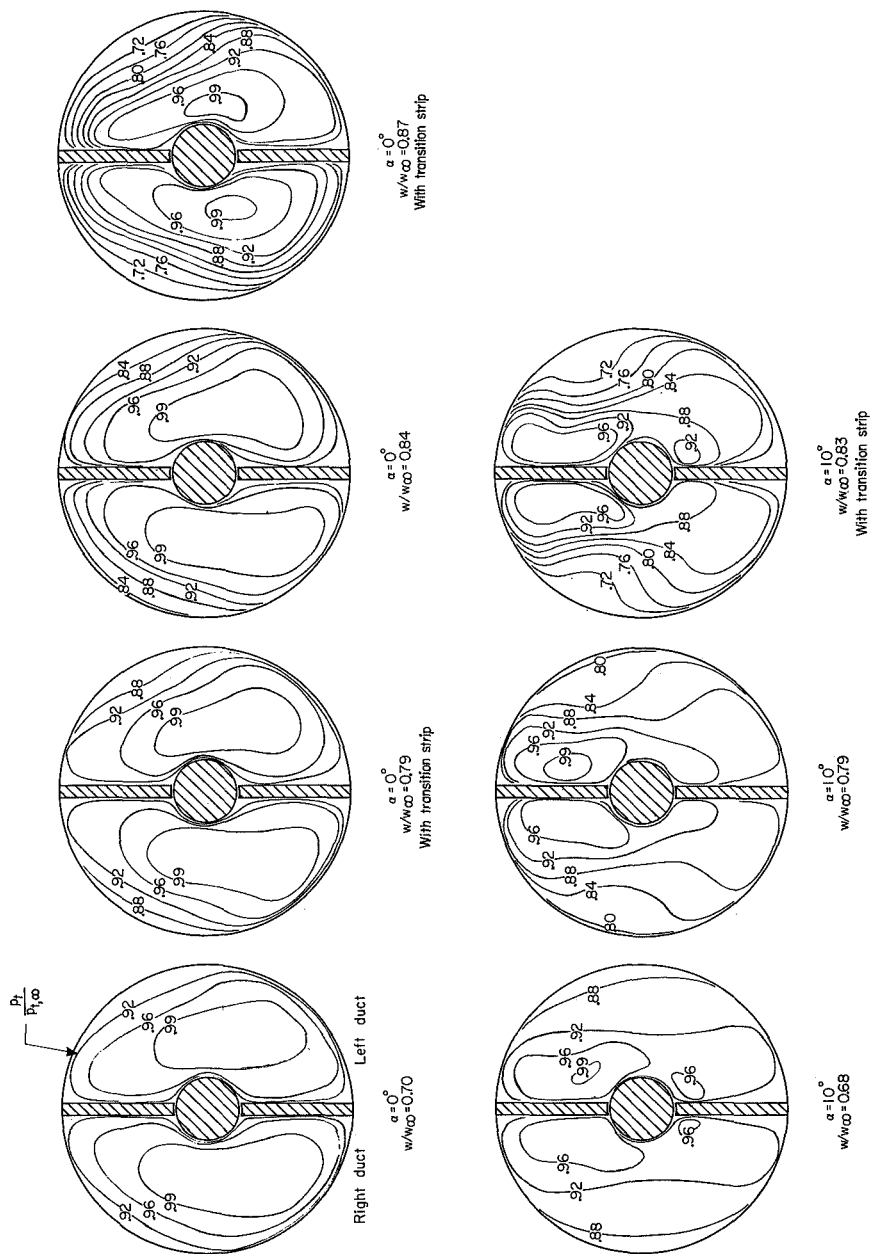
(a) $M = 0.90$.

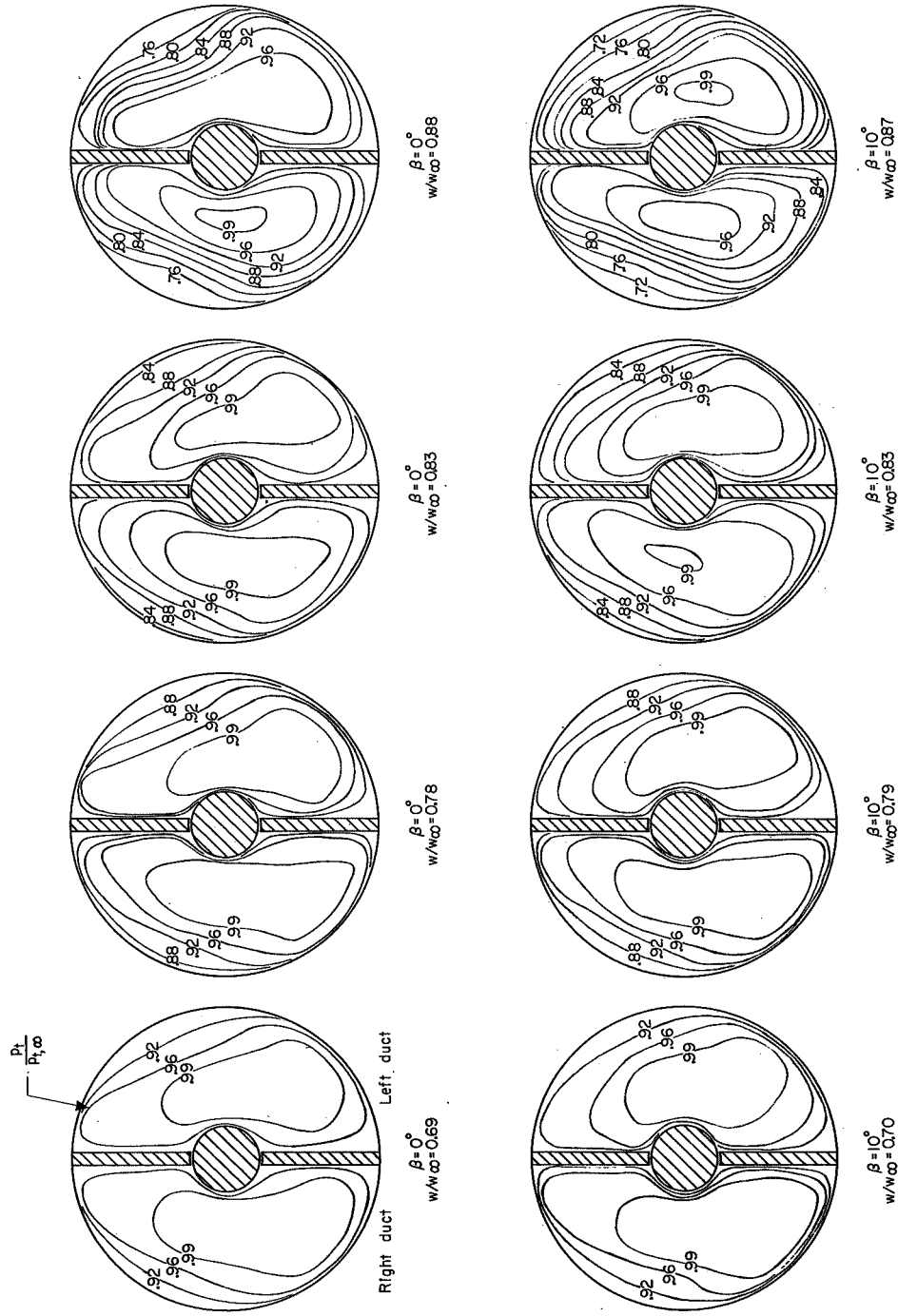
Figure 15.- Contour plots of total-pressure ratio at two angles of attack and several mass-flow ratios. View looking downstream. Basic configuration. $\beta = 0^\circ$.



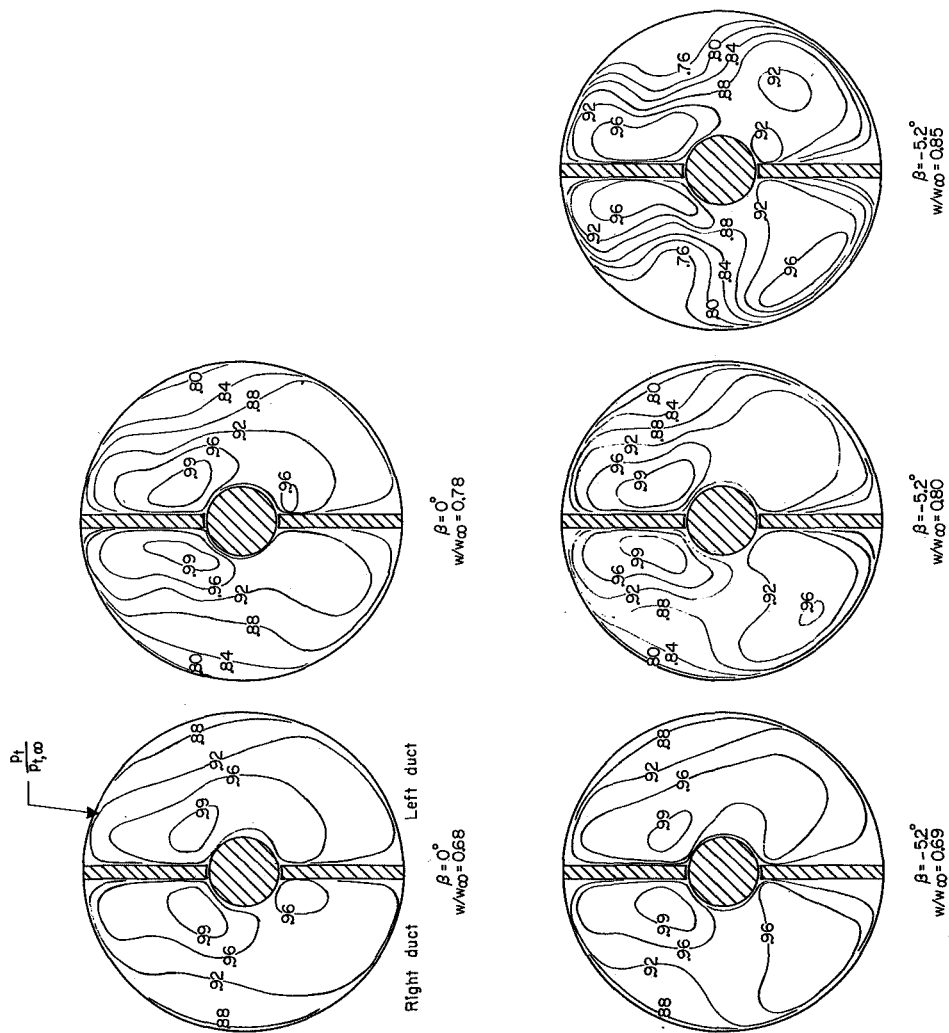


(c) $M = 1.10$.

Figure 15.- Concluded.



(3) $\alpha = 0^\circ$.



(b) $\alpha = 10^\circ$.

Figure 16.- Concluded.

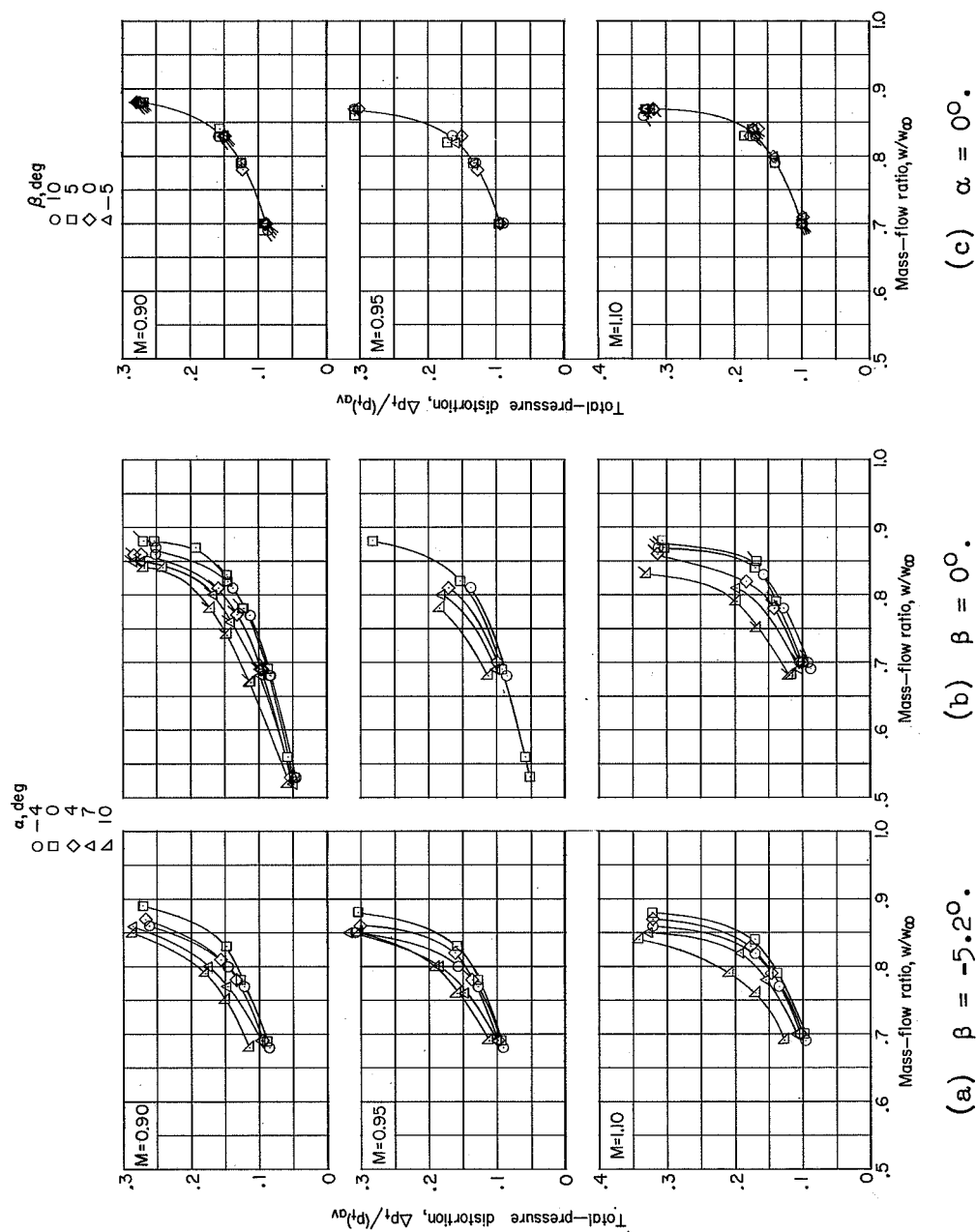
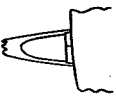

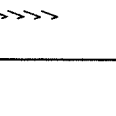
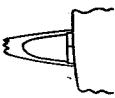

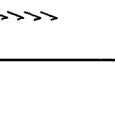
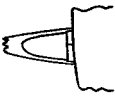

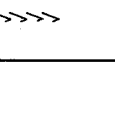
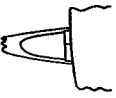

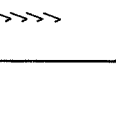


Figure 17.- Effect of mass-flow ratio on flow distortion at various angles of attack and sideslip. Upper flags indicate transition strip on fuselage, and lower flags indicate gloves on fuselage.

NOTES: (1) Reynolds number is based on the diameter of a circle with the same area as that of the capture area of the inlet.

(2) The symbol * denotes the occurrence of buzz.

Report and facility	Description			Test parameters					Test data			Performance		Remarks
				Number of oblique shocks	Type of boundary-layer control	Free-stream Mach number	Reynolds number $\times 10^{-6}$	Angle of attack, deg	Angle of yaw, deg	Drag profile	Inlet-flow picture	Discharge-flow picture	Maximum total-pressure recovery	
CONFID. NASA MEMO 3-9-59L Langley 8, transonic tunnel			Isentropic	Fuselage Diverter	0.60 .90 .95 1.10	0.71 .84 .84 .84	0 -4 to 10 -4 to 10 -4 to 10	-5 to 10 -4 to 10 -4 to 10 -4 to 10 for all Mach Nos.				0.93 .96 .96 .97	0.71 to 0.84 0.52 to 0.88 0.53 to 0.88 0.69 to 0.88	
CONFID. NASA MEMO 3-9-59L Langley 8, transonic tunnel			Isentropic	Fuselage Diverter	0.60 .90 .95 1.10	0.71 .84 .84 .84	0 -4 to 10 -4 to 10 -4 to 10	-5 to 10 -4 to 10 -4 to 10 -4 to 10 for all Mach Nos.				0.93 .98 .98 .97	0.71 to 0.84 0.52 to 0.88 0.53 to 0.88 0.69 to 0.88	
CONFID. NASA MEMO 3-9-59L Langley 8, transonic tunnel			Isentropic	Fuselage Diverter	0.60 .90 .95 1.10	0.71 .84 .84 .84	0 -4 to 10 -4 to 10 -4 to 10	-5 to 10 -4 to 10 -4 to 10 -4 to 10 for all Mach Nos.				0.99 .96 .98 .97	0.71 to 0.84 0.52 to 0.88 0.53 to 0.88 0.69 to 0.88	
CONFID. NASA MEMO 3-9-59L Langley 8, transonic tunnel			Isentropic	Fuselage Diverter	0.60 .90 .95 1.10	0.71 .84 .84 .84	0 -4 to 10 -4 to 10 -4 to 10	-5 to 10 -4 to 10 -4 to 10 -4 to 10 for all Mach Nos.				0.99 .98 .98 .97	0.71 to 0.84 0.52 to 0.88 0.53 to 0.88 0.69 to 0.88	

Bibliography

These strips are provided for the convenience of the reader and can be removed from this report to compile a bibliography of NASA inlet reports. This page is being added only to inlet reports and is on a trial basis.

1000

10

10

10

10

10

1000